SA/TR-5/91

Efficient Asymptotic Closed Form Approximation For Dyadic Green's Function For Anisotropic Substrates

Sina Barkeshli

Sabbagh Associates, Inc.
4639 Morningside Drive
Bloomington, IN 47401

August 15, 1991

Phase 1 Final Report
Grant No. DAAL02-91 C-0020

Harry Diamond Laboratories
2800 Powder Mill Road
Adelphi, MD 20783-1197

Contents

List of Figures

Chapter 1

1.1 Introduction

An efficient closed form asymptotic representation for a grounded double-layered anisotropic uniaxial geometry is developed. The large parameter of this asymptotic development is directly proportional to the lateral separation between the source and observation point. However the asymptotic solution remains accurate even for very small (a few tenths of a wavelength) lateral separation of the source and field points. The asymptotic closed form dyadic Green's function has been cast in such a form that the physical behavior of the electromagnetic fields due to anisotropy of the medium reveals itself through a simple mathematical parameters. Thus, the physical understanding of the interaction of the spatially confined source with an anisotropic (uniaxial) double-layered grounded slab is greatly enhanced through the newly developed asymptotic closed form representation of the dyadic Green's function.

Also, this efficient representation is very useful in the moment method (MM) solution of the current excited on the microstrip antennas and arrays in a grounded double-layered uniaxial geometry, as well as the volumetric current excited within a dielectric scatterer buried in a grounded double layered anisotropic uniaxial slab. The MM analysis, especially for microstrip arrays and guided wave structures, requires a very large number of computations where the lateral distance between the source and the field points in the dyadic Green's function can range from extremely small to very large values [1, 2]. The newly developed asymptotic Green's function can drastically improve the computational speed and the efficiency of the MM solution, as compared to the use of the conventional Sommerfeld form of the Green's function. For small lateral separation (less than a few tenths of the wavelength) between the source and observation points, one can switch to either modified Sommerfeld, or to the radially propagating integral representation of the dyadic Green's function which also developed during the project. For very small lateral separations, less than a quarter to half a free space wavelength, the modified Sommerfeld representation is more efficient; for the relatively small to moderately large the radially propagating integral representation of the dyadic Green's is should be used.

Hence, a systematic numerical algorithm is developed which can efficiently be used to compute the dyadic Green's function for a grounded anisotropic uniaxial double-layered

slab for the entire range of the separation of source and observation points.

The format of the report is as follows: Chapter 2 deals with the formulation of the electromagnetic dyadic Green's function in anisotropic uniaxial multi-layered media. A general formulation of the dyadic Green's function, and the theory of z-propagating modes in anisotropic uniaxial media is discussed in this chapter. The dyadic Green's function consists of the integral over the plane-wave spectrum of a continuum of vector-wave function, in which the vector-waves are guided (propagated) in the preferred $\hat{z}$-coordinate direction. Furthermore a related solution such as, the electromagnetic dyadic Green's function for an anisotropic uniaxial multi-layered medium due to periodic electric as well as magnetic point currents has also been developed. This solution is important in many applications involving anisotropic uniaxial stratified media, such as the design of high performance large phased array in mulit-layered envireoment, the analysis of the frequency selective surfaces (FSS), multi-layered guided structures, and grating. In Chapter 3 a general formulation presented in Chapter 2 will be specialized to a canonical geometry of a grounded anisotropic uniaxial double-layered slab where the electric point current located within the slab. A Sommerfeld and subsequently a radial propagation integral representation of the dyadic Green's function of this geometry will then be presented. Also in this chapter, two distinct efficient methods of the numerical integrations will be presented. The first method is based on removal of the singularity of the integrand of the Sommerfeld (z-propagating) integral representation of the dyadic Green's function. The second method results from the radially propagating integral representation of the Green's dyadic. The uniform asymptotic closed form approximation of the dyadic Green's function for anisotropic uniaxial double-layered grounded slab is the topic of Chapter 4. This asymptotic Green's function is developed employing the formal radial propagation integral representation of the Green's function presented in Chapter 3. Chapter 5 is devoted to numerical results based on the accuracy and efficiency of our newly developed asymptotic dyadic Green's function. The effect of the anisotropy of the material on the electromagnetic field and the physical interpretation of our result will also be presented in this chapter. The conclusion and the direction of our future research will be presented in Chapter 6. The analytical expressions for the vector-wave modes, for a general anisotropic uniaxial medium, is derived in Appendix A. In Appendix B the reciprocity and orthogonality relations for the vector-wave modes are presented. Some essential functions as well as residues of the surface waves which are being used to construct the radial propagation integral representation as well as the uniform asymptotic closed form dyadic Green's function are presented in Appendix C. Appendix D devoted to the asymptotic behavior of the integrands of the Green's functions which are employed in singularity removal technique.

Chapter 2

Formulation

2.1 Introduction

In this chapter a complete, plane-wave spectral, vector-wave function expansion of the electromagnetic, electric, and magnetic, dyadic Green's function for electric, as well as magnetic, point currents for a planar, anisotropic uniaxial multi-layered medium is presented. It is given in terms of z-propagating, solenoidal vector-wave functions, where $\hat{\mathbf{z}}$ is normal to the interfaces, and it is developed via a utilization of the Lorentz reciprocity theorem. For the completeness the electromagnetic dyadic Green's function for periodic electric as well as magnetic point current sources are also presented.

The geometry of the problem is shown in Figure 2.1, where the electrical parameters, $(\bar{\bar{\mu}}_n, \bar{\bar{\epsilon}}_n)$, in the n^{th} layer are assumed to be homogeneous and uniaxial ($\bar{\bar{\epsilon}} = \epsilon_t \mathbf{I}_t + \epsilon_z \hat{\mathbf{z}}\hat{\mathbf{z}}$; $\bar{\bar{\mu}} = \mu_t \mathbf{I}_t + \mu_z \hat{\mathbf{z}}\hat{\mathbf{z}}$). It is shown that the electromagnetic field at a given point within the multi-layered region consists of four distinct waves (two for each vector-wave type) caused by the presence of the multi-layered medium. Moreover, the presence of boundaries in anisotropic media cause mode-coupling at the planar interfaces; these modes are, in general, continuously coupled within the stratified region. However, due to the reflection symmetry of the anisotropic uniaxial structure considered here the modes are decoupled, and hence; the Green's dyadic within each of the layers can be expressed in terms of four uncoupled distinct waves (two for each mode), which resembles the dyadic Green's function for multi-layered isotropic medium.

A systematic formulation, presented here, is useful in many problems dealing with new types of anisotropic materials, such as advanced composites, ceramics, and honeycomb structures, which are finding increasingly important applications in high-frequency electromagnetics and optics. These applications range from microwave and millimeter-wave integrated circuits and optical devices, to antenna radomes and radar absorber materials. The importance of this analysis, besides the physical significance of understanding the interaction of electromagnetic sources with complex media, is due to a serious need for efficient design procedures for high performance monolithic integrated circuits that operate in the high frequency regime (millimeter to optical wavelength), as well as to a crucial

need for an analytical model for the non-destructive evaluation (NDE) of a variety of the increasingly-used advanced composite materials.

Due to the widespread application of complex materials, there has been considerable research on the interaction of electromagnetic waves with multi-layered anisotropic media. We restrict ourselves to those work which directly related to anisotropic uniaxial media. Wait [3] and Kong [4, 5] investigated the radiation of a dipole source over a uniaxial stratified media. Interaction of the electromagnetic source with anisotropic uniaxial media has also been extensively studied by Felsen and Marcuvitz [6]. Ali and Mahmoud [7] derived a Green's dyadic for a uniaxial stratified medium, using dyadic Green's function theory in conjunction with the primary and secondary dyadic Green's function. Tang [8], and Kwon and Wang [9] have investigated the problem of various types of the point sources in uniaxial stratified media. They derived the expressions for the electric and magnetic field components by satisfying the boundary conditions at each interface and a proper condition at the source point. Krowne [10] has given Green's function solutions for uniaxial and biaxial, layered, planar structures excited by a surface electric current. His results are given in terms of three different longitudinal-to-an-axis formulations of the differential coupled field component sets. The radiation of an electric dipole in the presence of the anisotropic uniaxial grounded layered media has been investigated by Tsalamengas and Uzunoglu [11]. An excellent review of wave propagation in general anisotropic media has recently been given by Chew [12].

In the present work the complete, spectral, vector-wave expansion for the electromagnetic (electric and magnetic) dyadic Green's function for electric, as well as magnetic, point current dipole sources for planar, anisotropic uniaxial multi-layered media, using solenoidal vector-wave functions [14] is derived. The orthogonality of the modes over a plane surface [6] transverse to the direction of the propagation, $\hat{\mathbf{z}}$, together with a reciprocity relation are employed to construct the Green's dyadics. Moreover, the method that is employed here utilizes only solenoidal vector-wave functions [13]; hence, the dyadic delta function term at the source point is included explicitly as a correction to the general solenoidal vector-wave expansion, which is valid outside the source point [13, 15].

The format of the chapter is as follows: Section 2.2 deals with the formulation of the electromagnetic dyadic Green's function. A general formulation of the dyadic Green's function in anisotropic media, and the theory of z-propagating modes in anisotropic media will be discussed in parts 2.2-A and 2.2-B respectively. In Section 2.3 the electromagnetic dyadic Green's function, $\overline{\overline{\Xi}}(\mathbf{r}, \mathbf{r}')$, for electric and magnetic point current sources in unbounded anisotropic uniaxial media is presented. The Green's function consists of an integral over the plane-wave spectrum of a continuum of eigenvectors, in which the eigenvectors are guided (propagated) in the preferred $\hat{\mathbf{z}}$-coordinate direction. This development uses the Lorentz reciprocity relation. The dyadic Green's function for anisotropic uniaxial multi-layered media, $\overline{\overline{\Xi}}_{m,n}(\mathbf{r}, \mathbf{r}')$, will be derived in section 2.4, using again the reciprocity relation in the multi-layered media. In Section 2.5 the Green's dyadic developed in the previous section will be used to derived the dyadic Green's function for the periodic electric

as well as magnetic point currents in anisotropic uniaxial multi-layered media.

2.2-A General dyadic Green's function formulation for anisotropic media

Maxwell's equations in a source-excited, unbounded, anisotropic, medium with ($e^{j\omega t}$) understood and suppressed, can be written in the operator form

$$\bar{\bar{\mathcal{L}}}\,\boldsymbol{\Sigma}(\mathbf{r},\mathbf{r}') = -\boldsymbol{\mathcal{J}} \quad , \tag{2.1}$$

where the dyadic operators are defined as

$$\bar{\bar{\mathcal{L}}} \equiv \begin{pmatrix} j\omega\epsilon_0\bar{\bar{\epsilon}} & -\nabla\times\mathbf{I} \\ \nabla\times\mathbf{I} & j\omega\mu_0\bar{\bar{\mu}} \end{pmatrix} \quad ; \boldsymbol{\Sigma} \equiv \begin{pmatrix} \mathbf{E} \\ \mathbf{H} \end{pmatrix} \quad ; \boldsymbol{\mathcal{J}} \equiv \begin{pmatrix} \mathbf{J}_e \\ \mathbf{J}_m \end{pmatrix} \quad , \tag{2.2}$$

and $\bar{\bar{\epsilon}}$, $\bar{\bar{\mu}}$ are respectively the relative permittivity and permeability tensors (with respect to free space) of the medium, $\mathbf{I}$ is a unit dyad, and $\boldsymbol{\mathcal{J}}$ represents the impressed electric as well as magnetic current sources. The electromagnetic field column-vector $\boldsymbol{\Sigma}$ can be represented, using the electromagnetic dyadic Green's function theory, as

$$\boldsymbol{\Sigma}(\mathbf{r}) = \int_v d\mathbf{r}'\, \boldsymbol{\Xi}(\mathbf{r},\mathbf{r}')\cdot\boldsymbol{\mathcal{J}}(\mathbf{r}') \quad , \tag{2.3}$$

where the electromagnetic dyadic Green's function, $\boldsymbol{\Xi}(\mathbf{r},\mathbf{r}')$, is 2×2 vector matrix of electric and magnetic dyadic Green's functions, and v contains the source region. In this general formulation the electric as well as magnetic dyadic Green's functions due to the impressed electric, e, and magnetic, m, current dipole sources are both considered. If $\boldsymbol{\mathcal{J}}$ is an arbitrarily oriented point column current dipole source,

$$\boldsymbol{\mathcal{J}} = \boldsymbol{\mathcal{P}}\delta(\mathbf{r}-\mathbf{r}') \; ; \quad \boldsymbol{\mathcal{P}} \equiv \begin{pmatrix} \mathbf{p}_{e,t} + \mathbf{p}_{e,z} \\ \mathbf{p}_{m,t} + \mathbf{p}_{m,z} \end{pmatrix} \quad , \tag{2.4}$$

where t, z stand for transverse and longitudinal directions respectively, then the electromagnetic field may be viewed as a distribution; namely,

$$\boldsymbol{\Sigma}(\mathbf{r}) = \boldsymbol{\Xi}(\mathbf{r},\mathbf{r}')\cdot\boldsymbol{\mathcal{P}} \quad , \tag{2.5}$$

where in vector-matrix notation, the above equation can be identified as,

$$\boldsymbol{\Sigma}(\mathbf{r}) = \begin{pmatrix} \mathcal{G}^{ee}(\mathbf{r},\mathbf{r}') & \mathcal{G}^{em}(\mathbf{r},\mathbf{r}') \\ \mathcal{G}^{me}(\mathbf{r},\mathbf{r}') & \mathcal{G}^{mm}(\mathbf{r},\mathbf{r}') \end{pmatrix} \cdot \begin{pmatrix} \mathbf{p}_e \\ \mathbf{p}_m \end{pmatrix} \quad . \tag{2.6}$$

The first and second superscripts denote the nature of the Green's dyadics, (i.e., electric or magnetic), and the type of the current sources, respectively.

Having established the relation between the electromagnetic field and its associated Green's dyadic, one may construct such a dyadic Green's function to find the electromagnetic field due to arbitrary electric and magnetic current distributions in unbounded anisotropic medium. One can utilize the guided wave mode theory [6] to construct such a dyadic Green's function from the spectrum of the guided (propagated) wave in an arbitrary z-direction. In the following the property of the guided wave modes for anisotropic media will be explained, and then the theory will be applied to find the Green's dyadic for unbounded, as well as multi-layered, uniaxial anisotropic media.

2.2-B The z-propagating mode description in anisotropic media

In order to effect the z-propagation representation of the eigenmodes, one can decompose the field operator into transverse, ∇_t, and longitudinal, $\frac{\partial}{\partial z}$, components, $(\nabla = \nabla_t + \frac{\partial}{\partial z})$, which yields,

$$\bar{\bar{\mathcal{L}}} = j(\bar{\bar{\mathcal{K}}} - j\bar{\bar{\mathbf{W}}}\frac{\partial}{\partial z}) \quad , \tag{2.7}$$

where

$$\bar{\bar{\mathcal{K}}} \equiv \begin{pmatrix} \omega\epsilon_0\bar{\bar{\epsilon}} & j\nabla_t \times \mathbf{I} \\ -j\nabla_t \times \mathbf{I} & \omega\mu_0\bar{\bar{\mu}} \end{pmatrix} \; ; \; \bar{\bar{\mathbf{W}}} \equiv \begin{pmatrix} 0 & -\hat{\mathbf{z}} \times \mathbf{I} \\ \hat{\mathbf{z}} \times \mathbf{I} & 0 \end{pmatrix} \; . \tag{2.8}$$

Also the dyadic $\bar{\bar{\epsilon}}$, and $\bar{\bar{\mu}}$, may be represented for a general anisotropic material as

$$\bar{\bar{\epsilon}} = \bar{\bar{\epsilon}}_{tt} + \hat{\mathbf{z}}\bar{\epsilon}_{zt} + \bar{\epsilon}_{tz}\hat{\mathbf{z}} + \hat{\mathbf{z}}\hat{\mathbf{z}}\epsilon_z \quad ; \quad \bar{\bar{\mu}} = \bar{\bar{\mu}}_{tt} + \hat{\mathbf{z}}\bar{\mu}_{zt} + \bar{\mu}_{tz}\hat{\mathbf{z}} + \hat{\mathbf{z}}\hat{\mathbf{z}}\mu_z \quad , \tag{2.9}$$

where for ($\beta = \epsilon$ or μ):

$$\bar{\bar{\beta}}_{tt} = \begin{pmatrix} \beta_{xx} & \beta_{xy} \\ \beta_{yx} & \beta_{yy} \end{pmatrix} ; \; \bar{\beta}_{tz} = \hat{\mathbf{x}}\beta_{xz} + \hat{\mathbf{y}}\beta_{yz} \; ; \; \bar{\beta}_{zt} = \hat{\mathbf{x}}\beta_{zx} + \hat{\mathbf{y}}\beta_{zy} \quad , \tag{2.10}$$

After decomposing the field components into transverse and longitudinal (i.e., $\mathbf{E} = \mathbf{E}_t + \hat{\mathbf{z}}\, E_z$; $\mathbf{H} = \mathbf{H}_t + \hat{\mathbf{z}}\, H_z$), and taking a dot product of (2.1) with $\hat{\mathbf{z}}$, in view of (2.4), (2.7) and (2.9), one will have

$$\begin{aligned} E_z &= -\frac{1}{\epsilon_z}\bar{\epsilon}_{zt} \cdot \mathbf{E}_t + \frac{1}{-j\omega\epsilon_0\epsilon_z}\nabla_t \cdot (\hat{\mathbf{z}} \times \mathbf{H}_t) - \frac{p_{e,z}}{j\omega\epsilon_0\epsilon_z}\delta(\mathbf{r} - \mathbf{r}') \quad , \\ H_z &= -\frac{1}{\mu_z}\bar{\mu}_{zt} \cdot \mathbf{H}_t + \frac{1}{-j\omega\mu_0\mu_z}\nabla_t \cdot (\mathbf{E}_t \times \hat{\mathbf{z}}) - \frac{p_{m,z}}{j\omega\mu_0\mu_z}\delta(\mathbf{r} - \mathbf{r}') \quad . \end{aligned} \tag{2.11}$$

Also, upon eliminating the longitudinal fields from (2.1), one can find the equation for the transverse field vectors [6]

$$\omega\epsilon_0\left[\bar{\bar{\epsilon}}_{tt}\cdot\ -\frac{\bar{\epsilon}_{tz}\,\bar{\epsilon}_{zt}}{\epsilon_z}+\frac{1}{\omega^2\epsilon_0\mu_0}\hat{\mathbf{z}}\times\nabla_t\frac{1}{\mu_z}\hat{\mathbf{z}}\cdot\nabla_t\times\right]\mathbf{E}_t$$
$$-j\left[\frac{\bar{\epsilon}_{tz}}{\epsilon_0}\hat{\mathbf{z}}\times\nabla_t-\hat{\mathbf{z}}\times\nabla_t\frac{\bar{\mu}_{zt}}{\mu_z}\right]\cdot\mathbf{H}_t+j\frac{\partial}{\partial z}\hat{\mathbf{z}}\times\mathbf{H}_t$$
$$=-\frac{\mathbf{p}_{et}\delta(\mathbf{r}-\mathbf{r}')}{j}+\frac{\bar{\epsilon}_{tz}}{j\epsilon_0}p_{ez}\delta(\mathbf{r}-\mathbf{r}')-\frac{1}{\omega\mu_0\mu_z}\hat{\mathbf{z}}\times\nabla_t\,p_{mz}\delta(\mathbf{r}-\mathbf{r}') \tag{2.12}$$

$$\omega\mu_0\left[\bar{\bar{\mu}}_{tt}\cdot\ -\frac{\bar{\mu}_{tz}\,\bar{\mu}_{zt}}{\mu_z}+\frac{1}{\omega^2\epsilon_0\mu_0\epsilon_0}\hat{\mathbf{z}}\times\nabla_t\frac{1}{\epsilon_z}\hat{\mathbf{z}}\cdot\nabla_t\times\right]\mathbf{H}_t$$
$$+j\left[\frac{\bar{\mu}_{tz}}{\mu_z}\hat{\mathbf{z}}\times\nabla_t-\hat{\mathbf{z}}\times\nabla_t\frac{\bar{\epsilon}_{zt}}{\epsilon_0}\right]\cdot\mathbf{E}_t-j\frac{\partial}{\partial z}\hat{\mathbf{z}}\times\mathbf{E}_t$$
$$=-\frac{\mathbf{p}_{mt}\delta(\mathbf{r}-\mathbf{r}')}{j}+\frac{\bar{\mu}_{tz}}{j\mu_z}p_{mz}\delta(\mathbf{r}-\mathbf{r}')+\frac{1}{\omega\epsilon_0\epsilon_z}\hat{\mathbf{z}}\times\nabla_t\,p_{ez}\delta(\mathbf{r}-\mathbf{r}')\,.$$

If the anisotropy of the medium is transverse to $\hat{\mathbf{z}}$; $\bar{\epsilon}_{tz},\bar{\epsilon}_{zt},\bar{\mu}_{tz}$, and $\bar{\mu}_{zt}$ identically vanish and (2.11) and (2.12) will be simplified to:

$$\begin{aligned}E_z &= \frac{1}{-j\omega\epsilon_0\epsilon_z}\nabla_t\cdot(\hat{\mathbf{z}}\times\mathbf{H}_t)-\frac{p_{e,z}}{j\omega\epsilon_0\epsilon_z}\delta(\mathbf{r}-\mathbf{r}')\quad,\\ H_z &= \frac{1}{-j\omega\mu_0\mu_z}\nabla_t\cdot(\mathbf{E}_t\times\hat{\mathbf{z}})-\frac{p_{m,z}}{j\omega\mu_0\mu_z}\delta(\mathbf{r}-\mathbf{r}')\quad,\end{aligned} \tag{2.13}$$

$$\omega\epsilon_0\left[\hat{\mathbf{z}}\times\bar{\bar{\epsilon}}_{tt}\cdot+\frac{1}{\omega^2\epsilon_0\mu_0\mu_z}\nabla_t(-\hat{\mathbf{z}}\cdot\nabla_t\times)\right]\mathbf{E}_t-j\frac{\partial}{\partial z}\mathbf{H}_t\ =$$
$$-\frac{\hat{\mathbf{z}}\times\mathbf{p}_{et}\delta(\mathbf{r}-\mathbf{r}')}{j}+\frac{1}{\omega\mu_0\mu_z}\nabla_t\,p_{ez}\delta(\mathbf{r}-\mathbf{r}')\quad, \tag{2.14}$$

$$\omega\mu_0\left[\hat{\mathbf{z}}\times\bar{\bar{\mu}}_{tt}\cdot+\frac{1}{\omega^2\epsilon_0\mu_0\epsilon_z}\nabla_t(-\hat{\mathbf{z}}\cdot\nabla_t\times)\right]\mathbf{H}_t-j\frac{\partial}{\partial z}\mathbf{E}_t\ =$$
$$-\frac{\hat{\mathbf{z}}\times\mathbf{p}_{mt}\delta(\mathbf{r}-\mathbf{r}')}{j}-\frac{1}{\omega\epsilon_0\epsilon_z}\nabla_t\,p_{mz}\delta(\mathbf{r}-\mathbf{r}')\,.$$

To obtain the mode function characteristics of the guided waves propagating along z for the (transversely) unbounded medium, one will seek the source-free solutions, ($\mathcal{P}=0$), of (2.1) with the generic form of

$$\boldsymbol{\Pi}_\alpha(\mathbf{r},\mathbf{k}_t)=\boldsymbol{\Psi}_\alpha(\boldsymbol{\rho})e^{-j\kappa_\alpha z}\quad;\quad\boldsymbol{\Psi}_\alpha(\boldsymbol{\rho})=\frac{1}{2\pi}\boldsymbol{\Psi}_\alpha e^{-j\mathbf{k}_t\cdot\boldsymbol{\rho}}\quad, \tag{2.15}$$

where $\boldsymbol{\Psi}_\alpha(\boldsymbol{\rho})$ and κ_α are the solenoidal eigenvectors and eigenvalues of the operator (2.7), respectively, and $\mathbf{k}_t$ is the transverse vector wavenumber (i.e. $\mathrm{k}_t = \sqrt{\mathbf{k}_t \cdot \mathbf{k}_t}$).

For the medium with a reflection-symmetric property (with respect to a plane transverse to $\hat{\mathbf{z}}$) [6], (i.e., the anisotropy confined in the transverse plane), if $\boldsymbol{\Psi}_\alpha{}^{>}(\boldsymbol{\rho})$ is the eigenvector corresponding to κ_α, then $\boldsymbol{\Psi}_\alpha{}^{<}(\boldsymbol{\rho}) = \bar{\bar{\mathcal{R}}}\boldsymbol{\Psi}_\alpha{}^{>}(\boldsymbol{\rho})$ is the eigenvector for $-\kappa_\alpha$, where the reflection operator $\bar{\bar{\mathcal{R}}}$ is defined as,

$$\bar{\bar{\mathcal{R}}} \equiv \begin{pmatrix} \mathbf{I}_t - \hat{\mathbf{z}}\hat{\mathbf{z}} & 0 \\ 0 & -\mathbf{I}_t + \hat{\mathbf{z}}\hat{\mathbf{z}} \end{pmatrix} \quad , \tag{2.16}$$

where $\mathbf{I}_t$ is the transverse unit dyad. This can be seen from (2.7) and (2.16) (in view of (2.13) and (2.14)), where $\bar{\bar{\mathcal{R}}}\bar{\bar{\mathcal{K}}} = \bar{\bar{\mathcal{K}}}\bar{\bar{\mathcal{R}}}$ and $\bar{\bar{\mathcal{R}}}\bar{\bar{\mathbf{W}}} = -\bar{\bar{\mathbf{W}}}\bar{\bar{\mathcal{R}}}$. Hence, the eigenvectors $\boldsymbol{\Psi}_\alpha^{\gtrless}(\boldsymbol{\rho})$ corresponding to $\pm\kappa_\alpha$ can be expressed as,

$$\boldsymbol{\Psi}_\alpha^{\gtrless}(\boldsymbol{\rho}) = \frac{1}{2\pi}\boldsymbol{\Psi}_\alpha^{\gtrless} e^{-j\mathbf{k}_t\cdot\boldsymbol{\rho}} \;\; ; \;\; \boldsymbol{\Psi}_\alpha^{\gtrless} = \begin{pmatrix} \mathbf{E}_{t,\alpha} \pm \mathbf{E}_{z,\alpha} \\ \pm\mathbf{H}_{t,\alpha} + \mathbf{H}_{z,\alpha} \end{pmatrix} = \begin{pmatrix} Z_\alpha \mathbf{e}_\alpha \pm \mathbf{e}_{z,\alpha} \\ \pm\mathbf{h}_\alpha + \mathbf{h}_{z,\alpha} \end{pmatrix} \quad , \tag{2.17}$$

where $\mathbf{e}_\alpha, \mathbf{h}_\alpha$ and $\mathbf{e}_{z,\alpha}, \mathbf{h}_{z,\alpha}$ are normalized mode-vectors transverse and parallel to z, respectively, for the eigenvalues of $\pm\kappa_\alpha$, and Z_α is the mode impedance [6, 14]. Thus, the eigenvectors $\boldsymbol{\Psi}_\alpha{}^{>}(\boldsymbol{\rho})$ and $\boldsymbol{\Psi}_\alpha{}^{<}(\boldsymbol{\rho})$ for $(\alpha = 1, 2)$ can be written in terms of identical mode-vectors which do not distinguish between the wavenumbers κ_α and $-\kappa_\alpha$.

The analytical expression for the wavenumber κ_α, and the eigenvector $\boldsymbol{\Psi}_\alpha(\boldsymbol{\rho})$ for $(\alpha = 1, 2)$, for a given transverse vector wavenumber $\mathbf{k}_t$ and the angular frequency of ω, are directly related to the relative permittivity and permeability tensors $(\bar{\bar{\epsilon}}, \bar{\bar{\mu}})$. Explicit expressions for $\kappa_\alpha, \mathbf{e}_\alpha, \mathbf{h}_\alpha, \mathbf{e}_{z,\alpha}, \mathbf{h}_{z,\alpha}$, and Z_α for a general uniaxial anisotropic medium, where $(\bar{\bar{\epsilon}} = \epsilon_t\mathbf{I}_t + \epsilon_z\hat{\mathbf{z}}\hat{\mathbf{z}} \;\; ; \;\; \bar{\bar{\mu}} = \mu_t\mathbf{I}_t + \mu_z\hat{\mathbf{z}}\hat{\mathbf{z}})$ are given by, (see also Appendix A for the derivations)

$$\begin{aligned} \mathbf{e}_1 &= \frac{k_x\hat{\mathbf{x}} + k_y\hat{\mathbf{y}}}{k_t} \quad , \\ \mathbf{h}_1 &= \hat{\mathbf{z}} \times \mathbf{e}_1 = \frac{k_x\hat{\mathbf{y}} - k_y\hat{\mathbf{x}}}{k_t} \quad , \end{aligned} \tag{2.18}$$

$$\begin{aligned} e_{z,1} &= -\frac{k_t}{\omega\epsilon_0\epsilon_z} \;\; ; \;\; h_{z,1} = 0 \quad , \\ \kappa_1 &= \sqrt{k_0^2\mu_t\epsilon_t - \frac{\epsilon_t}{\epsilon_z}k_t^2} \;\; ; \;\; Z_1 = \frac{\kappa_1}{\omega\epsilon_0\epsilon_t} \quad , \end{aligned} \tag{2.19}$$

$$\mathbf{e}_2 = \frac{k_x\hat{\mathbf{y}} - k_y\hat{\mathbf{x}}}{k_t} \quad ,$$

$$\mathbf{h}_2 = \hat{\mathbf{z}} \times \mathbf{e}_2 = -\frac{k_x \hat{\mathbf{x}} + k_y \hat{\mathbf{y}}}{k_t} \quad , \tag{2.20}$$

$$e_{z,2} = 0 \; ; \; h_{z,2} = -\frac{k_t}{\omega \mu_0 \mu_z} \quad ,$$

$$\kappa_2 = \sqrt{k_0^2 \mu_t \epsilon_t - \frac{\mu_t}{\mu_z} k_t^2} \; ; \; Y_2 = \frac{1}{Z_2} = \frac{\kappa_2}{\omega \mu_0 \mu_t} \quad , \tag{2.21}$$

where $k_0^2 = \omega^2 \epsilon_0 \mu_0$, and $k_t = \sqrt{k_x^2 + k_y^2}$. Note that $\alpha = 1$ and 2 are respectively correspond to transverse magnetic TM (or E-mode), and transverse electric TE (or H-mode) respectively. In the following section, the dyadic electromagnetic Green's function for a general uni-axial anisotropic unbounded medium will be formulated, and subsequently the dyadic Green's function for a uniaxial anisotropic multi-layered medium will be derived.

2.3 Dyadic Green's function for unbounded, uniaxial anisotropic media

In this section, the theory of the z-propagating (guided) eigenmode for a general uniaxial anisotropic medium, which has been established in the previous section, will be applied to obtain an explicit expression for the electromagnetic dyadic Green function, $\mathbf{\Xi}(\mathbf{r}, \mathbf{r}')$, which is associated with the electric and magnetic point sources, $\mathcal{P}\delta(\mathbf{r} - \mathbf{r}')$, in unbounded uniaxial anisotropic media. In the the next section the procedure developed here will be extended to obtain the dyadic Green's function for the uniaxial anisotropic multilayered medium.

The geometry of the problem dealing with full space uniaxial anisotropic medium with the relative constitutive parameters of ($\bar{\bar{\epsilon}} = \epsilon_t \mathbf{I}_t + \epsilon_z \hat{\mathbf{z}}\hat{\mathbf{z}}$; $\bar{\bar{\mu}} = \mu_t \mathbf{I}_t + \mu_z \hat{\mathbf{z}}\hat{\mathbf{z}}$) excited by $\mathcal{P}\delta(\mathbf{r} - \mathbf{r}')$ is shown in Figure 2.2. In the following formulation, the notation $\gtrless$ means that the entire space consists of two region, $z > z'$ and $z < z'$; and as shown in Figure 2.2, $z = z'$ is the plane S (normal to the $\hat{\mathbf{z}}$-axis) containing source, $\mathcal{P}\delta(\mathbf{r} - \mathbf{r}')$. The z-propagating representation of the dyadic electromagnetic Green's function for the full space anisotropic medium in terms of the solenoidal vector-wave functions can be expressed as [6, 14],

$$\mathbf{\Xi}(\mathbf{r}, \mathbf{r}') = \int d\mathbf{k}_t \, \tilde{\mathbf{\Xi}}^{\gtrless}(\mathbf{k}_t, \mathbf{r}, \mathbf{r}') + \hat{\mathbf{z}}\hat{\mathbf{z}}\bar{\Theta}_z \quad ; \quad \bar{\Theta}_z = \begin{pmatrix} \frac{1}{-j\omega\epsilon_0\epsilon_z} & 0 \\ 0 & \frac{1}{-j\omega\mu_0\mu_z} \end{pmatrix} \delta(\mathbf{r} - \mathbf{r}') \tag{2.22}$$

where the electromagnetic dyadic vector-wave function $\tilde{\mathbf{\Xi}}^{\gtrless}(\mathbf{k}_t, \mathbf{r}, \mathbf{r}')$ is defined as

$$\tilde{\mathbf{\Xi}}^{\gtrless}(\mathbf{k}_t, \mathbf{r}, \mathbf{r}') = \sum_{\alpha=1}^{2} \mathbf{\Pi}_{\alpha}^{\gtrless}(\mathbf{k}_t, \mathbf{r}) \bar{\mathcal{A}}_{\alpha}^{\lessgtr}(\mathbf{k}_t, \mathbf{r}') \quad , \tag{2.23}$$

and once again, the source-free solenoidal vector-wave function $\boldsymbol{\Pi}_{\alpha}^{\gtrless}(\mathbf{k}_t, \mathbf{r})$ can be expressed as

$$\boldsymbol{\Pi}_{\alpha}^{\gtrless}(\mathbf{k}_t, \mathbf{r}) = \frac{1}{2\pi} \boldsymbol{\Psi}_{\alpha}^{\gtrless} e^{-j\mathbf{k}_t \cdot \boldsymbol{\rho} \mp j\kappa_\alpha z} \quad . \tag{2.24}$$

Outside the source region, $z \gtrless z'$, the Green's dyadic can be represented in terms of the spectral integral of the source-free solenoidal vector-wave functions, eigenvectors, $\boldsymbol{\Pi}_{\alpha}^{\gtrless}$ as of (2.23). In order to make the representation complete in the source region at $\mathbf{r} = \mathbf{r}'$, the correction term, $\bar{\Theta}_z$, can simply be added to the spectral integral of the solenoidal vector-wave representation of the electromagnetic dyadic Green's function, which is, of course, valid outside the source region, [13]. The variable $\mathbf{k}_t$ (i.e.,$(\hat{\mathbf{x}}k_x + \hat{\mathbf{y}}k_y); d\mathbf{k}_t = dk_x\, dk_y$) are the continuous transverse eigenvalues which span the entire spectral domain ($-\infty < k_x < \infty; -\infty < k_y < \infty$), and the summation is over the discrete eigenmodes ($\alpha = 1$ and 2) propagating in the z direction. The unknown vector spectral amplitude $\bar{\mathcal{A}}_{\alpha}^{\gtrless}(\mathbf{k}_t, \mathbf{r}')$ is defined as a row vector,

$$\bar{\mathcal{A}}_{\alpha}^{\gtrless} = \left(\begin{array}{cc} \mathbf{a}_{\alpha}^{e} & \mathbf{a}_{\alpha}^{m} \end{array} \right)^{\gtrless} \tag{2.25}$$

where the superscript e and m stand for electric and magnetic sources, respectively, and will be found from the procedure using the reciprocity relation in uniaxial anisotropic media, (see Appendix B), to the fields, $\tilde{\boldsymbol{\Sigma}}^{\gtrless} = \tilde{\boldsymbol{\Xi}}^{\gtrless} \cdot \boldsymbol{\mathcal{P}}$, of (2.23) and the source free solenoidal vector-wave function of $\boldsymbol{\Pi}_{\alpha}^{\lessgtr}(-\mathbf{k}_t, \mathbf{r})$ in the region V, bounded by planar surface $S_>$ and $S_<$, which are slightly above and below the surface S of the Figure 2.2.1 respectively, [22, 13, pages 200–206][1]. Hence,

$$\begin{aligned} \int_{S_>} ds \left(\boldsymbol{\Pi}_{\alpha}^{\lessgtr}(-\mathbf{k}_t, \mathbf{r}) \,,\, \bar{\bar{\mathbf{W}}}\, \tilde{\boldsymbol{\Sigma}}^{\gtrless} \right) - \int_{S_<} ds \left(\boldsymbol{\Pi}_{\alpha}^{\lessgtr}(-\mathbf{k}_t, \mathbf{r}) \,,\, \bar{\bar{\mathbf{W}}}\, \tilde{\boldsymbol{\Sigma}}^{\gtrless} \right) \;\; = \\ - \int_V dv \left(\boldsymbol{\mathcal{P}} \delta(\mathbf{r} - \mathbf{r}') \,,\, \bar{\bar{U}} \left(\boldsymbol{\Pi}_{\alpha}^{\lessgtr}(-\mathbf{k}_t, \mathbf{r}) \right) \right) \\ = \; - \left(\boldsymbol{\mathcal{P}} \,,\, \bar{\bar{U}} \left(\boldsymbol{\Pi}_{\alpha}^{\lessgtr}(-\mathbf{k}_t, \mathbf{r}') \right) \right) \quad , \end{aligned} \tag{2.26}$$

where $\bar{\bar{U}}(\boldsymbol{\Pi}_\alpha)$ is a diagonal vector matrix comprised of the elements of the vector-wave mode, $\boldsymbol{\Pi}_\alpha$, (see (2.15) and (2.17); $\bar{\bar{U}}(\boldsymbol{\Pi}_\alpha)$ and $\bar{\bar{\mathbf{W}}}$ are defined as,

$$\bar{\bar{U}}(\boldsymbol{\Pi}_\alpha) = \left(\begin{array}{cc} \mathbf{E} & 0 \\ 0 & -\mathbf{H} \end{array} \right)_{\alpha} \quad ; \quad \bar{\bar{\mathbf{W}}} = \left(\begin{array}{cc} 0 & -\hat{\mathbf{z}} \times \mathbf{I} \\ -\hat{\mathbf{z}} \times \mathbf{I} & 0 \end{array} \right) \quad , \tag{2.27}$$

[1] The reciprocity theorem is applied to the volume V here with the radiation condition implied as $\rho \to \infty$.

and the operator notation of $(\boldsymbol{\Pi}_\alpha\ ,\ \bar{\bar{\mathbf{W}}}\ \boldsymbol{\Pi}_\beta)$ denotes the usual scalar product of the two column vectors:

$$(\boldsymbol{\Pi}_\alpha\ ,\ \bar{\bar{\mathbf{W}}}\ \boldsymbol{\Pi}_\beta) = \boldsymbol{\Pi}_\alpha^T \cdot \bar{\bar{\mathbf{W}}} \boldsymbol{\Pi}_\beta = \mathbf{E}_\alpha \cdot (\mathbf{H}_\beta \times \hat{\mathbf{z}}) - \mathbf{H}_\alpha \cdot (\hat{\mathbf{z}} \times \mathbf{E}_\beta) \quad . \tag{2.28}$$

Incorporating (2.23) into (2.26) and using the orthogonality relations developed in Appendix B, (see (B.8) and (B.9)) yields,

$$\bar{\mathcal{A}}_\alpha^{\gtrless}(\mathbf{k}_t, \mathbf{r}') \cdot \boldsymbol{\mathcal{P}} = \left(\begin{array}{cc} \mathbf{a}_\alpha^e \cdot \mathbf{p}_e & \mathbf{a}_\alpha^m \cdot \mathbf{p}_m \end{array} \right)^{\gtrless} = \frac{1}{2\pi} \frac{\boldsymbol{\mathcal{P}}^T \cdot \bar{\bar{U}}(\boldsymbol{\Psi}_\alpha^{\lessgtr}(-\mathbf{k}_t))}{-2\, Z_\alpha} e^{+j\mathbf{k}_t \cdot \boldsymbol{\rho}' \pm j\kappa_\alpha z'} \quad . \tag{2.29}$$

Therefore, from (2.29), (2.23), (2.17) and (2.22), the z-propagating plane-wave spectrum (PWS) integral representation for the full-space anisotropic uniaxial dyadic electromagnetic Green's function can be identified as,

$$\bar{\bar{\Xi}}(\mathbf{r}, \mathbf{r}') = \int \frac{d\mathbf{k}_t}{4\pi^2} \sum_{\alpha=1}^{2} \frac{\boldsymbol{\Psi}_\alpha^{\gtrless} \tilde{\boldsymbol{\Psi}}_\alpha^{\lessgtr}}{-2\, Z_\alpha} e^{-j\mathbf{k}_t \cdot (\boldsymbol{\rho} - \boldsymbol{\rho}')}\ e^{\mp j\kappa_\alpha (z - z')} + \hat{\mathbf{z}}\hat{\mathbf{z}} \bar{\Theta}_z \quad , \tag{2.30}$$

where, the vector-wave of $\tilde{\boldsymbol{\Psi}}_\alpha^{\gtrless}$ is identified as,

$$\tilde{\boldsymbol{\Psi}}_\alpha^{\gtrless}(\mathbf{k}_t) \equiv \left(1\ ,\ \bar{U} \left(\boldsymbol{\Psi}_\alpha^{\gtrless}(-\mathbf{k}_t) \right) \right) = \left(\begin{array}{c} \mathbf{E}_{t,\alpha} \mp \mathbf{E}_{z,\alpha} \\ \mp \mathbf{H}_{t,\alpha} + \mathbf{H}_{z,\alpha} \end{array} \right)^T = \left(\begin{array}{c} Z_\alpha \mathbf{e}_\alpha \mp \mathbf{e}_{z,\alpha} \\ \mp \mathbf{h}_\alpha + \mathbf{h}_{z,\alpha} \end{array} \right)^T \quad , \tag{2.31}$$

and $\mathbf{1}$ is a dyadic unit column vector-wave, (i.e., $\mathbf{1} \cdot \mathbf{E} = \mathbf{E}$), and T stands for transpose. The PWS representation of the Green 's dyadic for uniaxial anisotropic media resembles in many ways its counterpart of the dyadic Green's function for isotropic media [13]. The Green's dyadic $\bar{\bar{\Xi}}(\mathbf{r}, \mathbf{r}')$ can be decomposed into E- and H- type modes with the different propagation constants (eigenvalues) of $\kappa_\alpha (\alpha = 1, 2)$; moreover, the eigenmodes satisfy the reflection symmetry with respect to a plane transverse to the z-direction.

The (PWS) of the dyadic Green's function $\bar{\bar{\Xi}}(\mathbf{r}, \mathbf{r}')$ given above provides information on the general form of the (PWS) solution for the electromagnetic fields for multi-layered uniaxial anisotropic media. In the following the dyadic Green's function for the uniaxial anisotropic slab will be derived, which then will be generalized to multi-layered uniaxial anisotropic media.

2.4 Electromagnetic dyadic Green's functions for uniaxial anisotropic multi-layered media

The presence of a planar boundary in anisotropic media generally introduces coupling between the wave-vector modes which are traveling from and toward the source, and hence

makes any one amplitude dependent on the amplitudes of the others, [14]. Nevertheless, for uniaxial anisotropic multi-layered media the mode couplings do not occur.

The electromagnetic dyadic Green's function for uni-axial anisotropic multi-layered media can be expressed as sum of $\bar{\Xi}(\mathbf{r},\mathbf{r}')$ in (2.30) and another contribution to account for the field scattered by the layered media. The scattered field contribution can be expressed in terms of a PWS integral resembling that for $\bar{\Xi}(\mathbf{r},\mathbf{r}')$. Consider an arbitrarily oriented point column current dipole source as of (2.4) located in region (n) with constitutive parameters $(\bar{\bar{\epsilon}}_n = \epsilon_{t,n}\mathbf{I}_t + \epsilon_{z,n}\hat{\mathbf{z}}\hat{\mathbf{z}}\ ;\ \bar{\bar{\mu}}_n = \mu_{t,n}\mathbf{I}_t + \mu_{z,n}\hat{\mathbf{z}}\hat{\mathbf{z}})$. Let us represent the Green's dyadic for region m as

$$\bar{\Xi}_{m,n}(\mathbf{r},\mathbf{r}') = \int d\mathbf{k}_t\ \tilde{\bar{\Xi}}^{\gtrless}_{n,m}(\mathbf{k}_t,\mathbf{r},\mathbf{r}') \ + \ \hat{\mathbf{z}}\hat{\mathbf{z}}\bar{\Theta}_{z,n} \quad , \tag{2.32}$$

where the spectral Green's dyadic within the region m can be identified as

$$\tilde{\bar{\Xi}}^{\gtrless}_{m,n}(\mathbf{k}_t,\mathbf{r},\mathbf{r}') = \sum_{\alpha=1}^{2} \overline{\Pi}_{\alpha}^{m\lessgtr}(\mathbf{k}_t,\mathbf{r})\,\bar{\mathcal{D}}_{\alpha}^{m\gtrless}(\mathbf{k}_t,\mathbf{r}') \quad , \tag{2.33}$$

with $\overline{\Pi}_{\alpha}$ is defined as

$$\overline{\Pi}_{\alpha}^{m\gtrless}(\mathbf{k}_t,\mathbf{r}) \equiv \Phi^{m\gtrless}(\mathbf{k}_t,z)\,e^{-j\mathbf{k}_t\cdot\boldsymbol{\rho}}\ ;\ \Phi^{m\gtrless}(\mathbf{k}_t,z) \equiv \left(\Psi_{\alpha}{}^{m\gtrless}e^{\mp j\kappa_{\alpha}^{m}z} + R_{\alpha}^{m\gtrless}(0)\Psi_{\alpha}{}^{m\lessgtr}e^{\pm j\kappa_{\alpha}^{m}z}\right) \quad , \tag{2.34}$$

where subscripts (m,n) denote the field and source regions, respectively; $R_{\alpha}^{m\gtrless}(z)$ is the effective modal reflection coefficient at the interfaces $(m,m+1)$ and $(m,m-1)$ for $(>)$ and $(<)$, respectively evaluated at z, and the superscripts $\gtrless$ denote that the incident field travels in $\pm z$-directions; hence, (i.e., $R_{\alpha}^{m\gtrless}(z_j) = R_{\alpha}^{m\gtrless}(z_k)\,e^{\pm j2\kappa_{\alpha}^{m}(z_j-z_k)}$). The unknown $\bar{\mathcal{D}}_{\alpha}^{m\gtrless}$ is the vector-wave dyadic amplitude, for region m, and is defined as a row vector,

$$\bar{\mathcal{D}}_{\alpha}^{m\gtrless} = \begin{pmatrix} \mathbf{d}_{\alpha}^{e} & \mathbf{d}_{\alpha}^{m} \end{pmatrix}^{m\gtrless} \quad , \tag{2.35}$$

where subscripts e, and m denote the electric and magnetic type sources respectively, and will be determined from the Lorentz reciprocity relation shortly. The subscript $\gtrless$ here denotes the region of $z\gtrless z'$. The effective reflection coefficient $R_{\alpha}^{m\gtrless}(z)$ for region m, is a function of all successive layers, (i.e., $m\pm1, m\pm2,\ldots,\quad ;\begin{pmatrix} +\text{for} > \\ -\text{for} < \end{pmatrix}$) of the uni-axial anisotropic multi-layered media, and is given by the following recursive relation [13]

$$R_\alpha^{m\gtrless}(z_m) = \frac{\Gamma_\alpha^{m\gtrless} + R_\alpha^{m\pm1\gtrless}(z_{m\pm1})\, e^{-j2\kappa_\alpha^{m\pm1} d_{m\pm1}}}{1 + \Gamma_\alpha^{m\gtrless} R_\alpha^{m\pm1\gtrless}(z_{m\pm1})\, e^{-j2\kappa_\alpha^{m\pm1} d_{m\pm1}}} \quad , \tag{2.36}$$

where the reflection coefficient $\Gamma_\alpha^{m\gtrless}$ is given by

$$\Gamma_\alpha^{m\gtrless} = \frac{Z_\alpha^{m\pm1} - Z_\alpha^m}{Z_\alpha^{m\pm1} + Z_\alpha^m} \quad , \tag{2.37}$$

and the mode-impedances Z_α are defined (see also (2.18), (2.20), and Appendix A) as

$$Z_1^n = \frac{\kappa_1^n}{\omega\epsilon_0\epsilon_{t,n}} \; ; \; Z_2^n = \frac{\omega\mu_0\mu_{t,n}}{\kappa_2^n} \quad . \tag{2.38}$$

Also the modal dyadic coefficients $\bar{\mathcal{D}}_\alpha^{m\gtrless}$ of region m, and $\bar{\mathcal{D}}_\alpha^{n\gtrless}$ of region n on either side of the source are related via the effective transmission coefficient, $\Upsilon_{m,n;\alpha}^{\gtrless}$, and is given by [13][2]

$$\Upsilon_{m,n;\alpha}^{\gtrless} = e^{\pm j(\kappa_\alpha^n z_n - \kappa_\alpha^m z_m)} \prod_{i=n}^{m\pm1} T_\alpha^{i\gtrless}(z_i)\, e^{-j\kappa_\alpha^{i\pm1} d_{i\pm1}} \qquad ;\text{for} \quad n\gtrless m \quad , \tag{2.39}$$

where the transmission coefficient $T^{m\gtrless}$ at the interface $(m, m\pm1)$ is given by

$$T_\alpha^{m\gtrless}(z_m) = \frac{1 + \Gamma_\alpha^{m\gtrless}}{1 + \Gamma_\alpha^{m\gtrless} R_\alpha^{m\pm1\gtrless} e^{-j2\kappa_\alpha^{m\pm1} d_{m\pm1}}} \quad . \tag{2.40}$$

Hence, one only needs to find the modal coefficients $\bar{\mathcal{D}}^{\gtrless}$ in region n, in order to completely specify the fields in all regions. Specifying (2.33) for region n (i.e., $m = n$) and invoking the Lorentz reciprocity theorem to the fields, $\tilde{\boldsymbol{\Sigma}}_{n,n}^{\gtrless} = \tilde{\boldsymbol{\Xi}}_{n,n}^{\gtrless} \cdot \mathcal{P}$, of (2.33) and the source free solenoidal vector-wave function of $\overline{\boldsymbol{\Pi}}_\alpha^{n\lessgtr}(-\mathbf{k}_t, \mathbf{r})$, of (2.34), in region n of volume V, bounded by planar surface $S_>$ and $S_<$, which are slightly above and below the surface S of the Figure 2.1.2 respectively, yields

[2]Note that $\Upsilon_{m,n;\alpha}^{\gtrless}$ is the ratio of the modal incident wave-amplitudes of regions m and n; namely, $\mathcal{D}_\alpha^{m\gtrless} \cdot \mathcal{P} = \Upsilon_{m,n;\alpha}^{\gtrless}\, \mathcal{D}_\alpha^{n\gtrless} \cdot \mathcal{P}$.

$$\int_{S_>} ds \left(\overline{\overline{\Pi}}_\alpha^{n\,\lessgtr}(-\mathbf{k}_t, \mathbf{r}) , \bar{\bar{\mathbf{W}}}\, \tilde{\Sigma}_{n,n}^{\gtrless} \right) - \int_{S_<} ds \left(\overline{\overline{\Pi}}_\alpha^{n\,\lessgtr}(-\mathbf{k}_t, \mathbf{r}) , \bar{\bar{\mathbf{W}}}\, \tilde{\Sigma}_{n,n}^{\gtrless} \right) =$$

$$- \int_V dv \left(\mathcal{P}\delta(\mathbf{r}-\mathbf{r}') , \bar{\bar{U}} \left(\overline{\overline{\Pi}}_\alpha^{n\,\lessgtr}(-\mathbf{k}_t, \mathbf{r}) \right) \right) \qquad (2.41)$$

$$= - \left(\mathcal{P} , \bar{\bar{U}} \left(\overline{\overline{\Pi}}_\alpha^{n\,\lessgtr}(-\mathbf{k}_t, \mathbf{r}') \right) \right) ,$$

Incorporating (2.33) into (2.41) and using the orthogonality relations developed in Appendix B, (see (B.8) and (B.9)) yields,

$$\bar{\mathcal{D}}_\alpha^{n\,\gtrless}(\mathbf{k}_t, \mathbf{r}') \cdot \mathcal{P} = \begin{pmatrix} \mathbf{d}_\alpha^e \cdot \mathbf{p}_e & \mathbf{d}_\alpha^m \cdot \mathbf{p}_m \end{pmatrix}^{n\,\gtrless} = \frac{1}{2\pi} \frac{\mathcal{P}^T \cdot \bar{\bar{U}}(\mathbf{\Phi}^{n\,\lessgtr}(-\mathbf{k}_t, z'))}{-2\,\Lambda_\alpha^n} e^{+j\mathbf{k}_t \cdot \boldsymbol{\rho}'} \quad . \quad (2.42)$$

where

$$\Lambda_\alpha^n = Z_\alpha^n (1 - R_\alpha^{n<}(z_n) R_\alpha^{n>}(z_{n+1}) e^{-2j\kappa_\alpha^n d_{z_n}}) \quad . \qquad (2.43)$$

Therefore, from (2.42), (2.33), (2.17), and (2.31) the z-propagating plane-wave spectrum (PWS) integral representation for the electromagnetic dyadic Green's function of (2.32) can be identified as,

$$\bar{\Xi}_{m,n}(\mathbf{r}, \mathbf{r}') = \int \frac{d\mathbf{k}_t}{4\pi^2} \sum_{\alpha=1}^{2} \Upsilon_{m,n;\alpha}^{\gtrless} \frac{\mathbf{\Phi}_\alpha^{m\,\gtrless}(\mathbf{k}_t, z)\, \tilde{\mathbf{\Phi}}_\alpha^{n\,\lessgtr}(\mathbf{k}_t, z')}{-2\,\Lambda_\alpha^n} e^{-j\mathbf{k}_t \cdot (\boldsymbol{\rho} - \boldsymbol{\rho}')} + \hat{z}\hat{z}\bar{\Theta}_{z,n} \quad . \qquad (2.44)$$

where once more the wave-vectors $\mathbf{\Phi}$ and $\tilde{\mathbf{\Phi}}$ are given by

$$\begin{aligned} \mathbf{\Phi}_\alpha^{\gtrless} &= \mathbf{\Psi}_\alpha^{\gtrless} e^{\mp j\kappa_\alpha z} + R_\alpha^{\gtrless}(0) \mathbf{\Psi}_\alpha^{\lessgtr} e^{\pm j\kappa_\alpha z} \quad , \\ \tilde{\mathbf{\Phi}}_\alpha^{\gtrless} &= \tilde{\mathbf{\Psi}}_\alpha^{\gtrless} e^{\mp j\kappa_\alpha z'} + R_\alpha^{\gtrless}(0) \tilde{\mathbf{\Psi}}_\alpha^{\lessgtr} e^{\pm j\kappa_\alpha z'} \quad . \end{aligned} \qquad (2.45)$$

The resemblance of the electromagnetic Green's dyadic for the uni-axial anisotropic multi-layered media of (2.44) to its associated counterpart for the full-space uni-axial anisotropic medium should be noted. Both dyadic Green's functions are comprised of the vector-wave mode functions, which are the solutions of the source-free fields in the uni-axial anisotropic medium. In the full-space case, the excited modes are those which travel away from the source, whereas in the multi-layered case the modes which travel toward, as well as away from, the source will be excited.

In the following explicit expressions for the electric-electric $\mathcal{G}^{ee}$, magnetic-electric $\mathcal{G}^{me}$, electric-magnetic $\mathcal{G}^{em}$, and magnetic-magnetic $\mathcal{G}^{mm}$ dyadic Green's functions will be presented[3]. In view of (2.17) and (2.31) vector-wave functions $\boldsymbol{\Phi}$ and $\tilde{\boldsymbol{\Phi}}$ of (2.45) can be written in terms of the electric and magnetic mode functions as

$$\boldsymbol{\Phi}_{\alpha}^{\gtrless} = \begin{pmatrix} \boldsymbol{\Phi}_{\alpha,e}^{\gtrless} \\ \boldsymbol{\Phi}_{\alpha,m}^{\gtrless} \end{pmatrix} = \begin{pmatrix} (Z_\alpha \mathbf{e}_\alpha \pm \mathbf{e}_{z,\alpha})\, e^{\mp j\kappa_\alpha z} + R_\alpha^{\gtrless}(0)\,(Z_\alpha \mathbf{e}_\alpha \mp \mathbf{e}_{z,\alpha})\, e^{\pm j\kappa_\alpha z} \\ (\pm \mathbf{h}_\alpha + \mathbf{h}_{z,\alpha})\, e^{\mp j\kappa_\alpha z} + R_\alpha^{\gtrless}(0)\,(\mp \mathbf{h}_\alpha + \mathbf{h}_{z,\alpha})\, e^{\pm j\kappa_\alpha z} \end{pmatrix} , \quad (2.46)$$

and

$$\tilde{\boldsymbol{\Phi}}_{\alpha}^{\gtrless} = \begin{pmatrix} \tilde{\boldsymbol{\Phi}}_{\alpha,e}^{\gtrless} \\ \tilde{\boldsymbol{\Phi}}_{\alpha,m}^{\gtrless} \end{pmatrix}^T = \begin{pmatrix} (Z_\alpha \mathbf{e}_\alpha \mp \mathbf{e}_{z,\alpha})\, e^{\mp j\kappa_\alpha z} + R_\alpha^{\gtrless}(0)\,(Z_\alpha \mathbf{e}_\alpha \pm \mathbf{e}_{z,\alpha})\, e^{\pm j\kappa_\alpha z} \\ (\mp \mathbf{h}_\alpha + \mathbf{h}_{z,\alpha})\, e^{\mp j\kappa_\alpha z} + R_\alpha^{\gtrless}(0)\,(\pm \mathbf{h}_\alpha + \mathbf{h}_{z,\alpha})\, e^{\pm j\kappa_\alpha z} \end{pmatrix}^T , \quad (2.47)$$

therefore the electromagnetic dyadic Green's function can be identified as

$$\begin{aligned} \boldsymbol{\Xi}_{m,n}(\mathbf{r},\mathbf{r}') &= \begin{pmatrix} \mathcal{G}^{ee}(\mathbf{r},\mathbf{r}') & \mathcal{G}^{em}(\mathbf{r},\mathbf{r}') \\ \mathcal{G}^{me}(\mathbf{r},\mathbf{r}') & \mathcal{G}^{mm}(\mathbf{r},\mathbf{r}') \end{pmatrix}_{m,n} \qquad (2.48) \\ &= \int \frac{d\mathbf{k}_t}{4\pi^2}\, e^{-j\mathbf{k}_t\cdot(\boldsymbol{\rho}-\boldsymbol{\rho}')} \sum_{\alpha=1}^{2} \frac{\Upsilon_{m,n;\alpha}^{\gtrless}}{-2\,\Lambda_\alpha^n} \begin{pmatrix} \boldsymbol{\Phi}_{\alpha,e}^{m\gtrless}(\mathbf{k}_t,z)\,\tilde{\boldsymbol{\Phi}}_{\alpha,e}^{n\lessgtr}(\mathbf{k}_t,z') & \boldsymbol{\Phi}_{\alpha,e}^{m\gtrless}(\mathbf{k}_t,z)\,\tilde{\boldsymbol{\Phi}}_{\alpha,m}^{n\lessgtr}(\mathbf{k}_t,z') \\ \boldsymbol{\Phi}_{\alpha,m}^{m\gtrless}(\mathbf{k}_t,z)\,\tilde{\boldsymbol{\Phi}}_{\alpha,e}^{n\lessgtr}(\mathbf{k}_t,z') & \boldsymbol{\Phi}_{\alpha,e}^{m\gtrless}(\mathbf{k}_t,z)\,\tilde{\boldsymbol{\Phi}}_{\alpha,m}^{n\lessgtr}(\mathbf{k}_t,z') \end{pmatrix} \\ &\quad + \hat{\mathbf{z}}\hat{\mathbf{z}} \begin{pmatrix} \frac{1}{-j\omega\epsilon_0\epsilon_{z,n}} & 0 \\ 0 & \frac{1}{-j\omega\mu_0\mu_{z,n}} \end{pmatrix} \delta(\mathbf{r}-\mathbf{r}') \ . \end{aligned}$$

$$\begin{aligned} \mathcal{G}_{m,n}^{ee}(\mathbf{r},\mathbf{r}') &= \int \frac{d\mathbf{k}_t}{4\pi^2}\, e^{-j\mathbf{k}_t\cdot(\boldsymbol{\rho}-\boldsymbol{\rho}')} \sum_{\alpha=1}^{2} \frac{\Upsilon_{m,n;\alpha}^{\gtrless}}{-2\,\Lambda_\alpha^n} \cdot \qquad (2.49) \\ &\quad \left((Z_\alpha \mathbf{e}_\alpha \pm \mathbf{e}_{z,\alpha})_m\, e^{\mp j\kappa_\alpha^m z} + R_\alpha^{m\gtrless}(0)\,(Z_\alpha \mathbf{e}_\alpha \mp \mathbf{e}_{z,\alpha})_m\, e^{\pm j\kappa_\alpha^m z} \right) \cdot \\ &\quad \left((Z_\alpha \mathbf{e}_\alpha \pm \mathbf{e}_{z,\alpha})_n\, e^{\pm j\kappa_\alpha^n z'} + R_\alpha^{n\lessgtr}(0)\,(Z_\alpha \mathbf{e}_\alpha \mp \mathbf{e}_{z,\alpha})_n\, e^{\mp j\kappa_\alpha^n z'} \right) \\ &\quad + \hat{\mathbf{z}}\hat{\mathbf{z}} \frac{1}{-j\omega\epsilon_0\epsilon_{z,n}} \delta(\mathbf{r}-\mathbf{r}') \ . \end{aligned}$$

[3]Note that the expression in (2.44) is a compact representation of the electric as well as magnetic dyadic Green's function due to the electric and magnetic point sources in a uni-axial anisotropic multi-layered media.

$$\mathcal{G}^{me}_{m,n}(\mathbf{r},\mathbf{r}') = \int \frac{d\mathbf{k}_t}{4\pi^2} e^{-j\mathbf{k}_t\cdot(\boldsymbol{\rho}-\boldsymbol{\rho}')} \sum_{\alpha=1}^{2} \frac{\Upsilon^{\gtrless}_{m,n;\alpha}}{-2\,\Lambda^n_\alpha} \cdot \tag{2.50}$$
$$\left((\pm\mathbf{h}_\alpha + \mathbf{h}_{z,\alpha})_m\, e^{\mp j\kappa^m_\alpha z} + R^{m\gtrless}_\alpha(0)\,(\mp\mathbf{h}_\alpha + \mathbf{h}_{z,\alpha})_m\, e^{\pm j\kappa^m_\alpha z} \right) \cdot$$
$$\left((Z_\alpha \mathbf{e}_\alpha \pm \mathbf{e}_{z,\alpha})_n\, e^{\pm j\kappa^n_\alpha z'} + R^{n\lessgtr}_\alpha(0)\,(Z_\alpha \mathbf{e}_\alpha \mp \mathbf{e}_{z,\alpha})_n\, e^{\mp j\kappa^n_\alpha z'} \right) \quad ,$$

$$\mathcal{G}^{em}_{m,n}(\mathbf{r},\mathbf{r}') = \int \frac{d\mathbf{k}_t}{4\pi^2} e^{-j\mathbf{k}_t\cdot(\boldsymbol{\rho}-\boldsymbol{\rho}')} \sum_{\alpha=1}^{2} \frac{\Upsilon^{\gtrless}_{m,n;\alpha}}{-2\,\Lambda^n_\alpha} \cdot \tag{2.51}$$
$$\left((Z_\alpha \mathbf{e}_\alpha \pm \mathbf{e}_{z,\alpha})_m\, e^{\mp j\kappa^m_\alpha z} + R^{m\gtrless}_\alpha(0)\,(Z_\alpha \mathbf{e}_\alpha \mp \mathbf{e}_{z,\alpha})_m\, e^{\pm j\kappa^m_\alpha z} \right) \cdot$$
$$\left((\pm\mathbf{h}_\alpha + \mathbf{h}_{z,\alpha})_n\, e^{\pm j\kappa^n_\alpha z'} + R^{n\lessgtr}_\alpha(0)\,(\mp\mathbf{h}_\alpha + \mathbf{h}_{z,\alpha})_n\, e^{\mp j\kappa^n_\alpha z'} \right) \quad ,$$

$$\mathcal{G}^{mm}_{m,n}(\mathbf{r},\mathbf{r}') = \int \frac{d\mathbf{k}_t}{4\pi^2} e^{-j\mathbf{k}_t\cdot(\boldsymbol{\rho}-\boldsymbol{\rho}')} \sum_{\alpha=1}^{2} \frac{\Upsilon^{\gtrless}_{m,n;\alpha}}{-2\,\Lambda^n_\alpha} \cdot \tag{2.52}$$
$$\left((\pm\mathbf{h}_\alpha + \mathbf{h}_{z,\alpha})_m\, e^{\mp j\kappa^m_\alpha z} + R^{m\gtrless}_\alpha(0)\,(\mp\mathbf{h}_\alpha + \mathbf{h}_{z,\alpha})_m\, e^{\pm j\kappa^m_\alpha z} \right) \cdot$$
$$\left((\pm\mathbf{h}_\alpha + \mathbf{h}_{z,\alpha})_n\, e^{\pm j\kappa^n_\alpha z} + R^{n\lessgtr}_\alpha(0)\,(\mp\mathbf{h}_\alpha + \mathbf{h}_{z,\alpha})_n\, e^{\mp j\kappa^n_\alpha z'} \right)$$
$$+ \hat{\mathbf{z}}\hat{\mathbf{z}} \frac{1}{-j\omega\mu_0\mu_{z,n}} \delta(\mathbf{r}-\mathbf{r}') \quad .$$

2.5 Electromagnetic dyadic Green's functions for uniaxial anisotropic multi-layered media due to periodic electric and magnetic point currents

In the following the dyadic Green's function for an infinite periodic array of an arbitrarily oriented current point source in a uni-axial anisotropic multi-layered media will be derived. The geometry of the problem is shown in Figure 2.3.

The starting point for this analysis is based on the following theorem. Consider a

periodic impulse train, f with an spatial phase variation ω_0 and period X:

$$f(x) = \sum_{n=-\infty}^{\infty} \delta(x - n\,X) e^{-j\omega_0 x} \quad . \tag{2.53}$$

the Fourier transform of this function,denoted by F is given by

$$\begin{aligned} F(\omega) &= \int dx\, e^{j\omega x} f(x) \\ &= \sum_{n=-\infty}^{\infty} \int dx\, e^{j(\omega-\omega_0)x} \delta(x - n\,X) \qquad (2.54) \\ &= \sum_{n=-\infty}^{\infty} e^{j(\omega-\omega_0)nX} \quad , \qquad (2.55) \end{aligned}$$

but from the distribution theory [16]

$$\sum_{n=-\infty}^{\infty} e^{j\omega\, n\, T} = \frac{2\pi}{T} \sum_{n=-\infty}^{\infty} \delta(\omega - \frac{2\pi\, n}{T}) \quad , \tag{2.56}$$

so, it follows that,

$$F(\omega) = \frac{2\pi}{X} \sum_{n=-\infty}^{\infty} \delta((\omega - \omega_0) - \frac{2\pi\, n}{X}) \quad , \tag{2.57}$$

which simply state that a periodic impulse train has a Fourier transform which is also a periodic impulse train.

Let us assume that the current elements are spatially periodic with the period of X' and Y' in $\hat{\mathbf{x}}'$ and $\hat{\mathbf{y}}'$ directions respectively, where (x', y') coordinate are skwed α, and β degrees with respect to (x, y) global coordinate respectively, as shown in Figure 2.3. Thus the location of (i, q)th element $\overline{OP}$ can be represented as

$$\begin{aligned} \overline{OP} &= i\,X'\hat{\mathbf{x}}' + q\,Y'\hat{\mathbf{y}}' \\ &= i\,X'(\hat{\mathbf{x}}\cos\alpha - \hat{\mathbf{y}}\sin\alpha) + q\,Y'(\hat{\mathbf{x}}\sin\beta + \hat{\mathbf{y}}\cos\beta) \qquad (2.58) \\ &= (i\,X'\cos\alpha + q\,Y'\sin\beta)\,\hat{\mathbf{x}} + (-i\,X'\sin\alpha + q\,Y'\cos\beta)\,\hat{\mathbf{y}} \quad . \end{aligned}$$

Let also assume that the current elements are phased at an angle (θ, ϕ); thus, the discrete periodic current distribution can be denoted by

$$\begin{aligned} \mathcal{J}(\mathbf{r}, \mathbf{r}') &= \sum_{i,q=-\infty}^{\infty} \mathcal{P}\, e^{-j\omega_x x - j\omega_y y} \delta(z - z') \cdot \\ &\delta\left(x - (i\,X'\cos\alpha + q\,Y'\sin\beta)\right)\ \delta\left(y - (-i\,X'\sin\alpha + q\,Y'\cos\beta)\right) \quad , \qquad (2.59) \end{aligned}$$

where

$$\omega_x = k_0 \sin\theta\cos\phi \quad ; \quad \omega_y = k_0 \sin\theta\sin\phi \quad . \tag{2.60}$$

The Fourier transform $\tilde{\mathcal{J}}$ of $\mathcal{J}$ is given by

$$\tilde{\mathcal{J}}(\mathbf{k}_t) = \frac{4\pi^2}{X'Y'} \sum_{i,q=-\infty}^{\infty} \mathcal{P}\,\delta(z-z')\;\delta\left(k_x\cos\alpha - k_y\sin\alpha - C_1(i)\right)\delta\left(k_x\sin\beta + k_c os\beta - C_2(q)\right) \quad , \tag{2.61}$$

where the parameters $C_1(i)$ and $C_2(q)$ are defined as

$$\begin{aligned} C_1(i) &= \omega_x\cos\alpha - \omega_y\sin\alpha + \frac{2\pi\, i}{X'} \\ C_2(q) &= \omega_x\sin\beta + \omega_y\cos\beta + \frac{2\pi\, q}{Y'} \quad . \end{aligned} \tag{2.62}$$

If $\tilde{\mathcal{J}}$ and $\mathcal{U}$ are related through a following dyadic operator

$$\mathcal{U}(\mathbf{r}) = \int d\mathbf{k}_t \mathcal{L}\left[\tilde{\mathcal{J}}(\mathbf{k}_t)\right] \quad , \tag{2.63}$$

then, in view of (2.57) and the following definition of the *delta* function:

$$F(x) = \int d\xi\, F(\xi)\delta(\xi - x) \quad , \tag{2.64}$$

$\mathcal{U}(\mathbf{r})$ can be identified as, [17]

$$\mathcal{U}(\mathbf{r}) = \sum_{i,q=-\infty}^{\infty} \mathcal{L}\left[\tilde{\mathcal{J}}(k_x^{i,q}, k_y^{i,q})\right] \quad , \tag{2.65}$$

where the discrete spectral eigen-values $k_x^{i,q}$ and $k_y^{i,q}$ are given by

$$\begin{aligned} k_x^{i,q} &= \frac{C_1(i)\cos\beta + C_2(q)\sin\alpha}{\cos(\alpha-\beta)} \\ k_y^{i,q} &= \frac{-C_1(i)\sin\beta + C_2(q)\cos\alpha}{\cos(\alpha-\beta)} \quad . \end{aligned} \tag{2.66}$$

In the special case of the $\hat{\mathbf{x}}' = \hat{\mathbf{x}}$ and $\hat{\mathbf{y}}' = \hat{\mathbf{y}}$ ($\alpha = 0 = \beta$), spectral values of $k_x^{i,q}$ and $k_y^{i,q}$ will be simplified to

$$k_x^{i,q} = \omega_x + \frac{2\pi}{X'} \quad ; \quad k_y^{i,q} = \omega_y + \frac{2\pi}{Y'} \quad . \tag{2.67}$$

In the light of the above discussion, the electromagnetic dyadic Green's function for the periodic current point source can be expressed as,

$$\begin{aligned}
\Xi^{p}_{m,n}(\mathbf{r},\mathbf{r}') &= \begin{pmatrix} \mathcal{G}^{ee}(\mathbf{r},\mathbf{r}') & \mathcal{G}^{em}(\mathbf{r},\mathbf{r}') \\ \mathcal{G}^{me}(\mathbf{r},\mathbf{r}') & \mathcal{G}^{mm}(\mathbf{r},\mathbf{r}') \end{pmatrix}_{m,n} \qquad (2.68)\\
&= \frac{1}{X'Y'} \sum_{i,q=-\infty}^{\infty} e^{-j\mathbf{k}_t^{i,q}\cdot(\boldsymbol{\rho}-\boldsymbol{\rho}')} \cdot \\
&\qquad \sum_{\alpha=1}^{2} \frac{\Upsilon^{\gtrless}_{m,n;\alpha}(\mathbf{k}_t^{i,q})}{-2\,\Lambda^{n}_{\alpha}(\mathbf{k}_t^{i,q})} \begin{pmatrix} \Phi^{m\,\gtrless}_{\alpha,e}(\mathbf{k}_t^{i,q},z)\,\tilde{\Phi}^{n\,\lessgtr}_{\alpha,e}(\mathbf{k}_t^{i,q},z') & \Phi^{m\,\gtrless}_{\alpha,e}(\mathbf{k}_t^{i,q},z)\,\tilde{\Phi}^{n\,\lessgtr}_{\alpha,m}(\mathbf{k}_t^{i,q},z') \\ \Phi^{m\,\lessgtr}_{\alpha,m}(\mathbf{k}_t^{i,q},z)\,\tilde{\Phi}^{n\,\gtrless}_{\alpha,e}(\mathbf{k}_t^{i,q},z') & \Phi^{m\,\gtrless}_{\alpha,e}(\mathbf{k}_t^{i,q},z)\,\tilde{\Phi}^{n\,\lessgtr}_{\alpha,m}(\mathbf{k}_t^{i,q},z') \end{pmatrix} + \\
&\hat{\mathbf{z}}\hat{\mathbf{z}} \begin{pmatrix} \frac{1}{-j\omega\epsilon_0\epsilon_{z,n}} & 0 \\ 0 & \frac{1}{-j\omega\mu_0\mu_{z,n}} \end{pmatrix} \delta(z-z') \cdot \sum_{i,q=-\infty}^{\infty} \delta\left(x-(i\,X'\cos\alpha+q\,Y'\sin\beta)\right)\ \delta\left(y-(-i\,X'\sin\alpha+q\,Y'\cos\beta)\right)\ ,
\end{aligned}$$

where subscript p denotes the periodic type Green's function, and $\mathbf{k}_t^{i,q}$ is discrete transverse eigen-value, and is given by defines as

$$\mathbf{k}_t^{i,q} = k_x^{i,q}\,\hat{\mathbf{x}} + k_y^{i,q}\,\hat{\mathbf{y}}\ , \qquad (2.69)$$

where $k_x^{i,q}$ and $k_y^{i,q}$ are defined in (2.66). Likewise explicit expressions for the periodic electric-electric $\mathcal{G}^{p:ee}$, magnetic-electric $\mathcal{G}^{p:me}$, electric-magnetic $\mathcal{G}^{p:em}$, and magnetic-magnetic $\mathcal{G}^{p:mm}$ dyadic Green's functions can be expressed as

$$\begin{aligned}
\mathcal{G}^{p:ee}_{m,n}(\mathbf{r},\mathbf{r}') &= \frac{1}{X'Y'} \sum_{i,q=-\infty}^{\infty} e^{-j\mathbf{k}_t^{i,q}\cdot(\boldsymbol{\rho}-\boldsymbol{\rho}')} \sum_{\alpha=1}^{2} \frac{\Upsilon^{\gtrless}_{m,n;\alpha}(\mathbf{k}_t^{i,q})}{-2\,\Lambda^{n}_{\alpha}(\mathbf{k}_t^{i,q})} \cdot \qquad (2.70)\\
&\qquad \left((Z_\alpha \mathbf{e}_\alpha \pm \mathbf{e}_{z,\alpha})_m\, e^{\mp j\kappa^m_\alpha z} + R^{m\,\gtrless}_{\alpha}(0)\,(Z_\alpha \mathbf{e}_\alpha \mp \mathbf{e}_{z,\alpha})_m\, e^{\pm j\kappa^m_\alpha z} \right)^{i,q} \cdot \\
&\qquad\qquad \left((Z_\alpha \mathbf{e}_\alpha \pm \mathbf{e}_{z,\alpha})_n\, e^{\pm j\kappa^n_\alpha z'} + R^{n\,\lessgtr}_{\alpha}(0)\,(Z_\alpha \mathbf{e}_\alpha \mp \mathbf{e}_{z,\alpha})_n\, e^{\mp j\kappa^n_\alpha z'} \right)^{i,q} + \\
&\hat{\mathbf{z}}\hat{\mathbf{z}}\, \frac{1}{-j\omega\epsilon_0\epsilon_{z,n}} \delta(z-z') \cdot \sum_{i,q=-\infty}^{\infty} \delta\left(x-(i\,X'\cos\alpha+q\,Y'\sin\beta)\right)\ \delta\left(y-(-i\,X'\sin\alpha+q\,Y'\cos\beta)\right)\ ,
\end{aligned}$$

$$\begin{aligned}
\mathcal{G}^{p:me}_{m,n}(\mathbf{r},\mathbf{r}') &= \frac{1}{X'Y'} \sum_{i,q=-\infty}^{\infty} e^{-j\mathbf{k}_t^{i,q}\cdot(\boldsymbol{\rho}-\boldsymbol{\rho}')} \sum_{\alpha=1}^{2} \frac{\Upsilon^{\gtrless}_{m,n;\alpha}(\mathbf{k}_t^{i,q})}{-2\,\Lambda^{n}_{\alpha}(\mathbf{k}_t^{i,q})} \cdot \qquad (2.71)\\
&\qquad \left((\pm\mathbf{h}_\alpha + \mathbf{h}_{z,\alpha})_m\, e^{\mp j\kappa^m_\alpha z} + R^{m\,\gtrless}_{\alpha}(0)\,(\mp\mathbf{h}_\alpha + \mathbf{h}_{z,\alpha})_m\, e^{\pm j\kappa^m_\alpha z} \right)^{i,q} .
\end{aligned}$$

$$\left((Z_\alpha \mathbf{e}_\alpha \pm \mathbf{e}_{z,\alpha})_n \, e^{\pm j\kappa_\alpha^n z'} + R_\alpha^{n\gtrless}(0) \, (Z_\alpha \mathbf{e}_\alpha \mp \mathbf{e}_{z,\alpha})_n \, e^{\mp j\kappa_\alpha^n z'} \right)^{i,q} \quad ,$$

$$\mathcal{G}_{m,n}^{p:em}(\mathbf{r},\mathbf{r}') = \frac{1}{X'Y'} \sum_{i,q=-\infty}^{\infty} e^{-j\mathbf{k}_t^{i,q}\cdot(\boldsymbol{\rho}-\boldsymbol{\rho}')} \sum_{\alpha=1}^{2} \frac{\Upsilon_{m,n;\alpha}^{\gtrless}(\mathbf{k}_t^{i,q})}{-2\,\Lambda_\alpha^n(\mathbf{k}_t^{i,q})} \cdot \tag{2.72}$$

$$\left((Z_\alpha \mathbf{e}_\alpha \pm \mathbf{e}_{z,\alpha})_m \, e^{\mp j\kappa_\alpha^m z} + R_\alpha^{m\lessgtr}(0) \, (Z_\alpha \mathbf{e}_\alpha \mp \mathbf{e}_{z,\alpha})_m \, e^{\pm j\kappa_\alpha^m z} \right)^{i,q} \cdot$$

$$\left((\pm \mathbf{h}_\alpha + \mathbf{h}_{z,\alpha})_n \, e^{\pm j\kappa_\alpha^n z'} + R_\alpha^{n\gtrless}(0) \, (\mp \mathbf{h}_\alpha + \mathbf{h}_{z,\alpha})_n \, e^{\mp j\kappa_\alpha^n z'} \right)^{i,q} \quad ,$$

$$\mathcal{G}_{m,n}^{p:mm}(\mathbf{r},\mathbf{r}') = \frac{1}{X'Y'} \sum_{i,q=-\infty}^{\infty} e^{-j\mathbf{k}_t^{i,q}\cdot(\boldsymbol{\rho}-\boldsymbol{\rho}')} \sum_{\alpha=1}^{2} \frac{\Upsilon_{m,n;\alpha}^{\gtrless}(\mathbf{k}_t^{i,q})}{-2\,\Lambda_\alpha^n(\mathbf{k}_t^{i,q})} \cdot \tag{2.73}$$

$$\left((\pm \mathbf{h}_\alpha + \mathbf{h}_{z,\alpha})_m \, e^{\mp j\kappa_\alpha^m z} + R_\alpha^{m\gtrless}(0) \, (\mp \mathbf{h}_\alpha + \mathbf{h}_{z,\alpha})_m \, e^{\pm j\kappa_\alpha^m z} \right)^{i,q} \cdot$$

$$\left((\pm \mathbf{h}_\alpha + \mathbf{h}_{z,\alpha})_n \, e^{\pm j\kappa_\alpha^n z} + R_\alpha^{n\lessgtr}(0) \, (\mp \mathbf{h}_\alpha + \mathbf{h}_{z,\alpha})_n \, e^{\mp j\kappa_\alpha^n z'} \right)^{i,q} +$$

$$\hat{\mathbf{z}}\hat{\mathbf{z}} \frac{1}{-j\omega\mu_0\mu_{z,n}} \delta(z-z') \cdot \sum_{i,q=-\infty}^{\infty} \delta\left(x - (i\,X'\cos\alpha + q\,Y'\sin\beta)\right) \; \delta\left(y - (-i\,X'\sin\alpha + q\,Y'\cos\beta)\right) \quad .$$

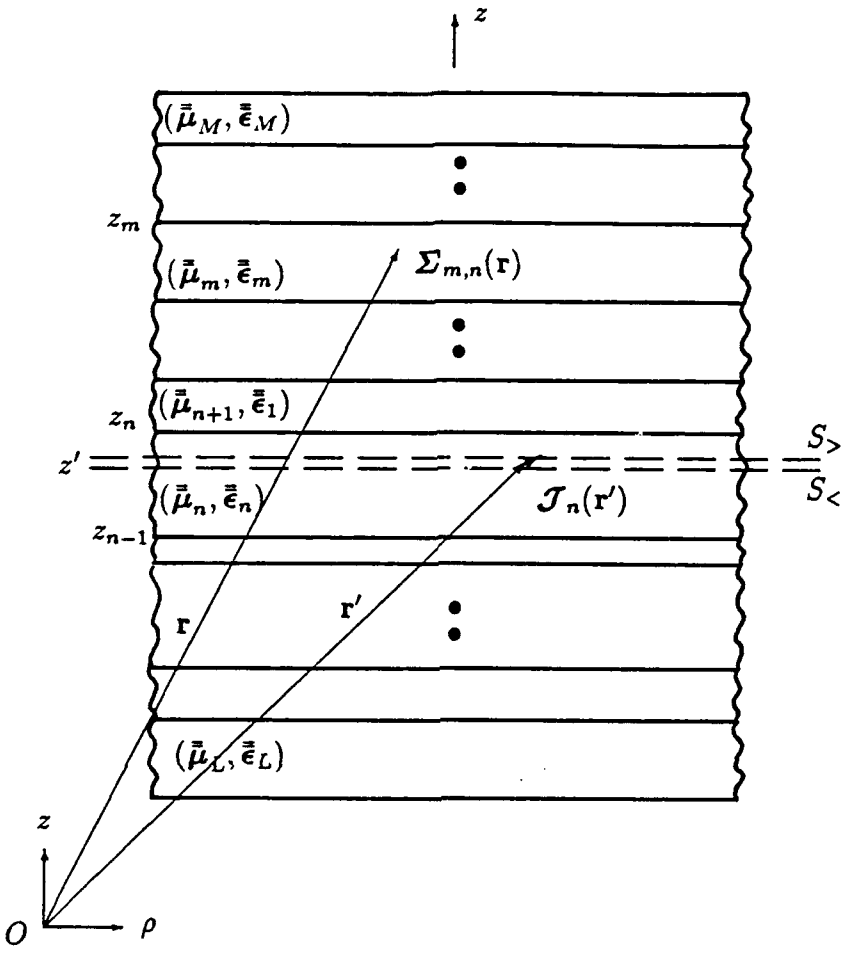

$$\bar{\bar{\epsilon}}_i = \epsilon_{i,t}\mathbf{I}_t + \epsilon_{i,z}\hat{\mathbf{z}}\hat{\mathbf{z}} \;\; ; \;\; \bar{\bar{\mu}}_i = \mu_{i,t}\mathbf{I}_t + \mu_{i,z}\hat{\mathbf{z}}\hat{\mathbf{z}}$$

Figure 2.1: Electric and magnetic point current dipole sources in anisotropic uniaxial multi-layered media, ($\bar{\bar{\epsilon}} = \epsilon_t\mathbf{I}_t + \epsilon_z\hat{\mathbf{z}}\hat{\mathbf{z}}$; $\bar{\bar{\mu}} = \mu_t\mathbf{I}_t + \mu_z\hat{\mathbf{z}}\hat{\mathbf{z}}$). Also the planar surface $S_>$ and $S_<$ slightly above and below the source are shown.

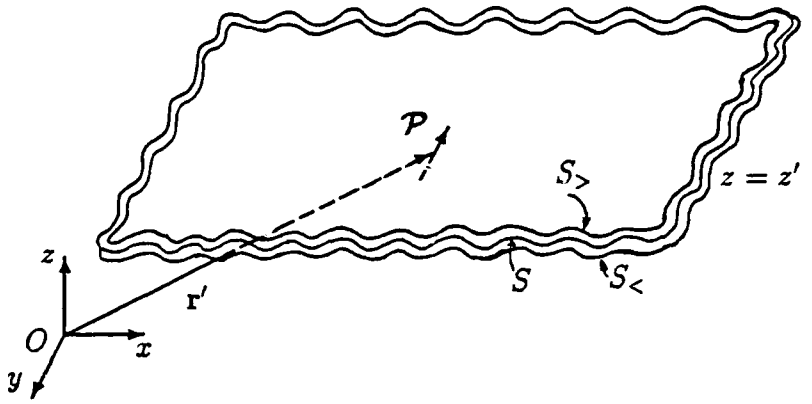

Figure 2.2: Imaginary plane S, parallel to xy plane, passing through the source at $z = z'$ in unbounded anisotropic uniaxial media. Also plotted are planar surfaces $S_>$ and $S_<$ slightly above and below the source.

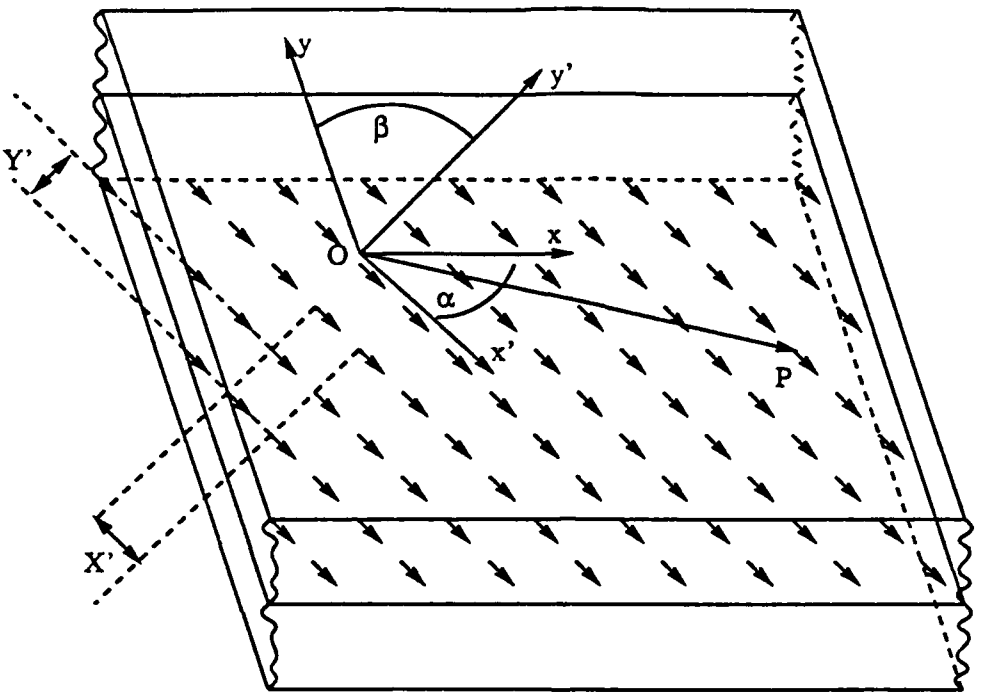

$$\bar{\bar{\epsilon}}_i = \epsilon_{i,t}\mathbf{I}_t + \epsilon_{i,z}\hat{z}\hat{z} \;\; ; \;\; \bar{\bar{\mu}}_i = \mu_{i,t}\mathbf{I}_t + \mu_{i,z}\hat{z}\hat{z}$$

Figure 2.3: Infinite periodic array of arbitrarily oriented current point sources in a uni-axial anisotropic multi-layered media. The current elements are spatially periodic with the period of X' and Y' in $\hat{x}'$ and $\hat{y}'$ directions respectively, where (x', y') coordinate are skwed α, and β degrees with respect to (x, y) global coordinate respectively. $\overline{OP}$ is the spatial position of (i, q)th element. Also current elements are phased at an angle (θ, ϕ) (not shown).

Chapter 3

Electric dyadic green's function for a grounded uniaxial anisotropic double layered slab due to an electric point source

3.1 Formulation of the Sommerfeld representation for the dyadic Green's function

The planewave spectrum (PWS) integral representation of the electromagnetic dyadic Green's function for a general uniaxial anisotropic multi-layered medium, which has been derived in the previous chapter will be specialized to a grounded double layered unaxial anisotropic slab as shown in Figure 3.1, where an electric point source, ($\mathbf{p}_e\delta(\mathbf{r}-\mathbf{r}')$, $\mathbf{p}_e = \mathbf{p}_{te} + \mathbf{p}_{ze}$), is located in region (2). Then the Sommerfeld z-propagation integral representation, and subsequently, the radially propagating integral representations of the electric dyadic Green's function will be derived. The Sommerfeld integral representation leads to the singularity removal technique which is very efficient when the observation point is very close to source point. Nevertheless, as the lateral separation between the source and observation points increases, the Sommerfeld integrand starts to oscillate rapidly, and eventually the method loses its efficiency. These oscillations are due to the rapid growth of the argument of the Bessel function in the integrand which causes the singularity extraction method to eventually lose its efficiency. The radial propagation representation of the dyadic Green's function is very efficient when the source and observation points are laterally separated. This efficiency is due to the imaginary argument of the Hankel function which is present in the radial propagation of the dyadic Green's function.

The electric field is related to the electric dyadic Green's function as

$$\mathbf{E}_m(\mathbf{r}) = \int_V dv' \mathcal{G}^{ee}_{m,2}(\mathbf{r},\mathbf{r}') \cdot \mathbf{J}_e(\mathbf{r}') \ ; \ \ m = 1 \text{ or } 2 \ , \tag{3.1}$$

where $\mathbf{J}_e$ is the impressed electric current within the slab, and V contains the source region. If the $\mathbf{J}(\mathbf{r}')$ is an arbitrarily-oriented point current source of $\mathbf{p}_e\delta(\mathbf{r}-\mathbf{r}')$, the electric field may be viewed as the distribution

$$\mathbf{E}_m(\mathbf{r}) = \mathcal{G}^{ee}_{m,2}(\mathbf{r},\mathbf{r}') \cdot \mathbf{p}_e \ , \tag{3.2}$$

The electric dyadic Green's function due to the electric source can be expressed, using (2.49), as

$$\mathcal{G}^{ee}_{m,2}(\mathbf{r},\mathbf{r}') = \int \frac{d\mathbf{k}_t}{4\pi^2}\, e^{-j\mathbf{k}_t\cdot(\boldsymbol{\rho}-\boldsymbol{\rho}')}\, \tilde{\mathcal{G}}^{\gtrless}_{m,2}(\mathbf{k}_t,z,z') + \hat{\mathbf{z}}\hat{\mathbf{z}}\frac{1}{-j\omega\epsilon_0\epsilon_{z,2}}\delta(\mathbf{r}-\mathbf{r}') \ , \tag{3.3}$$

where

$$\mathbf{k}_t\cdot(\boldsymbol{\rho}-\boldsymbol{\rho}') = k_x(x-x') + k_y(y-y') \ ; \ d\,\mathbf{k}_t = d\,k_x\,d\,k_y \ , \tag{3.4}$$

and $\tilde{\mathcal{G}}^{\gtrless}_{m,2}(\mathbf{k}_t,z,z')$ can be represented in the matrix form

$$\tilde{\mathcal{G}}^{\gtrless}_{m,2}(\mathbf{k}_t,z,z') = \begin{pmatrix} \tilde{\mathcal{G}}^{\gtrless}_{tt}(\mathbf{k}_t,z,z') & \tilde{\mathcal{G}}^{\gtrless}_{tz}(\mathbf{k}_t,z,z') \\ \tilde{\mathcal{G}}^{\gtrless}_{zt}(\mathbf{k}_t,z,z') & \tilde{\mathcal{G}}^{\gtrless}_{zz}(\mathbf{k}_t,z,z') \end{pmatrix}_{m,2} \ , \tag{3.5}$$

the first and second subscripts denote the electric field and electric point current directions, respectively. Using analytical expressions for the modal fields, $\mathbf{e}_\alpha, \mathbf{e}_{z\alpha}, \mathbf{h}_\alpha, \mathbf{h}_{z\alpha}$ and the modal impedance Z_α given in Appendix A, the Green's dyadics inside the bracket for $m = 2$ (i.e., field points located in region 2) are explicitly defined as,

$$\tilde{\mathcal{G}}^{\gtrless}_{tt}(\mathbf{k}_t,z,z') = \frac{1}{-2\omega\epsilon_0}\left[\frac{\kappa_2'}{\epsilon_t}\tilde{g}'^{\gtrless}_{tt}(\mathbf{k}_t,z,z')\hat{\mathbf{k}}_t'\hat{\mathbf{k}}_t' + k_0^2\frac{\mu_t}{\kappa_2''}\tilde{g}''^{\gtrless}_{tt}(\mathbf{k}_t,z,z')\hat{\mathbf{k}}_t''\hat{\mathbf{k}}_t''\right] \ , \tag{3.6}$$

$$\tilde{\mathcal{G}}^{\gtrless}_{tz}(\mathbf{k}_t,z,z') = \frac{k_t}{2\omega\epsilon_0\epsilon_z}\tilde{g}'^{\gtrless}_{tz}(\mathbf{k}_t,z,z')\hat{\mathbf{k}}_t'\hat{\mathbf{z}} \ , \tag{3.7}$$

$$\tilde{\mathcal{G}}^{\gtrless}_{zt}(\mathbf{k}_t,z,z') = \frac{k_t}{2\omega\epsilon_0\epsilon_z}\tilde{g}'^{\gtrless}_{zt}(\mathbf{k}_t,z,z')\hat{\mathbf{z}}\hat{\mathbf{k}}_t' \ , \tag{3.8}$$

$$\tilde{\mathcal{G}}^{\gtrless}_{zz}(\mathbf{k}_t,z,z') = -\frac{\epsilon_t}{2\omega\epsilon_0\epsilon_z\epsilon_z}\frac{k_t^2}{\kappa_2'}\tilde{g}'^{\gtrless}(\mathbf{k}_t,z,z')\hat{\mathbf{z}}\hat{\mathbf{z}} \ , \tag{3.9}$$

where

$$\hat{\mathbf{k}}_t' = \frac{\hat{\mathbf{x}}\,k_x + \hat{\mathbf{y}}\,k_y}{k_t} \ ; \ \hat{\mathbf{k}}_t'' = \hat{\mathbf{z}}\times\hat{\mathbf{k}}_t' = \frac{\hat{\mathbf{y}}\,k_x - \hat{\mathbf{x}}\,k_y}{k_t} \ , \tag{3.10}$$

and the functions $\tilde{g}'(\mathbf{k}_t,z,z')$ and $\tilde{g}''(\mathbf{k}_t,z,z')$ are defined in Appendix C. The prime ($'$) and double prime ($''$) here are respectively correspond to $\alpha = 1$, and $\alpha = 2$.

The Green's dyadic can be written in terms of scalar functions if one notes

$$\hat{\mathbf{k}}_t'\hat{\mathbf{k}}_t' \longrightarrow -\frac{\nabla_t\nabla_t}{k_t^2} \ ; \ \hat{\mathbf{k}}_t''\hat{\mathbf{k}}_t'' \longrightarrow -\frac{(\hat{\mathbf{z}}\times\nabla_t)(\hat{\mathbf{z}}\times\nabla_t)}{k_t^2} \ , \tag{3.11}$$

and uses the identity of

$$\nabla_t \nabla_t \longrightarrow (\hat{\mathbf{x}}\frac{\partial}{\partial x} + \hat{\mathbf{y}}\frac{\partial}{\partial y})(\hat{\mathbf{x}}\frac{\partial}{\partial x} + \hat{\mathbf{y}}\frac{\partial}{\partial y})$$
$$\equiv \hat{\mathbf{x}}\hat{\mathbf{x}}\frac{\partial^2}{\partial x^2} + \hat{\mathbf{y}}\hat{\mathbf{y}}\frac{\partial^2}{\partial y^2} + (\hat{\mathbf{x}}\hat{\mathbf{y}} + \hat{\mathbf{y}}\hat{\mathbf{x}})\frac{\partial^2}{\partial x \partial y} \ , \tag{3.12}$$

and

$$(\hat{\mathbf{z}} \times \nabla_t)(\hat{\mathbf{z}} \times \nabla_t) \longrightarrow \hat{\mathbf{x}}\hat{\mathbf{x}}\frac{\partial^2}{\partial y^2} + \hat{\mathbf{y}}\hat{\mathbf{y}}\frac{\partial^2}{\partial x^2} - (\hat{\mathbf{x}}\hat{\mathbf{y}} + \hat{\mathbf{y}}\hat{\mathbf{x}})\frac{\partial^2}{\partial x \partial y} \tag{3.13}$$
$$\equiv \hat{\mathbf{x}}\hat{\mathbf{x}}(\nabla_t^2 - \frac{\partial^2}{\partial x^2}) + \hat{\mathbf{y}}\hat{\mathbf{y}}(\nabla_t^2 - \frac{\partial^2}{\partial y^2}) - (\hat{\mathbf{x}}\hat{\mathbf{y}} + \hat{\mathbf{y}}\hat{\mathbf{x}})\frac{\partial^2}{\partial x \partial y} \ .$$

Thus, the planewave spectral dyadic Green's function (3.3) (in view (3.5)-(3.9)) can be expressed as

$$\mathcal{G}_{tt}^{\gtrless}(\mathbf{r},\mathbf{r}') = \frac{1}{2\omega\epsilon_0}\left\{\hat{\mathbf{x}}\hat{\mathbf{x}}\left(-k_0^2\mathcal{U}^{\gtrless}(\mathbf{r},\mathbf{r}') + \frac{\partial^2}{\partial x^2}\mathcal{W}^{\gtrless}(\mathbf{r},\mathbf{r}')\right)\right.$$
$$+\hat{\mathbf{y}}\hat{\mathbf{y}}\left(-k_0^2\mathcal{U}^{\gtrless}(\mathbf{r},\mathbf{r}') + \frac{\partial^2}{\partial y^2}\mathcal{W}^{\gtrless}(\mathbf{r},\mathbf{r}')\right)$$
$$\left.+(\hat{\mathbf{x}}\hat{\mathbf{y}} + \hat{\mathbf{y}}\hat{\mathbf{x}})\frac{\partial^2}{\partial x \partial y}\mathcal{W}^{\gtrless}(\mathbf{r},\mathbf{r}')\right\} \ , \tag{3.14}$$

$$\mathcal{G}_{tz}^{\gtrless}(\mathbf{r},\mathbf{r}') = \frac{j}{2\omega\epsilon_0\epsilon_{2,z}}\nabla_t\left[g_{tz}'^{\gtrless}(\mathbf{r},\mathbf{r}')\right]\hat{\mathbf{z}} \ , \tag{3.15}$$

$$\mathcal{G}_{zt}^{\gtrless}(\mathbf{r},\mathbf{r}') = \frac{j}{2\omega\epsilon_0\epsilon_{2,z}}\hat{\mathbf{z}}\nabla_t\left[g_{zt}'^{\gtrless}(\mathbf{r},\mathbf{r}')\right] \ , \tag{3.16}$$

$$\mathcal{G}_{zz}^{\gtrless}(\mathbf{r},\mathbf{r}') = -\frac{\epsilon_{2,t}}{2\omega\epsilon_0\epsilon_{2,z}\epsilon_{2,z}}\mathcal{V}^{\gtrless}(\mathbf{r},\mathbf{r}') \ , \tag{3.17}$$

where

$$g^{\gtrless}(\mathbf{r},\mathbf{r}') = \int \frac{d\mathbf{k}_t}{4\pi^2}\, e^{-j\mathbf{k}_t\cdot(\boldsymbol{\rho}-\boldsymbol{\rho}')}\,\tilde{g}^{\gtrless}(k_t,z,z') \ , \tag{3.18}$$

$$\mathcal{U}^{\gtrless}(\mathbf{r},\mathbf{r}') = \int \frac{d\mathbf{k}_t}{4\pi^2}\, e^{-j\mathbf{k}_t\cdot(\boldsymbol{\rho}-\boldsymbol{\rho}')}\,\frac{\mu_{2,t}}{\kappa_2''}\tilde{g}''^{\gtrless}(k_t,z,z') \ , \tag{3.19}$$

$$\mathcal{W}^{\gtrless}(\mathbf{r},\mathbf{r}') = \int \frac{d\mathbf{k}_t}{4\pi^2} e^{-j\mathbf{k}_t\cdot(\boldsymbol{\rho}-\boldsymbol{\rho}')} \cdot \left[\frac{\kappa_2'}{\epsilon_{2,t}k_t^2}\tilde{g}_{tt}'^{\gtrless}(k_t,z,z') - k_0^2\frac{\mu_{2,t}}{\kappa_2''k_t^2}\tilde{g}''^{\gtrless}(k_t,z,z')\right] , \tag{3.20}$$

$$\mathcal{V}^{\gtrless}(\mathbf{r},\mathbf{r}') = \int \frac{d\mathbf{k}_t}{4\pi^2} e^{-j\mathbf{k}_t\cdot(\boldsymbol{\rho}-\boldsymbol{\rho}')} \frac{k_t^2}{\kappa_2'}\tilde{g}_{zz}'^{\gtrless} . \tag{3.21}$$

The Equation (3.18) has a Fourier-Bessel representation given by

$$g^{\gtrless}(\mathbf{r},\mathbf{r}') = \frac{k_0^2}{2\pi}\sum_{n=-\infty}^{\infty} e^{-jn(\phi-\phi')}\int_0^{\infty}\tilde{g}^{\gtrless}(\xi,z,z')J_n(k_0\xi\rho)\,J_m(k_0\xi\rho')\xi\,d,\xi , \tag{3.22}$$

which can be obtained from (3.18) by employing the following transformations

$$k_t = k_0\xi \;;\; k_x = k_0\xi\cos\alpha \;;\; k_y = k_0\xi\sin\alpha \tag{3.23}$$

$$(x-x') = \rho\cos\phi - \rho'\cos\phi' \;;\; y-y' = \rho\sin\phi - \rho'\sin\phi' . \tag{3.24}$$

If the coordinate system is chosen so that $\rho' = 0$, then the expression (3.22) reduces (in view of $J_0(0) = 1$, and $J_m(0) = 0$ for $m \neq 0$) to

$$g(\mathbf{r},\mathbf{r}') = \frac{k_0^2}{2\pi}\int_0^{\infty}\tilde{g}(\xi,z,z')J_0(\xi\,k_0\,\rho)\xi\,d\,\xi . \tag{3.25}$$

The Fourier-Bessel representation of the $\mathcal{U}$, $\mathcal{W}$, and $\mathcal{V}$ are obtained using the same procedure as of g and are given by:

$$\mathcal{U}^{\gtrless}(\mathbf{r},\mathbf{r}') = \frac{k_0}{2\pi}\int_0^{\infty}\frac{\mu_{2,t}}{\kappa_2''}\tilde{g}_{tt}''^{\gtrless}(\xi,z,z')\,J_0(\xi\,k_0\,\rho)\,\xi\,d\,\xi , \tag{3.26}$$

$$\mathcal{W}^{\gtrless}(\mathbf{r},\mathbf{r}') = \frac{k_0}{2\pi}\int_0^{\infty}\left[\frac{\kappa_2'}{\epsilon_{2,t}}\tilde{g}_{tt}'^{\gtrless}(\xi,z,z') - \frac{\mu_{2,t}}{\kappa_2''}\tilde{g}_{tt}''^{\gtrless}(\xi,z,z')\right]J_0(\xi\,k_0\,\rho)\,\frac{d\,\xi}{\xi} , \tag{3.27}$$

$$\mathcal{V}^{\gtrless}(\mathbf{r},\mathbf{r}') = \frac{k_0^3}{2\pi}\int_0^{\infty}\frac{\xi^2}{\kappa_2'}\tilde{g}_{zz}'^{\gtrless}(\xi,z,z')\,J_0(\xi\,k_0\,\rho)\,\xi\,d\,\xi . \tag{3.28}$$

Expressions in (3.25)-(3.28) are the Sommerfeld type integral representations of g, $\mathcal{U}$, $\mathcal{W}$, and $\mathcal{V}$ given in terms of planewave spectral (PWS) integral representation given in (3.20)-(3.25). It should be noted that the wavenumbers κ_i' and κ_i'' in (3.25)-(3.28) are normalized with respect to k_0, namely by

$$\kappa_i' = \sqrt{n_i - n_i'\,\xi^2} \;\;;\;\; \kappa_i'' = \sqrt{n_i - n_i''\,\xi^2} , \tag{3.29}$$

where $n_i = \epsilon_{i,t}\mu_{i,t}$, $n_i' = \frac{\epsilon_{i,t}}{\epsilon_{i,z}}$, and $n_i'' = \frac{\mu_{i,t}}{\mu_{i,z}}$.

Each term in the integrand of (3.27) exhibits a spurious pole at $\xi = 0$. This leads to an integral with a logarithmic singularity and it is a consequence of interchanging the derivative and integration operations. Strictly speaking, this interchange is not allowed (because of the convergence of difficulty as $\xi \to 0$). However the expressions in (3.27) as a whole converge, which means that the integrand of

$$\left[\frac{\kappa_2'}{\epsilon_{2,t}}\tilde{g}_{tt}'^{\gtrless}(\xi, z, z') - \frac{\mu_{2,t}}{\kappa_2''}\tilde{g}_{tt}''^{\gtrless}(\xi, z, z')\right] J_0(\xi\, k_0\, \rho)\frac{1}{\xi} \tag{3.30}$$

is regular at $\xi = 0$. This can be shown by explicit substitution of $\tilde{g}_{tt}'$ and $\tilde{g}_{tt}''$ and taking the limit of the integrand of the above expression as $\xi \to 0$. So in a distributional sense an interchange of the operators is justified.

The convergence behavior of these functions in (3.25)-(3.28) depends strongly upon the value of $|z - z'|$ (vertical separation between the source and observation points). For the cases of planar structures, such as microstrip arrays, the factor which exhibits an exponential decay, $e^{-\xi k_0|z-z'|}$, goes to unity. Thus, as $\xi \to \infty$, the Sommerfeld type integrands decay algebraically as $\sim \frac{1}{\sqrt{\xi k_0 \rho}}$ rather than exponentially; the algebraic decay results from the asymptotic behavior of $J_0(\xi\, k_0\, \rho)$ for large $\xi\, k_0\, \rho$.

It is a well known fact that the numerical integration of oscillatory functions are very time consuming, particularly when they have an end point at infinity. To overcome this difficulty, which is inherent in any open structure involving multilayered media one may use the singularity removal technique. This technique is very efficient when the lateral separation ($k_0\rho$) is small (i.e., if $k_0\rho < 1$). It deals with asymptotic behavior of the integrands, which in turn is dictated by the behavior of $J_o(\xi k_0\rho)$. These asymptotic values can be integrated in closed form; therefore, if one subtracts these asymptotic values from the integrands, then the resulting integrands are relatively smooth and fast decaying so that they can be integrated efficiently.

The singularity removal technique [19] which improves the convergence of the conventional Sommerfeld integral representation is described as follows.

Let I be a typical value of g, $\mathcal{U}$, $\mathcal{W}$, or $\mathcal{V}$ of (3.25)-(3.28) which in general has the form

$$I = \int_0^\infty \xi^m\, F(\xi, z, z')\, J_0(\xi\, k_0\, \rho)\, d\, \xi \quad , \tag{3.31}$$

where $\xi^m\ F(\xi, z, z')$ is recognizable from (3.25) through (3.28). As $\xi \to \infty$, the value of $F(\xi, z, z')$ asymptotically approaches some complex value, say $\sum_n C_n\, e^{-\xi\delta n}$; (where the explicit expressions associated with g, $\mathcal{U}$, $\mathcal{W}$, and $\mathcal{V}$ can be found from (3.25)-(3.28), and the limiting values of $\tilde{g}_{ij}'^{\gtrless}(\xi, z, z')$ and $\tilde{g}_{ij}''^{\gtrless}(\xi, z, z')$ as $\xi \to \infty$ which are given in Appendix D. But

$$\int_0^\infty J_0(\xi\, k_0\rho)\; e^{-\xi\, k_0\, \delta}\; \xi^m\; d\xi \;=\; (-1)^m \frac{d^m}{d(k_0\delta)^m} \int_0^\infty J_0(\xi\, k_0\rho)\; e^{-\xi\, k_0\, \delta}\; d\xi$$

$$= (-1)^m \frac{d^m}{d(k_0\delta)^m} \left(\frac{1}{k_0\sqrt{(\rho^2+\delta^2)}} \right) \quad . \tag{3.32}$$

Therefore

$$I = \int_0^\infty (F(\xi) - \sum_n C_n\, e^{-\xi\, k_0\, \delta}) \xi^m\; J_0(\xi\, k_0\, \rho)\; d\xi + \sum_n C_n\, (-1)^m \frac{d^m}{d(k_0\delta)^m} \left(\frac{1}{k_0\sqrt{(\rho^2+\delta^2)}} \right) \quad . \tag{3.33}$$

Mathematically, Equations (3.31) and (3.33) are equivalent; numerically however, the integral of (3.33) possessed a much smoother function; therefore an eight or sixteen point Gaussian integration routine is sufficient to achieve a reasonable accuracy in evaluating such an integral. More discussion about the behavior of integrands in (3.31) and (3.33) will be presented in Chapter 5 which is devoted to numerical results.

It should be pointed out however that the smoothness of the integrand in (3.33) deteriorates as the lateral separation of the source and observation popints increases (i.e., as $k_0\rho$ becomes large). The second method involves the use of a radially propagating integral representation which overcomes the difficulty associated with the first method, and converges very fast if the source and observation points are separated laterally rather than vertically. This technique also leads to the uniform asymptotic closed form solution which will be discussed in the following chapter.

3.2 Alternative radial ρ-propagation representation for the dyadic Green's function

The starting point in the derivation of the radial propagation microstrip Green's function is Equation (3.25) which constitute the Sommerfeld representation of $g(\mathbf{r}, \mathbf{r}')$ as

$$g(\mathbf{r}, \mathbf{r}') = \frac{k_0^2}{2\pi} \int_0^\infty \tilde{g}(\xi, z, z')\; J_0\; (\xi k_0\, \rho)\; \xi\; d\; \xi \quad . \tag{3.34}$$

The above integral in (3.34) can be written in terms of the Hankel function where the integral has the lower limit as $\infty e^{-j\pi}$, and the upper limit at ∞, provided that $\tilde{g}$ is an even function of ξ. Thus, (3.34) becomes

$$g(\mathbf{r}, \mathbf{r}') = \frac{k_0^2}{4\pi} \int_{\infty\; e^{-j\pi}}^\infty \tilde{g}(\xi, z, z')\; H_0^{(2)}(\xi\, k_0\, \rho)\; \xi\; d\; \xi \quad , \tag{3.35}$$

in which the contour of integration is such that the branch point at $\xi = 0$ introduced by the transformation is avoided as shown in Figure 3.2.

An alternative ρ-propagation representation of g can be derived by deforming the integration contour of (3.35) so that it encloses all the singularities of the z-dependent function $\tilde{g}(\xi, z,')$ in the integrand. General techniques for arriving at alternative representations for Green's functions have been discussed in [6, 18].

In order to enclose al' .he singularities of $\tilde{g}(\xi, z, z')$ in the ξ plane, the analytic property of $\tilde{g}(\xi, z, z')$ needs to be studied. As mentioned earlier, explicit expressions for $\tilde{g}''^{\gtrless}$ and $\tilde{g}'^{\gtrless}$ are given in Appendix C (in particular see (C.1) - (C.11) and (C.32) - (C.39)). The $\tilde{g}''^{\gtrless}$ and $\tilde{g}'^{\gtrless}$ are functions of the propagation constants κ'_m, κ''_m, $m = 0, 1$ and 2, and in the complex ξ plane they have a pair of branch points at $\xi = \pm 1$ and a pair of branch cuts from $\xi = \pm 1$ to infinity. These branch cuts must be defined in such a way that $Im\left(\sqrt{1-\xi^2}\right) < 0$ on the entire top sheet. This is the only pair of branch cuts that allow the analytic continuation of $\tilde{g}''^{\gtrless}$ and $\tilde{g}'^{\gtrless}$ into the entire top sheet of ξ such that they satisfy the radiation condition. Therefore, the deformation of the real axis path of integration into the complex plane is possible as long as it stays on the top Riemann sheet as $|\xi| \to \infty$; of course, one must account for residues associated with any poles in the integrals ($\tilde{g}''^{\gtrless}$ and $\tilde{g}'^{\gtrless}$) which are enclosed in this contour deformation. As mentioned previously, Figure 3.2 shows a typical complex ξ plane containing branch cuts due to the Hankel function and $\tilde{g}''^{\gtrless}$ in the integrand of (3.35) as well as the path of integration from $\infty e^{-j\pi}$ to ∞. In general there also exist a finite number of pole singularities (i.e. N number of poles) on the top Riemann sheet; these poles are called proper surface wave poles (whose residues are modal waves because they satisfy the radiation condition at infinity). There can also exist an infinite number of pole singularities on the bottom Riemann sheet; the latter poles are called leaky wave poles (giving rise to non-modal waves since they do not satisfy the radiation condition at infinity). A finite number of surface wave poles have also been depicted in Figure 3.2.

Equation (3.34) and (3.35) constitute a Sommerfeld or z-propagation integral representation; on the other hand, the ρ-propagation representation for g can be derived by enclosing all the singularities of $\tilde{g}$ in the plane via a contour deformation. The original contour is thus deformed as shown in Figure 3.2 to arrive at

$$g(\mathbf{r}, \mathbf{r}') = \frac{k_0^2}{4\pi}\left[\int_{C_B} \tilde{g}(\xi, z, z')\, H_0^{(2)}(\xi\, k_0\, \rho)\, \xi\, d\, \xi - 2\pi j \sum_{p=1}^{N} Res\left(\tilde{g}(\xi_p, z, z')\right) \xi_p\, H_0^{(2)}(\xi_p \rho)\right], \tag{3.36}$$

where the finite sum refers to the discrete spectral or pole wave contribution to g and the integral of C_B is the continuous spectral contribution to g; also, the Res is defined as the residue of $\tilde{g}$ at the poles $\xi = \xi_p$; i.e., (see also (C.16) and (C.38))

$$Res(\tilde{g}(\xi_p, z, z')) = \lim_{\xi \to \xi_p} (\xi - \xi_p)\ \tilde{g}(\xi, z, z') \tag{3.37}$$

The integral contour C_B can be transformed to the real axis by introducing the change of variable

$$\zeta = \sqrt{1 - \xi^2} \quad ; \quad d\xi = \frac{-\zeta d\zeta}{\sqrt{1-\zeta^2}}. \tag{3.38}$$

It is noted that as ξ varies along the contour C_B of the Figure 3.2, the new variable of integration ζ will vary from $+\infty$ to $-\infty$ along the real ζ axis as shown in Figure 3.3. Note that the circular contour which encircles the branch point does not contribute. Finally, one obtains

$$\begin{aligned} g(\mathbf{r}, \mathbf{r}') \;=\; & \frac{k_0^2}{4\pi} \left[\int_{-\infty}^{\infty} \tilde{g}(\zeta, z, z')\ H_0^{(2)}\left(k_0 \rho \sqrt{1-\zeta^2}\right)\ \zeta\ d\,\zeta \right. \\ & \left. -2\pi j \left(\sum_p Res\left(\tilde{g}(\xi_p, z, z)\ \xi_p\ H_0^{(2)}(\xi_p k_0 \rho)\right)\right)\right]. \end{aligned} \tag{3.39}$$

The above result in (3.39) represents the alternative ρ-propagation representation of g which is obtained from its Sommerfeld representation in (3.34).

The radial propagation of a grounded uniaxial anisotropic double layered dyadic Green's function can be constructed after incorporating g of (3.39), $\mathcal{U}$, $\mathcal{W}$, and $\mathcal{V}$ given in the following into (3.14) - (3.17)

$$\begin{aligned} \mathcal{U}^{\gtrless}(\mathbf{r}, \mathbf{r}') \;=\; & \frac{k_0}{4\pi} \left[\int_{-\infty}^{\infty} \frac{\mu_{2,t}}{\kappa_2''} \tilde{g}_{tt}''^{\gtrless}(\zeta, z, z')\, H_0^{(2)}(k_0 \rho \sqrt{1-\zeta^2})\, \zeta\, d\,\zeta \right. \\ & \left. -2\pi j \sum_{p''} \frac{\mu_{2,t}}{\kappa_2''} Res\left(\tilde{g}_{tt}''^{\gtrless}(\xi_{p''}, z, z')\right)\ H_0^{(2)}(k_0 \rho \xi_{p''}) \right] , \end{aligned} \tag{3.40}$$

$$\begin{aligned} \mathcal{W}^{\gtrless}(\mathbf{r}, \mathbf{r}') \;=\; & \frac{k_0}{2\pi} \left\{ \int_{-\infty}^{\infty} \left[\frac{\kappa_2'}{\epsilon_{2,t}} \tilde{g}_{tt}'^{\gtrless}(\zeta, z, z') - \frac{\mu_{2,t}}{\kappa_2''} \tilde{g}_{tt}''^{\gtrless}(\zeta, z, z') \right]\ H_0^{(2)}(k_0 \rho \sqrt{1-\zeta^2})\, \frac{\zeta}{1-\zeta^2}\, d\,\zeta \right. \\ & -2\pi j \left(\sum_{p'} \frac{\kappa_2'}{\epsilon_{2,t} \xi_{p'}} Res\left(\tilde{g}_{tt}'^{\gtrless}(\xi_{p'}, z, z')\right)\ H_0^{(2)}(k_0 \rho \xi_{p'})) \right. \\ & \left. \left. - \sum_{p''} \frac{\mu_{2,t}}{\kappa_2'' \xi_{p''}} Res\left(\tilde{g}_{tt}''^{\gtrless}(\xi_{p''}, z, z')\right)\ H_0^{(2)}(k_0 \rho \xi_{p''}) \right) \right\} , \end{aligned} \tag{3.41}$$

$$\mathcal{V}^{\gtrless}(\mathbf{r},\mathbf{r}') = \frac{k_0^3}{2\pi}\left[\int_{-\infty}^{\infty}\frac{1-\zeta^2}{\kappa_2'}\tilde{g}_{zz}'^{\gtrless}(\zeta,z,z')\,H_0^{(2)}(k_0\rho\sqrt{1-\zeta^2})\zeta\,d\zeta\right. \tag{3.42}$$
$$\left. -2\pi j\sum_{p'}\frac{\xi_{p'}^3}{\kappa_2'}Res\left(\tilde{g}_{zz}'^{\gtrless}(\xi_{p'},z,z')\right)H_0^{(2)}(k_0\rho\xi_{p'})\right]\ .$$

The prime ($'$) and double prime ($''$) in (3.40) - (3.42) refer to TM (or E-mode; $\alpha = 1$) and TE (or H-mode; $\alpha = 2$) respectively; see also Appendix C. One can now see that the radial propagation representation of the dyadic Green's function exhibits fast convergence for laterally separated source and field points. This is due to the fact that for the $\zeta > 1$, the Hankel functions associated with the integrand in (3.39) - (3.42) decay exponentially. Therefore it is more efficient to utilize this representation for the planar geometries when dealing with a solution for currents within a planar uniaxial anisotropic materials. The logarithmic singularity of the Hankel function at $\zeta = \pm 1$ can be removed via the following transformations

$$\zeta = \sqrt{1-\xi^2}\ \ ,\ \ |\zeta| < 1\ \ ;\ \ \zeta = \sqrt{1+\xi^2}\ \ ,\ \ |\zeta| > 1\ . \tag{3.43}$$

Hence, the final form of $g, \mathcal{U}, \mathcal{W}$, and $\mathcal{V}$ after transforming the integrtal (0,-1) to (0,1), and $(-\infty,-1)$ and $(1,\infty)$ to $(0,\infty)$, which will be used in the numerical integrarion are given by:

$$g(\mathbf{r},\mathbf{r}') = \frac{k_0^2}{4\pi}\left[\int_0^1\left[\tilde{g}(\zeta,z,z')-\tilde{g}(-\zeta,z,z')\right]_{|_{\zeta=\sqrt{1-\xi^2}}}H_0^{(2)}(k_0\rho\xi)\ \xi\ d\ \xi\right.$$
$$+\quad\int_0^{\infty}\left[\tilde{g}(\zeta,z,z')-\tilde{g}(-\zeta,z,z')\right]_{|_{\zeta=\sqrt{1+\xi^2}}}H_0^{(2)}(-jk_0\rho\xi)\ \xi\ d\ \xi$$
$$\left.-2\pi j\left(\sum_p Res\left(\tilde{g}(\xi_p,z,z)\ \xi_p\ H_0^{(2)}(\xi_p k_0\rho)\right)\right)\right]. \tag{3.44}$$

$$\mathcal{U}^{\gtrless}(\mathbf{r},\mathbf{r}') = \frac{k_0}{4\pi}\left[\int_0^1\frac{\mu_{2,t}}{\kappa_2''(\zeta)}\left[\tilde{g}_{tt}''^{\gtrless}(\zeta,z,z')-\tilde{g}_{tt}''^{\gtrless}(-\zeta,z,z')\right]_{|_{\zeta=\sqrt{1-\xi^2}}}H_0^{(2)}(k_0\rho\xi)\,\xi\,d\xi\right.$$
$$+\quad\int_0^{\infty}\frac{\mu_{2,t}}{\kappa_2''(\zeta)}\left[\tilde{g}_{tt}''^{\gtrless}(\zeta,z,z')-\tilde{g}_{tt}''^{\gtrless}(-\zeta,z,z')\right]_{|_{\zeta=\sqrt{1+\xi^2}}}H_0^{(2)}(-jk_0\rho\xi)\,\xi\,d\xi$$
$$\left.-2\pi j\sum_{p''}\frac{\mu_{2,t}}{\kappa_2''}Res\left(\tilde{g}_{tt}''^{\gtrless}(\xi_{p''},z,z')\right)\ H_0^{(2)}(k_0\rho\xi_{p''})\right]\ , \tag{3.45}$$

$$
\begin{aligned}
\mathcal{W}^{\gtrless}(\mathbf{r},\mathbf{r}') \;=\; & \frac{k_0}{2\pi}\left\{\int_0^1 \left(\frac{\kappa_2'(\zeta)}{\epsilon_{2,t}}\left[\tilde{g}_{tt}'^{\gtrless}(\zeta,z,z') - \tilde{g}_{tt}'^{\gtrless}(-\zeta,z,z')\right]\right.\right. \\
& \left.\left. - \frac{\mu_{2,t}}{\kappa_2''(\zeta)}\left[\tilde{g}_{tt}''^{\gtrless}(\zeta,z,z') - \tilde{g}_{tt}''^{\gtrless}(-\zeta,z,z')\right]\right)\Big|_{\zeta=\sqrt{1-\xi^2}} H_0^{(2)}(k_0\rho\xi)\,\frac{d\xi}{\xi}\right. \\
& - \int_0^\infty \left(\frac{\kappa_2'(\zeta)}{\epsilon_{2,t}}\left[\tilde{g}_{tt}'^{\gtrless}(\zeta,z,z') - \tilde{g}_{tt}'^{\gtrless}(-\zeta,z,z')\right]\right. \\
& \left. - \frac{\mu_{2,t}}{\kappa_2''(\zeta)}\left[\tilde{g}_{tt}''^{\gtrless}(\zeta,z,z') - \tilde{g}_{tt}''^{\gtrless}(-\zeta,z,z')\right]\right)\Big|_{\zeta=\sqrt{1+\xi^2}} H_0^{(2)}(-jk_0\rho\xi)\,\frac{d\xi}{\xi} \\
& -2\pi j\left(\sum_{p'}\frac{\kappa_2'}{\epsilon_{2,t}\xi_{p'}} Res\left(\tilde{g}_{tt}'^{\gtrless}(\xi_{p'},z,z')\right) H_0^{(2)}(k_0\rho\xi_{p'})\right. \\
& \left.\left. - \sum_{p''}\frac{\mu_{2,t}}{\kappa_2''\xi_{p''}} Res\left(\tilde{g}_{tt}''^{\gtrless}(\xi_{p''},z,z')\right) H_0^{(2)}(k_0\rho\xi_{p''})\right)\right\}\;,
\end{aligned}
\tag{3.46}
$$

$$
\begin{aligned}
\mathcal{V}^{\gtrless}(\mathbf{r},\mathbf{r}') \;=\; & \frac{k_0^3}{2\pi}\left[\int_0^1 \frac{\xi^2}{\kappa_2'(\zeta)}\left[\tilde{g}_{zz}'^{\gtrless}(\zeta,z,z') - \tilde{g}_{zz}'^{\gtrless}(-\zeta,z,z')\right]\Big|_{\zeta=\sqrt{1-\xi^2}} H_0^{(2)}(k_0\rho\xi)\xi\,d\xi\right. \\
& + \int_0^\infty \frac{\xi^2}{\kappa_2'(\zeta)}\left[\tilde{g}_{zz}'^{\gtrless}(\zeta,z,z') - \tilde{g}_{zz}'^{\gtrless}(-\zeta,z,z')\right]\Big|_{\zeta=\sqrt{1+\xi^2}} H_0^{(2)}(-jk_0\rho\xi)\xi\,d\xi \\
& \left. -2\pi j\sum_{p'}\frac{\xi_{p'}^3}{\kappa_2'} Res\left(\tilde{g}_{zz}'^{\gtrless}(\xi_{p'},z,z')\right) H_0^{(2)}(k_0\rho\xi_{p'})\right]\;.
\end{aligned}
\tag{3.47}
$$

The behavior of the integrand of the radially propagating integral representation in (3.44) to (3.47) will be discussed in Chapter 5 of numerical results.

As mentioned earlier, the formal representation of the radially propagating integral representation of the dyadic Green's function developed in this chapter leads to a very efficient closed form asymptotic approximation of the Green's dyadic which remain accurate even for very small lateral separation of the source and observation points. The developement of this asymptotic representation will be discussed in the next chapter.

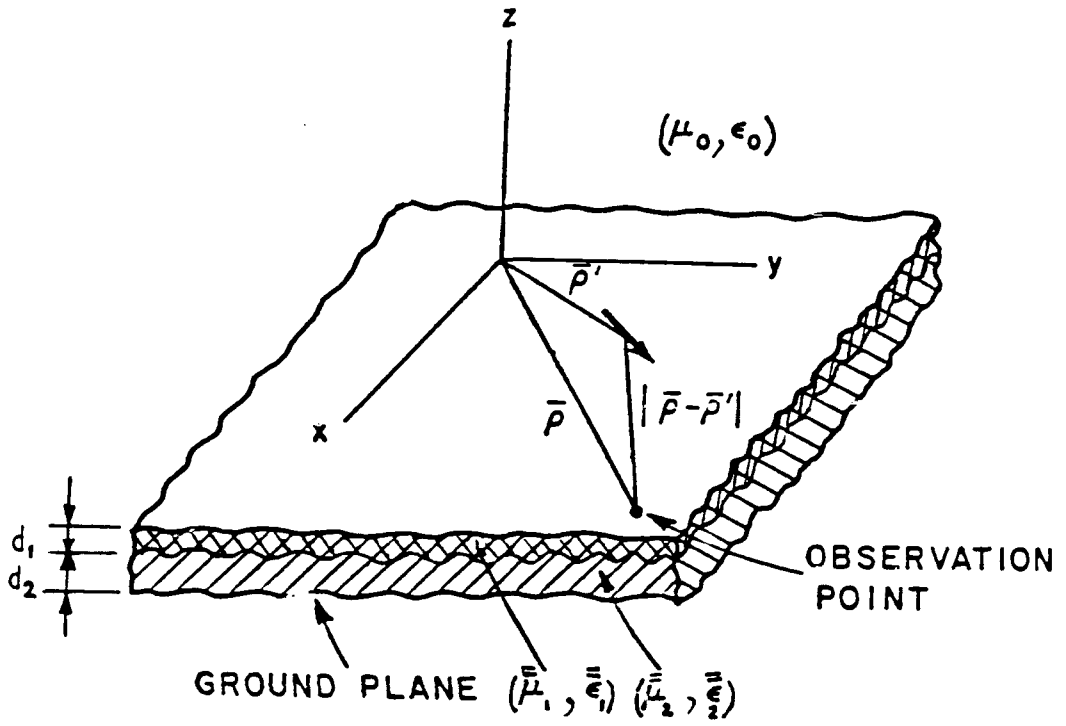

Figure 3.1: Electric point current dipole source in a grounded anisotropic uniaxial double layered slab, ($\bar{\bar{\epsilon}}_i = \epsilon_{i,t}\mathbf{I}_t + \epsilon_{i,z}\hat{z}\hat{z}$; $\bar{\bar{\mu}}_i = \mu_{i,t}\mathbf{I}_t + \mu_{i,z}\hat{z}\hat{z}$).

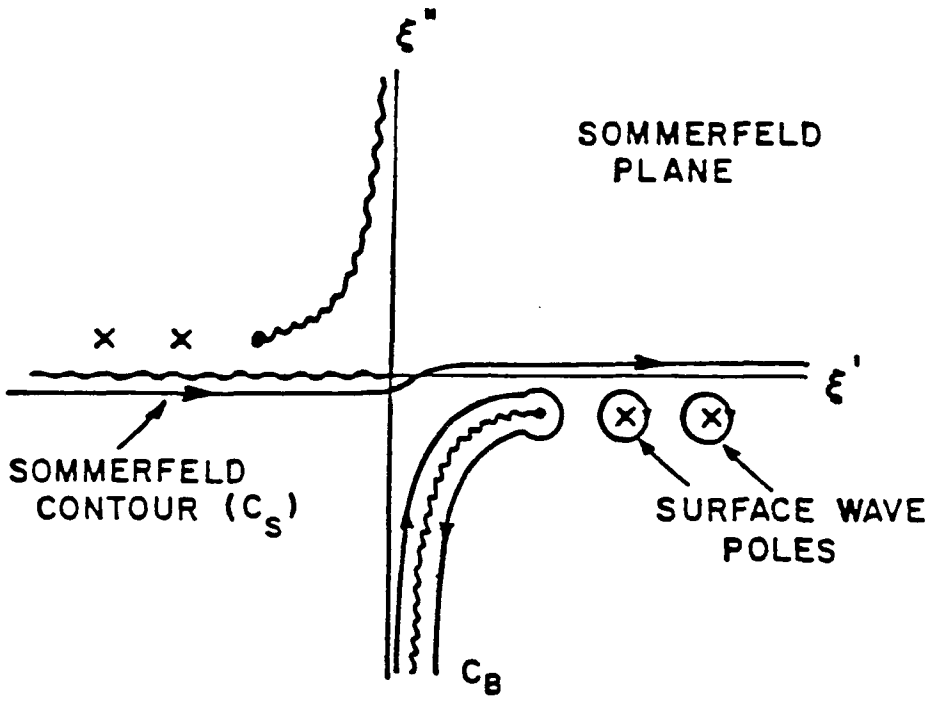

Figure 3.2: Analytic properties of $\tilde{g}(\xi, z, z')$ in the complex ξ plane; surface wave poles and branch cuts. Also depicted here are, the original Sommerfeld contour, the contour deformation for ρ-representation as a sum of the enclosed residues plus the integral around the branch cut C_B of $\tilde{g}(\xi, z, z')$.

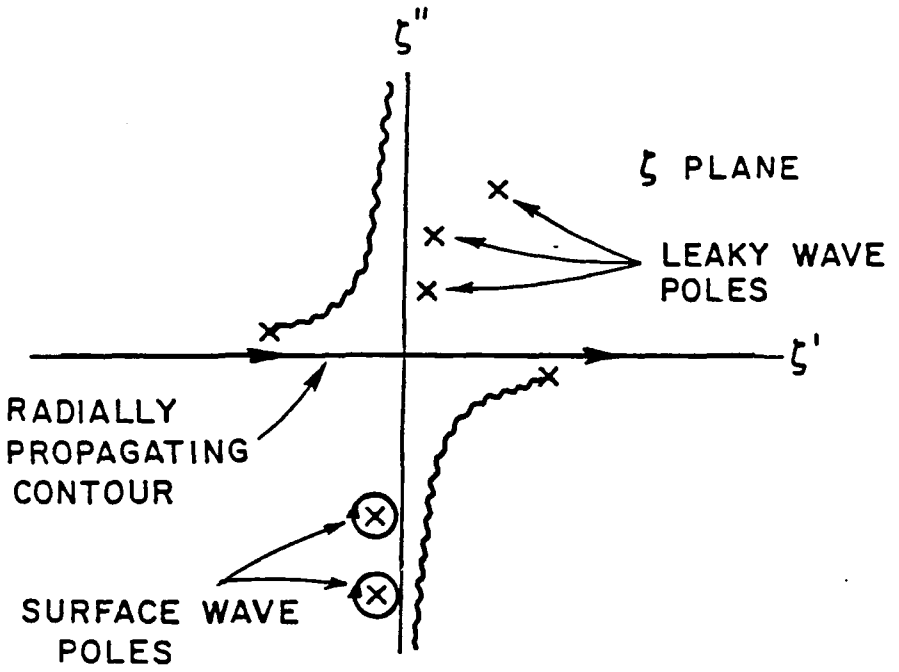

Figure 3.3: Complex ζ plane and the real axis contour of integration of (3.39).

Chapter 4

Uniform asymptotic closed-form representation for the dyadic Green's function

This chapter deals with the development of an asymptotic representation for the dyadic Green's function for the uniaxial anisotropic double layered geometry in which the large parameter directly depends on the lateral separation between the source and observation points; however, this asymptotic result is found to remain accurate even for source and field points separated by only a few tenths of a free space wavelength. As mentioned earlier, the radially propagating integral representation given in the previous chapter can be used as a starting point to find an approximate closed form asymptotic solution of the dyadic Green's function which remains valid in the entire range of $k_0\rho$ except for very small $k_0\rho$. The details of this asymptotic development are shown in the following.

Consider the integral I of the form

$$I = \int_{-\infty}^{\infty} F(\zeta, z, z') H_0^{(2)}(k_0 \rho \sqrt{1-\zeta^2})\ \zeta\ d\zeta\ , \tag{4.1}$$

in which $(k_0\rho)$ is assumed to be a large parameter. This integral is similar to the the radially propagating part of g, $\mathcal{U}$, $\mathcal{W}$, and $\mathcal{V}$; $F(\zeta, z, z')$ has the following functional form

$$F(\zeta, z, z') \rightarrow K(\zeta) e^{-jk_0\,\delta\zeta} \qquad ;\quad \delta \rightarrow \pm(z \pm z') \tag{4.2}$$

If one performs the angular spectrum mapping

$$\zeta = \cos\gamma;\quad d\zeta = -\sin\gamma d\gamma,\quad \text{and}\quad \sqrt{1-\zeta^2} = \sin\gamma, \tag{4.3}$$

then,

$$I \sim \int_\Gamma K(\gamma) \sqrt{\frac{2}{\pi k_0 r \sin\gamma}}\, e^{+j\frac{\pi}{4}} \left(1 + \frac{j}{8k_0 r \sin\gamma}\right) e^{-jk_0 r\cos(\theta-\gamma)} \cos\gamma\ \sin\gamma\ d\gamma \tag{4.4}$$

where,

$$\delta = r\cos\theta \quad ; \quad \rho = r\sin\theta, \quad \text{and} \quad \tan\theta = \frac{\rho}{\delta} \quad , \tag{4.5}$$

and use has been made of the large argument approximation of the Hankel function

$$H_0^{(2)}(x) \sim \sqrt{\frac{2}{\pi x}}\left(1+\frac{j}{8x}\right)e^{-j(x-\frac{\pi}{4})} \quad ; \quad x \gg 1 \quad . \tag{4.6}$$

The integrand exhibits a saddle point at $\gamma_s = \theta$. Let

$$q(\gamma) = -j\cos(\theta-\gamma). \tag{4.7}$$

Then,

$$q'(\gamma) = j\sin(\theta-\gamma) \quad ; \quad \gamma_s = \theta \,(\text{saddle point}) \quad ; \quad q(\gamma_s) = -j \; . \tag{4.8}$$

Figures 4.1 and 4.2 show the double sheeted ζ and complex γ planes respectively, with the original path Γ and steepest descent path Γ_{SDP} depicted in the complex γ plane. Note that the steepest descent path is the path on which the following condition holds,

$$Im(q(\gamma)) = Im(q(\gamma_s)), \quad \text{or} \quad Re(\cos(\theta-\gamma)) = 1, \tag{4.9}$$

so,

$$\begin{aligned} I \;\sim\; & \int_{\Gamma_{SDP}} K(\gamma)\sqrt{\frac{2}{\pi k_0 r\sin\gamma}}e^{j\frac{\pi}{4}}\left(1+\frac{j}{8\,k_0 r\sin\gamma}\right)e^{-jk_0 r\cos(\theta-\gamma)}\cos\gamma\sin\gamma\, d\gamma \\ & + 2\pi j\sum_s Res(I(\gamma_s)) - 2\pi j\sum_l Res(I(\gamma_l)) \quad , \end{aligned} \tag{4.10}$$

where Γ_{SDP} is the SDP contour, and the summation terms of s and l, stand for the residue contributions arising from the presence of the surface wave and leaky wave poles respectively which may be intercepted during the path deformation. It is noted that unless $\theta \approx \frac{\pi}{2}$ ($k_0\rho \gg 1$; $k_0\delta \ll 1$), there exists the possibility of crossing one or more of those surface wave poles which are closest to the Real γ axis (see Figure 4.2) which have been captured during the derivation of ρ-propagation representation (see (3.39) - (3.42)). This results in the cancellation of some fo the surface wave residue contributions in the sum on the right hand sides of (3.39) - (3.42). It is also noted that the same SDP will result if one starts from the Sommerfeld representation (rather than the ρ-propagation representation) since only one SDP exists in each strip of 2π radians in the γ plane, but in this case, the surface wave poles must be found in γ plane. In the following we will map the SDP onto a contour along the real axis in the new complex plane s defined by

$$q(\gamma) - q(\gamma_s) = s^2 \quad ; \quad \cos(\theta - \gamma) = 1 - js^2, \tag{4.11}$$

or

$$\frac{d\gamma}{ds} = \frac{2j}{\sqrt{s^2+2j}} \quad ; \quad \text{(branch points at } \sqrt{s^2+2j} = 0). \tag{4.12}$$

This transformation maps the steepest descent path Γ_{SDP}, on the real axis of the complex s plane as indicated above. The saddle point at $\gamma_s = \theta$ is now mapped to $s = 0$ (see Figure 4.3). For the $\theta \approx \frac{\pi}{2}$ the source and the observation points laterally separated (i.e. $(k_0\rho \gg 1;\ k_0\delta \ll 1)$, one will have

$$\sin\gamma = 1 - js^2, \quad \cos\gamma = |s|\sqrt{s^2+2j} \quad . \tag{4.13}$$

It is useful to note that

$$\zeta = s\sqrt{s^2+2j} \quad ; \quad \frac{d\zeta}{ds} = \frac{2j(s^2-1)}{\sqrt{s^2+2j}} \quad . \tag{4.14}$$

therefore the SDP representation of I in the s-plane can be expressed as

$$I \sim \sqrt{\frac{2}{\pi k_0\rho}}\, e^{i\frac{\pi}{4}}\, e^{-jk_0\rho} \int_{-\infty}^{\infty} G(s) e^{-k_0\rho s^2}\, ds - 2\pi j \sum_l Res(I(\gamma_l)) \quad , \tag{4.15}$$

where, in view of (4.1), $G(s)$ are given by

$$G(s) = \left(1 + \frac{j}{8\, k_0\rho(1-js^2)}\right) 2js\sqrt{(1-js^2)}\, F(\zeta, z, z')_{|_{\zeta = s\sqrt{s^2+2j}}} \tag{4.16}$$

It should be noted that for the particular case of $\theta \approx \frac{\pi}{2}$ no surface wave pole will be intercepted during the path deformation.

The uniform asymptotic approximation of I can be represented as, [19]

$$\begin{aligned} I \;\sim\; & \sqrt{2j}\,\frac{e^{-jk_0\rho}}{k_0\rho} \left\{ \frac{G''(0)}{4k_0\rho} \right. \\ & + \left. \sum_\sigma \frac{Res(G(s_\sigma))}{s_\sigma} \left(1 - \mathcal{F}(jk_0\rho s_\sigma^2) + \frac{1}{2k_0\rho s_\sigma^2}\right) \right\} \\ & - 2\pi j \sum_l Res(I(s_l)) \quad , \end{aligned} \tag{4.17}$$

where s_σ's are the poles (surface wave as well as leaky wave poles) that are considered to be close to the saddle point at $s = 0$; and $Res(G(s_\sigma))$ is related to $Res(F(\zeta_\sigma))$ (of ρ-representation) and $Res(F(\xi_\sigma))$ (of the Sommerfeld representation) by

$$\begin{aligned} Res(G(s_\sigma)) &= \left(1 + \frac{j}{8\,k_0\rho\sqrt{1-\zeta_\sigma^2}}\right) \frac{\zeta_\sigma}{\sqrt{\sqrt{1-\zeta_\sigma^2}}}\, Res(F(\zeta_\sigma)) \ , \\ &= \left(1 + \frac{j}{8\,k_0\rho\xi_\sigma}\right) \sqrt{\xi_\sigma}\, Res(F(\xi_\sigma)) \ , \end{aligned} \tag{4.18}$$

and $s_\sigma = \pm\sqrt{j}\sqrt{\xi_\sigma - 1}$; $\zeta_\sigma = \pm\sqrt{1-\xi_\sigma^2}$, also $s_\sigma = \pm\sqrt{j}\sqrt{\sqrt{1-\zeta_\sigma^2} - 1}$. The value of $G''(s)_{|_{s=0}}$ is related to the first derivative of $F(s)$ by

$$\begin{aligned} G''(s)_{|_{s=0}} &= 4j(1 + \frac{j}{8k_0\,\rho})\frac{d}{ds}F(s)_{|_{s=0}} \ , \\ &= -4j(1 + \frac{j}{8k_0\,\rho})\sqrt{2j}\lim_{\xi\to 1}\left[\sqrt{1-\xi^2}\,\frac{d}{d\xi}F(\xi)\right] \ , \end{aligned} \tag{4.19}$$

where use has been made of $\frac{d}{ds} = \frac{d\xi}{ds}\frac{d}{d\xi}$, and $\xi = 1 - js^2$; $\frac{d\xi}{ds} = -2js$. The transition function $\mathcal{F}(\alpha)$ is defined [19, 20]

$$\mathcal{F}(\alpha) = 2j\sqrt{\alpha}e^{j\alpha}\int_{\sqrt{\alpha}}^{\infty} e^{-j\tau^2}d\tau \ , \tag{4.20}$$

the analytical property of the transition function is also discussed in [19].

The function $F(\xi)$ can in general be represented as

$$F(\xi, z, z') = f(\xi)\frac{N(\xi, z, z')}{D(\xi)} \ , \tag{4.21}$$

where

$$\lim_{\xi\to 1}\left[\sqrt{1-\xi^2}\ f(\xi)\right] = 0 \ ; \ \lim_{\xi\to 1}\left[\sqrt{1-\xi^2}\,\frac{d}{d\xi}f(\xi)\right] = 0 \ . \tag{4.22}$$

thus

$$\begin{aligned} \lim_{\xi\to 1}\left[\sqrt{1-\xi^2}\,\frac{d}{d\xi}F(\xi, z, z')\right] &= \lim_{\xi\to 1}\sqrt{1-\xi^2}\,\left[\frac{f'(\xi)\,N(\xi, z, z') + f(\xi)\,N'(\xi, z, z')}{D(\xi)} - \right. \\ &\qquad \left. f(\xi)\,N(\xi, z, z')\,\frac{D'(\xi)}{D^2(\xi)}\right] \ , \\ &= \frac{f(1)}{D(1)}\left[\lim_{\xi\to 1}\sqrt{1-\xi^2}\,N'(\xi) - \frac{N(1, z, z')}{D(1)}\lim_{\xi\to 1}\sqrt{1-\xi^2}\,D'(\xi)_{|_{\xi=1}}\right] \ . \end{aligned} \tag{4.23}$$

Hence the uniform asymptotic representation of a grounded uniaxial anisotropic double layered dyadic Green's function can be constructed after incorporating (4.17) (in view of (4.18), (4.19), (3.39) - (3.42)) into (3.14) - (3.17), where $F_{g'}(\xi), F_{\mathcal{U}}(\xi), F_{\mathcal{W}}(\xi)$, and $F_{\mathcal{V}}(\xi)$ used in (4.18) and (4.19) are given in the following:

$$F_{g'}(\xi,z,z') = \frac{N_E^{\gtrless}(\xi,z,z')}{D_E(\xi)} \quad , \tag{4.24}$$

$$F_{\mathcal{U}}(\xi,z,z') = k_0\frac{\mu_{2,t}}{\kappa_2''}\frac{N_{tt,E}^{\gtrless}(\xi,z,z')}{D_E(\xi)} \quad , \tag{4.25}$$

$$F_{\mathcal{W}}(\xi,z,z') = \frac{k_0}{\xi^2}\left(\frac{\kappa_2'}{\epsilon_{2,t}}\frac{N_{tt,E}^{\gtrless}(\xi,z,z')}{D_E(\xi)} - \frac{\mu_{2,t}}{\kappa_2''}\frac{N_{tt,H}^{\gtrless}(\xi,z,z')}{D_H(\xi)}\right) \quad , \tag{4.26}$$

$$F_{\mathcal{V}}(\xi,z,z') = k_0^3\frac{\xi^2}{\kappa_2'}\frac{N_{zz,E}^{\gtrless}(\xi,z,z')}{D_E(\xi)} \quad , \tag{4.27}$$

and expressions for $N_{\substack{E\\H}}^{\gtrless}(1), \lim_{\xi\to 1}\left[\sqrt{1-\xi^2}\,\frac{d}{d\xi}N_{\substack{E\\H}}^{\gtrless}(\xi)\right], D_{\substack{E\\H}}(1), \lim_{\xi\to 1}\left[\sqrt{1-\xi^2}\,\frac{d}{d\xi}D_{\substack{E\\H}}(\xi)\right]$, and the residues of $\tilde{g}_{ij}^{'\gtrless}(z,z')$ and $\tilde{g}_{ij}^{''\gtrless}(z,z')$ are all given in Appendix C.

The uniform asymptotic closed form approxiamtion of the dyadic Green's function developed here has been cast in such a form that the physical behavior of the electromagnetic fields due to anisotropy of the medium reveals itself through a simple mathematical parameters (see also Appendic C). Moreover, the asymptotic solution of each of the $g(\mathbf{r},\mathbf{r}')$, $\mathcal{U}(\mathbf{r},\mathbf{r}')$, $\mathcal{W}(\mathbf{r},\mathbf{r}')$, and $\mathcal{V}(\mathbf{r},\mathbf{r}')$ consists of the contribution of the space wave (the saddle ponit contribution), surface waves, leaky waves (if any), and the transitoin effects of the surface and leaky wave poles which are close to the saddle point. Thus, the physical understanding of the interaction of the spatially confined source with an anisotropic (uniaxial) double-layered grounded slab is greatly enhanced through the newly developed asymptotic closed form representation of the dyadic Green's function.

Becuase there are infinite number of leaky wave poles in the bottom sheet of the Sommerfeld plane; the question may arise which poles should be cosiderd close to the saddle point. For the loss-less case, there are two sets of leaky wave poles on the bottom sheet of the Sommerfeld plane; the complex poles and the real poles. During the investigation it is found that the inclusion of the real poles[1], which may be called improper surface wave poles [20, 23, 24], (because they are the same species as of surface wave poles lying on the

[1] They are lying on the positive imaginary axis of ζ plane, the radially propagating plane.

bottom sheet of the Sommerfeld plane), would be sufficient for achieving a good accuracy for the asymptotic representation.

In fact the proper surface wave poles are originally improper surface waves [20, 24]; of course except for the first TM (E-mode) surface wave mode which is always present independent of material properties and thicknesses of the layers. As the materials become more dense and/or the substrates become electrically thicker, an improper surface wave pole moves toward the brach point, and it eventually passes through the branch point and appears in the upper sheet of the Sommerfeld plane; and hence, it becomes a proper surface wave pole. It is easy to verify that the condition for any surface wave mode to "turn-on" is $\xi_p = 1.0$, (note that the variable ξ has been normalized with respect to k_0). From (C.12) for TM (E-mode), one will have

$$D_E(\xi_p)_{|_{\xi_p=1.0}} = 0 \quad , \tag{4.28}$$

or

$$\frac{L_1'}{\epsilon_{1,t}\bar{d}_1} \tan L_1' = -\frac{L_2'}{\epsilon_{2,t}\bar{d}_2} \tan L_2' \quad , \tag{4.29}$$

where $L_i' = \bar{d}_i\sqrt{n_i - n_i'}, n_i = \mu_{i,t}\,\epsilon_{i,t}, n_i' = \frac{\epsilon_{i,t}}{\epsilon_{i,s}}$, and $\bar{d}_i = k_0\, d_i$. By the same token, from (C.34) for TE (H-mode), one will have

$$D_H(\xi_p)_{|_{\xi_p=1.0}} = 0 \quad , \tag{4.30}$$

or

$$\frac{L_1''}{\mu_{1,t}\bar{d}_1} \tan L_1'' = \frac{L''}{\mu_{2,t}\bar{d}_2} \cot L_2'' \quad , \tag{4.31}$$

where $L_i'' = \bar{d}_i\sqrt{n_i - n_i''}$, and $n_i'' = \frac{\mu_{i,t}}{\mu_{i,s}}$.

Simillar equations for the isotropic case have already been reported by Alexopoulos and Jackson [25]. Equations (4.29) and (4.31) respectively represent parametric conditions for any TM and TE surface wave modes to turn-on. The loci of these equations for the isotropic case have been studied by Marin and Pathak [26]. It is evident that by controlling different parameters invloved in (4.29) and (4.31), one can excite or suppress a certain number of poles. A complete elimination of the surface wave excitation is also possible if one lets $\kappa_2'(\xi_p) = 0$ for TM (E-mode), and $\kappa_2''(\xi_p) = 0$ for TE (H-mode). This is due to the fact that since there is no variation of the surface wave modes in z-direction with these conditions, and the tangential electric field must vanish on a perfectly conducting ground plane; by reciprocity this impies that these modes are not excited [25].

It is also important to realize that because the proper and improper surface wave poles are lying on the real axis of the Sommerfeld plane (positive imaginary axis of the radially propagating plane), they can easily be found[2]; and hence, rendering to the efficeincy of the newly developed asymptotic solution.

In the following chapter the accuracy and the efficiency of the asymptotic solution as a function of lateral separation of the soure and observation points with different material parameters and thicknesses.

[2]A Newton-Raphson search procedure with a good initial guess can be employed to find the poles in a few iterations.

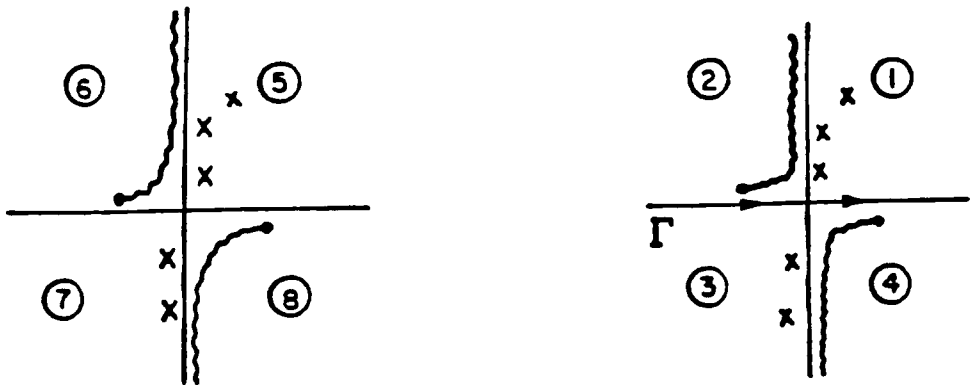

$Im(\sqrt{1-\zeta^2}) > 0$ $Im(\sqrt{1-\zeta^2}) < 0$

Figure 4.1: Two sheeted ζ plane. First sheet, $Im(\sqrt{1-\zeta^2}) < 0$; and the second sheet, $Im(\sqrt{1-\zeta^2}) > 0$.

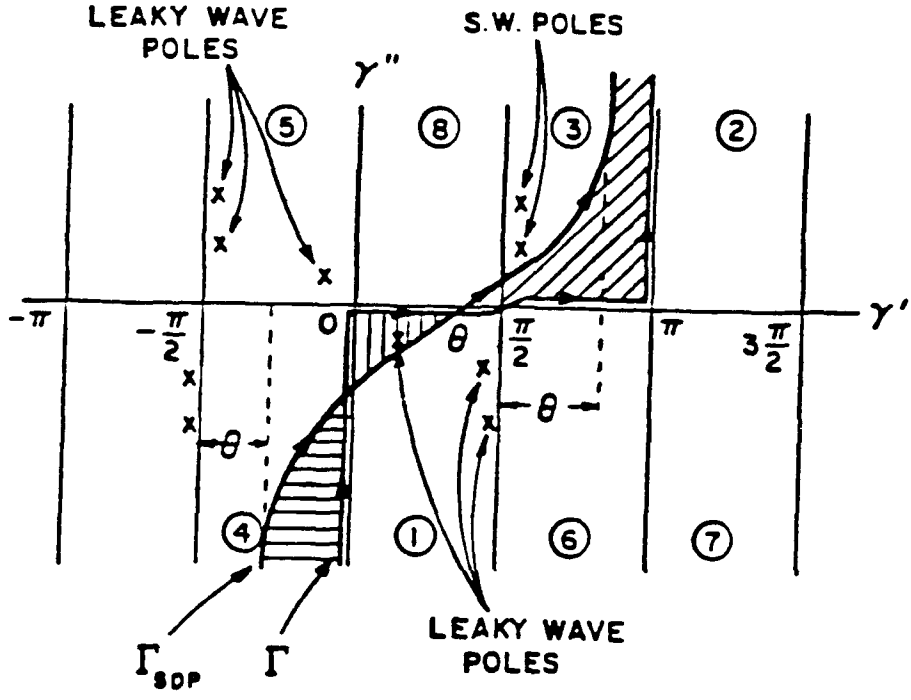

Figure 4.2: Angular spectrum mapping where $\zeta = cos\gamma$; the leaky and surface wave poles and the contour of integration Γ and Γ_{SDP}

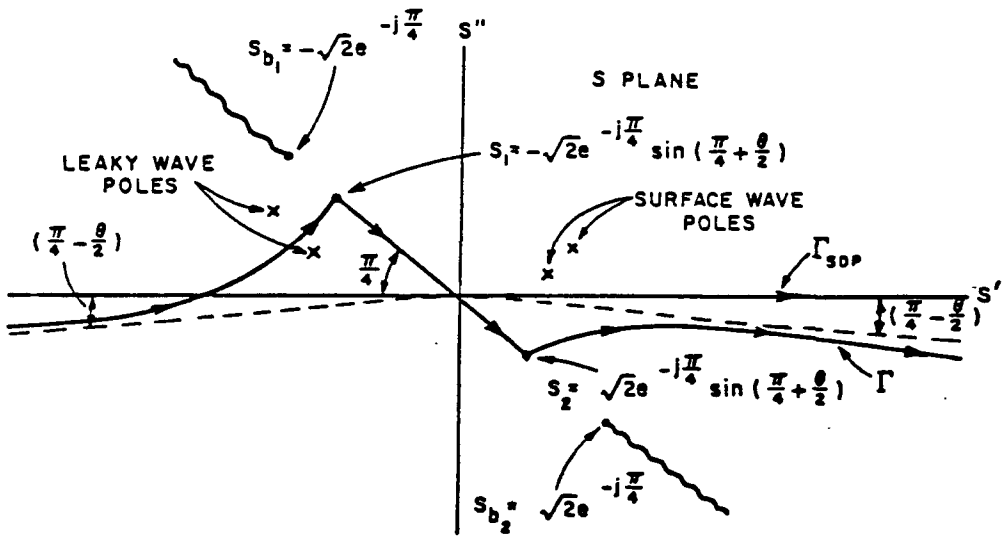

Figure 4.3: Complex s plane, original path Γ maps on solid curve, the SDP maps onto the real axis $(-\infty < s < -\infty)$, the saddle point $\gamma_s = \theta$, and branch points at $s_{b_{12}} = \pm\sqrt{2}e^{-j\pi/4}(\sqrt{s^2 + 2j} = 0)$.

Chapter 5

Numerical Results

Figure 5.1 shows the typical behavior of the integrand of the function $\mathcal{W}$ of (3.31) for $\rho/\lambda_0 = 0.1$ versus ξ as $|z - z'| \to 0$. The integrand is an oscillatory function (typical behavior of the Bessel function), and decays very slowly. Figure 5.2 shows the numerical behavior of the integrand of $\mathcal{W}$ of (3.33) for $\rho/\lambda_0 = 0.1$ as $|z - z'| \to 0$ when the singularity of the integrand is removed. The significance of the singularity removal technique is vivid if one compares the smoothness of the plots in Figures 5.1 and 5.2 for $\rho/\lambda_0 = 0.1$. It is now evident that (for the small lateral separation) the method of singularity removal technique can efficiently be utilized to evaluate the dyadic Green's function. Nevertheless as the lateral separation of the source and observation points increases ($k_0\rho$ becomes large) the integrand starts to oscillate. Figure 5.3 shows the typical behavior of the integrand of $\mathcal{W}$ of (3.33) for $\rho/\lambda_0 = 4.7$. This oscillation is due to rapid growth of the argument of the Bessel function which causes the method to lose its efficiency. This is the main difficulty of the singularity removal technique which motivates us to construct the alternative radial propagation representation of the dyadic Green's function. Figures 5.4 and 5.5 show a typical behavior of the integrand of $\mathcal{W}$ of (3.46) as a function of its argument ξ for different lateral distances ρ/λ_0 =0.5, and 2.0. It is important to note that as the separation between the source and observation points increases, the infinite integral decays faster, but the number of oscillations in the finite integrals increases. This can be seen from Figure 5.5. These oscillation are due to the behavior of the Hankel function as its argument becomes larger. It is interesting to note that in the Sommerfeld representation, the total number of oscillation of the integrand between 0 and 1 of its semi-infinite interval of integration are the same as the number of oscillations of the integrand of the radial propagation representation which exist only over the finite limits from 0 to 1.0. Over the rest of the interval of the integration from 1.0 to infinity, however, the Sommerfeld integrand exhibits an infinite number of oscillations; no such oscillations exist for the radial propagation representation. The advantage of the radial propagation representation against the Sommerfeld representation is now apparent.

Figures 5.6-5.13 show the numerical integration and the closed form asymptotic representation of $\mathcal{W}$ given in (4.17) versus ρ/λ_0 for various substrate and superstrates thicknesses with high and low material constants and various degree of anisotropy. The numerical values of these parameters are given in the captions of the Figures. The accuracy of the new

representation is quite impressive. This new asymptotic solution remains valid for the field points very close to the source. The efficiency and hence its usefulness of the new asymptotic expansion is now clear. The error bound of the solution is less than one to five percent for lateral separations between the source and field points as small as 0.5-1.0 of free space wavelength. Also it is note worthy that as the lateral separation of the source and observation increases, the computational time for the numerical integration also increases. This time increase is due to rapid growth of the argument of the Bessel and Hankel functions which are present in the integrand. Nevertheless, the computational time for the asymptotic representation remains constant since no Sommerfeld type integral is involved in this solution; and moreover, the accuracy of the asymptotic solution improves as the lateral separation of the source and observation point increases.

As expected, it is found that the accuracy of the new representation, particularly for small lateral separation of the source and observation points, indeed depends on the material thicknesses and parameters. In the case of thin slabs with low material parameters, the dominant effect is due to space waves arising from the saddle point contribution, whereas for thick and dense material constants, the dominant effect is due to the surface waves. For the uniform asymptotic approximation only one TM surface wave pole to be considered close to the saddle point for thin and low-dense material slabs. For thicker and/or more dense material slabs, a TE improper surface wave pole also comes close to saddle point, and as discussed in the previous chapter, when a certain condition met, (see (4.31)), the TE improper surface pole eventually becomes the first TE proper surface wave. In most practical applications, the uniform asymptotic dyadic Green's function needs one TM surface wave and one TE proper or improper surface wave pole singularities close to the saddle point. It is noted that the improper surface poles are located on the positive imaginary axis of the ζ plane (radially propagating plane), which are the same improper surface wave poles lying on the positive real axis of the bottom sheet of the original Sommerfeld plane.

The accuracy of the uniform asymptotic representations of $g(\mathbf{r}, \mathbf{r}')$, $\mathcal{U}(\mathbf{r}, \mathbf{r}')$, and $\mathcal{V}(\mathbf{r}, \mathbf{r}')$ have been tested, and they are at least as accurate as of $\mathcal{W}(\mathbf{r}, \mathbf{r}')$. Those results have not been reported here.

A comparison between the numerical and asymptotic evaluation of electric fields, E_x, E_y, of an electric point current parallel to the interface (horizontally oriented) over the dielectric interface for the grounded double-layered anisotropic uniaxial slab versus ϕ at $\rho = 0.5\lambda_0$ are shown in Figures 5.14 - 5.17. It can be seen from the figures that the accuracy of the asymptotic representation is quite accurate and remains valid even for the field points very close to the source.

With the new asymptotic solution the effect of the material anisotropy over the field components can easily be investigated. The parameters $n_i' = \frac{\epsilon_{i,z}}{\epsilon_{i,t}}$, and $n_i'' = \frac{\mu_{i,z}}{\mu_{i,t}}$ represent the degree of anisotropy of the material, and can have any value in complex plane. It should be noted that as n_i' and n_i'' go to one the material becomes isotropic. Also if the thickness of the first layer goes to zero, or its material parameters approach to the free space constitutive parameters the solution will give the dyadic Green's function for a single

layer grounded anisotropic uniaxial slab.

The effect of the anisotropy on the $\mathcal{W}(\mathbf{r}, \mathbf{r}')$, can be seen if one compares the plots of Figure 5.6 (for the isotropic case), and Figure 5.7 (for $n_1' = n_2' = 1.5$), and Figure 5.8 (for $n_1' = n_2' = 0.75$). It seems that the strength of the field increases as the value of n_i' decreases. Similar conclusion can be drawn from the plots of the surface electric fields of shown in Figures 5.14 - 5.16.

More numerical results and the physical interpretations based on the newly developed closed form asymptotic representation of the dyadic Green's function for a double-layered anisotropic uniaxial grounded slab will be reported in the second phase of this research.

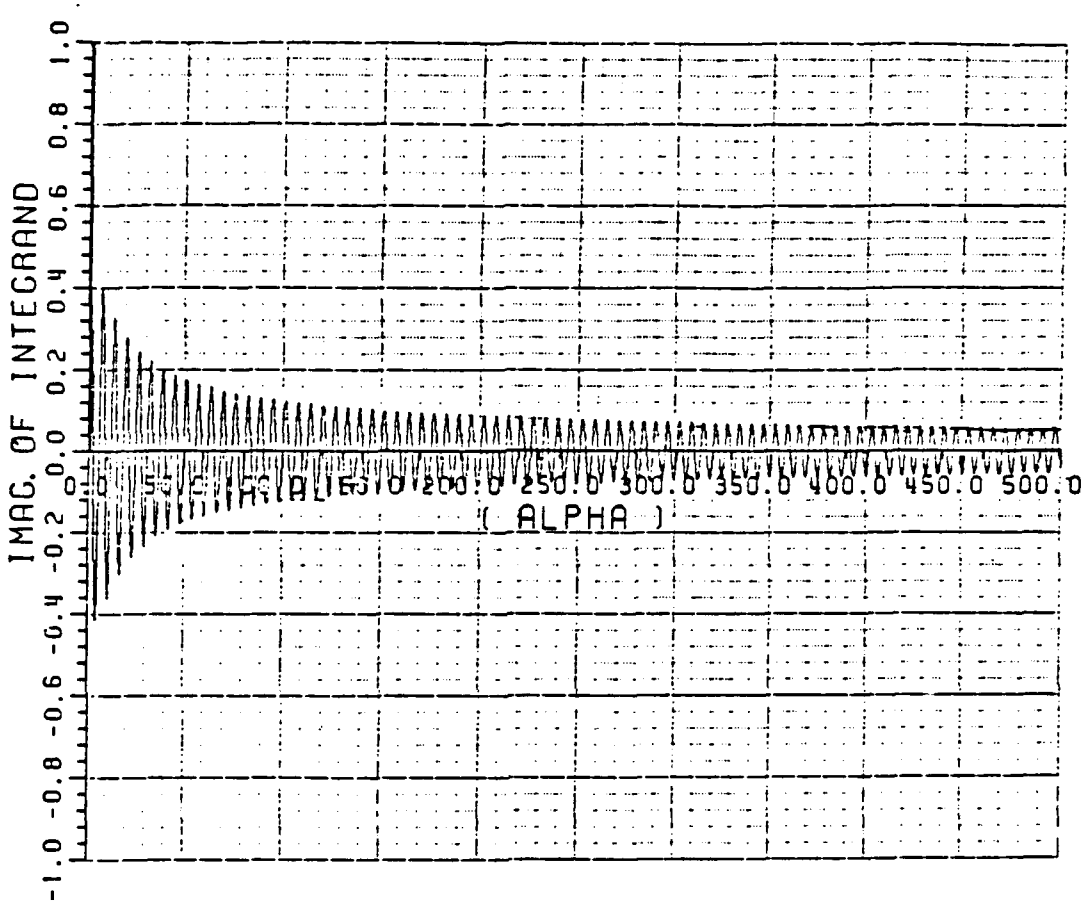

$\xi \equiv$ ALPHA

$\rho = 0.1\ \lambda_0$

Figure 5.1: Behavior of the integrand of the Sommerfeld type integral of $\mathcal{W}$ (3.31) for $\rho/\lambda_0 = 0.1$ versus ξ as $|z - z'| \to 0$.

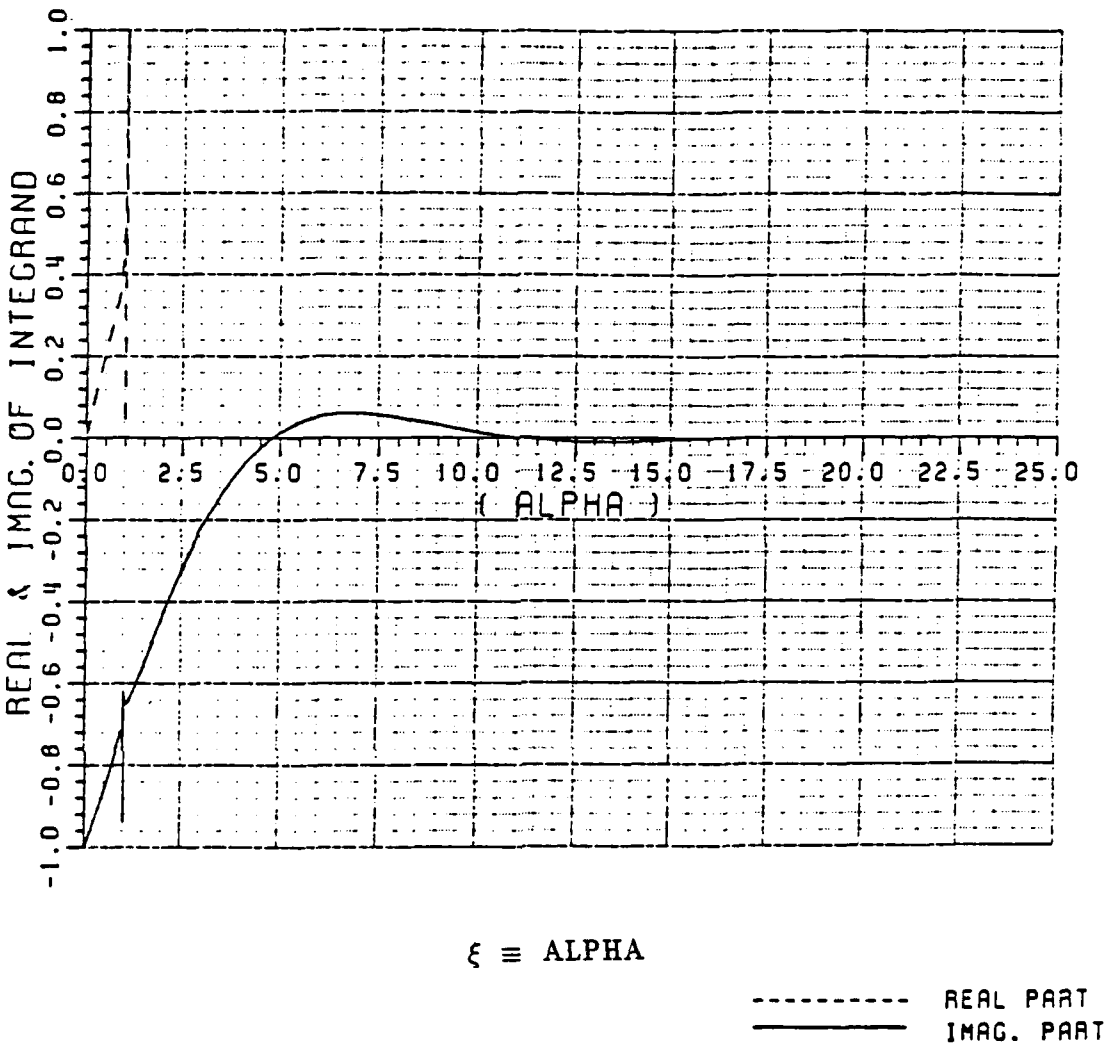

$\xi \equiv$ ALPHA

$\rho = 0.1\ \lambda_0$

Figure 5.2: Behavior of the integrand of the Sommerfeld type integral of $\mathcal{W}$ in (3.33) for $\rho/\lambda_0 = 0.1$ versus ξ as $|z - z'| \to 0$, when the singularity removel technique is employed

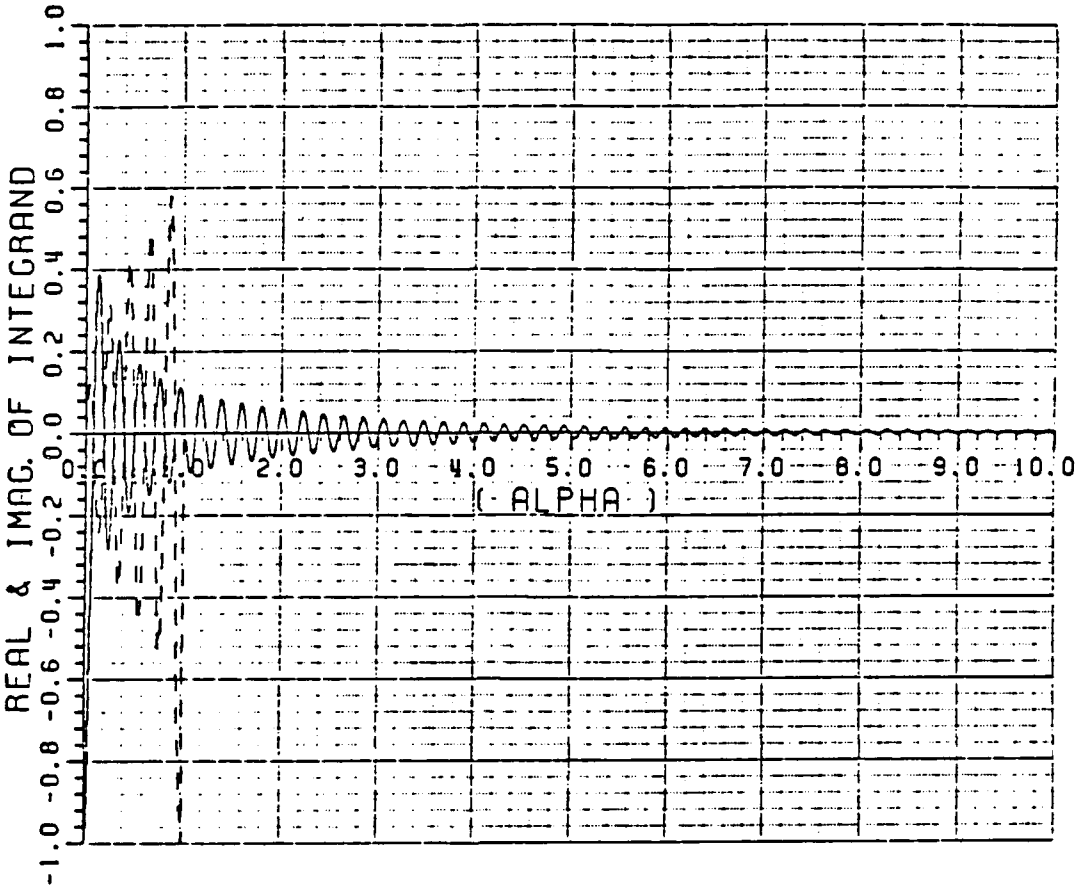

$\xi \equiv$ ALPHA

---------- REAL PART
———————— IMAG. PART

$\rho = 4.7\ \lambda_0$

Figure 5.3: Behavior of the integrand of the Sommerfeld type integral of $\mathcal{W}$ in (3.33) for $\rho/\lambda_0 = 4.7$ versus ξ as $|z - z'| \to 0$, when the singularity removel technique is employed

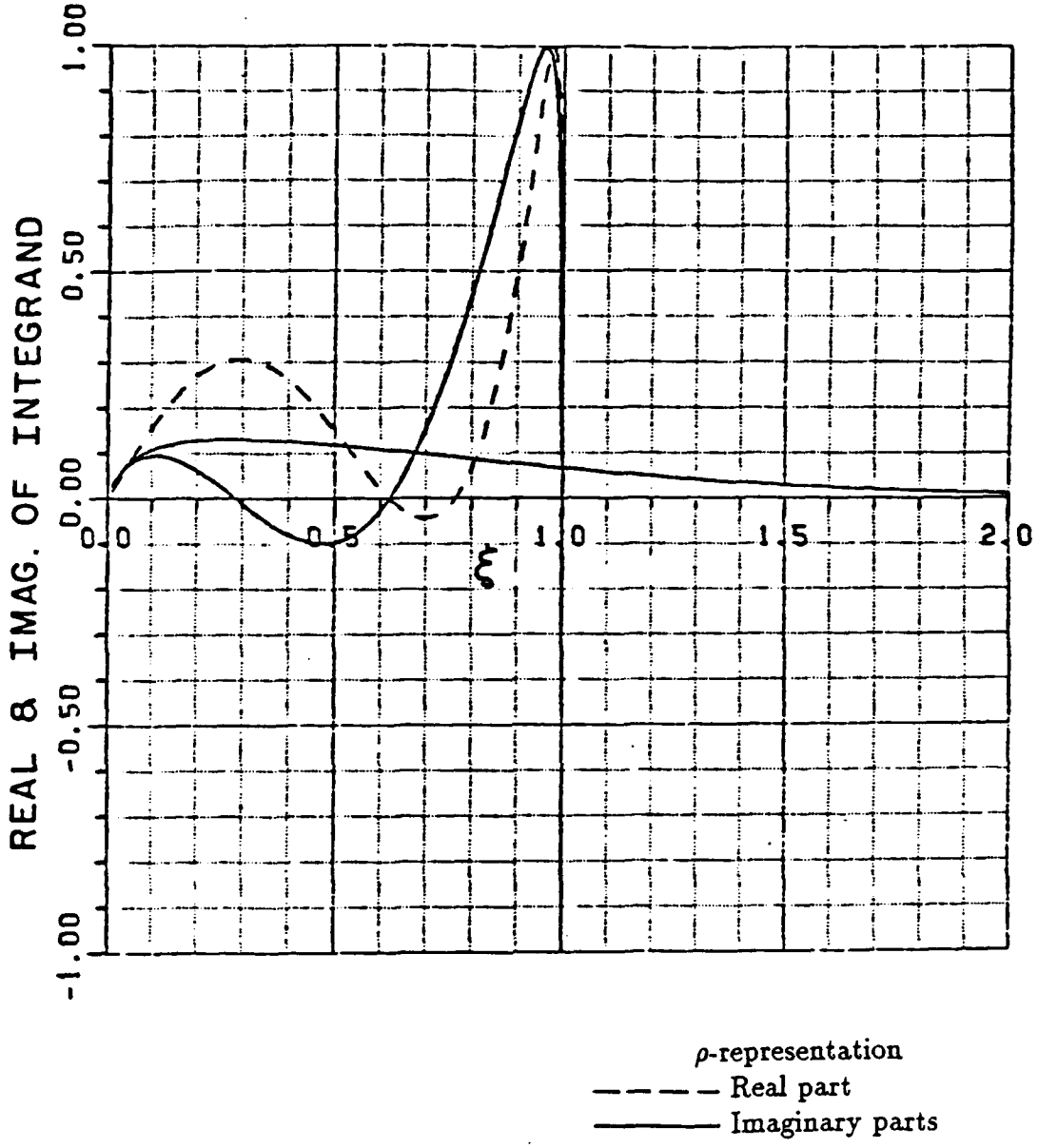

Figure 5.4: Behavior of the integrand of the radially propagating type integral of $\mathcal{W}$ in (3.46) for $\rho/\lambda_0 = 0.5$ versus ξ as $|z - z'| \to 0$.

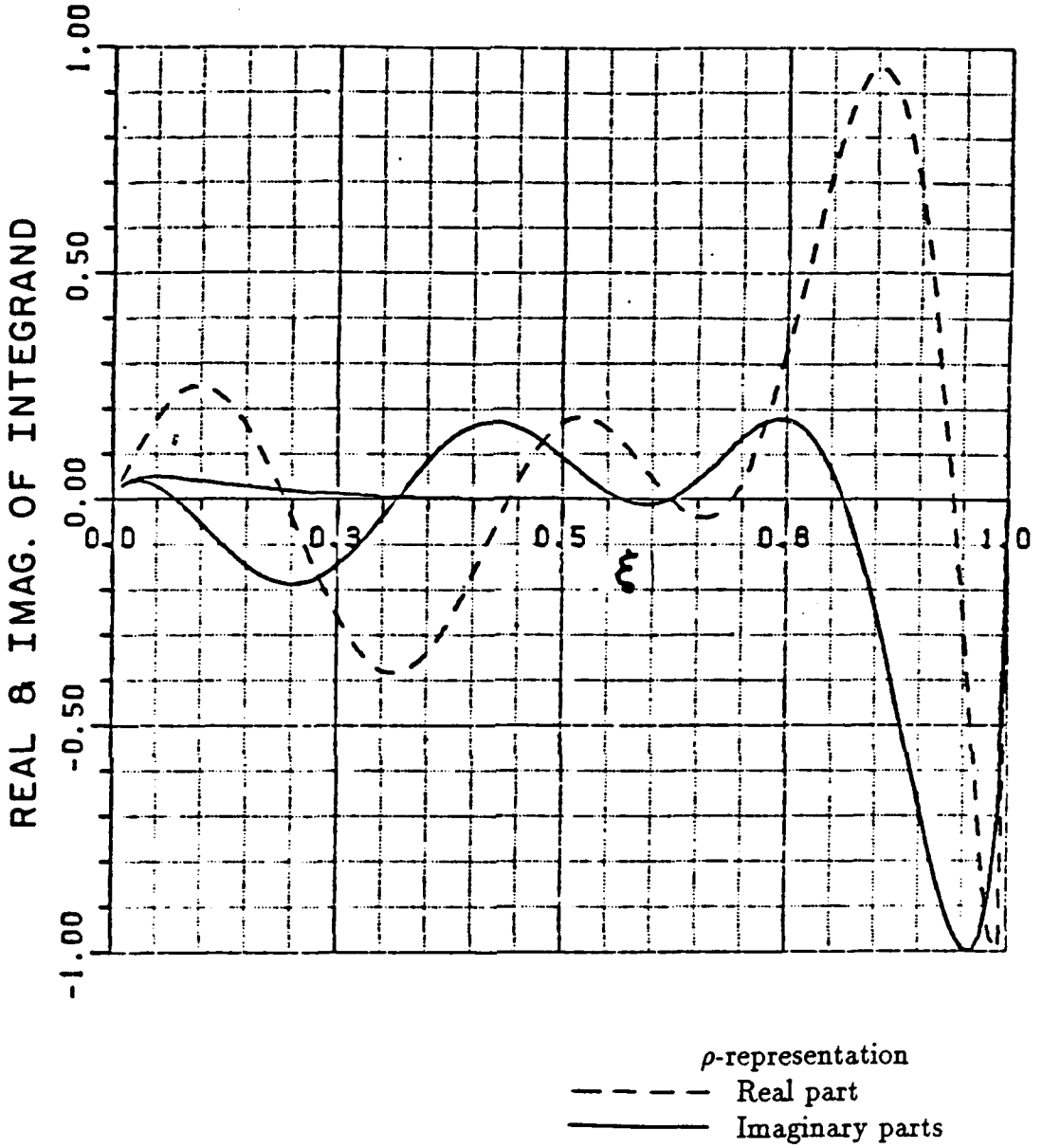

Figure 5.5: Behavior of the integrand of the radially propagating type integral of $\mathcal{W}$ in (3.46) for $\rho/\lambda_0 = 2.0$ versus ξ as $|z - z'| \to 0$.

$d_1/\lambda_0 = 0.05, \epsilon_{1,t} = 2.25, \epsilon_{1,t}/\epsilon_{1,z} = 1.0, \mu_{1,t} = 1.0, \mu_{1,t}/\mu_{1,z} = 1.0$
$d_2/\lambda_0 = 0.05, \epsilon_{2,t} = 3.25, \epsilon_{2,t}/\epsilon_{2,z} = 1.0, \mu_{2,t} = 1.0, \mu_{2,t}/\mu_{2,z} = 1.0$

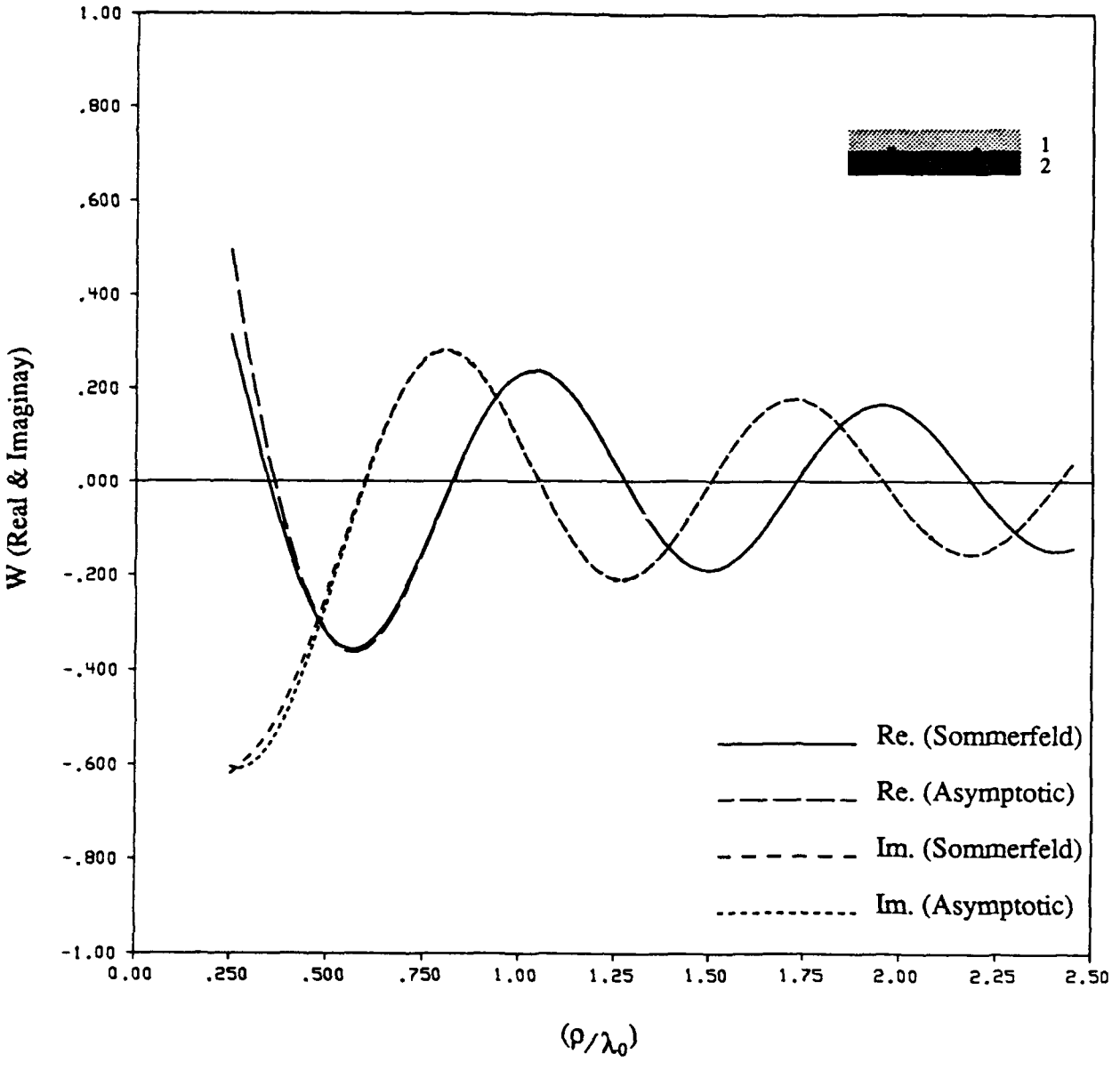

Figure 5.6: Comparison between the numerical integration and asymptotic value of $\mathcal{W}$ versus ρ/λ_0 in (4.17) for $|z - z'| \to 0$.

$$d_1/\lambda_0 = 0.05, \epsilon_{1,t} = 2.25, \epsilon_{1,t}/\epsilon_{1,z} = 1.5, \mu_{1,t} = 1.0, \mu_{1,t}/\mu_{1,z} = 1.0$$
$$d_2/\lambda_0 = 0.05, \epsilon_{2,t} = 3.25, \epsilon_{2,t}/\epsilon_{2,z} = 1.5, \mu_{2,t} = 1.0, \mu_{2,t}/\mu_{2,z} = 1.0$$

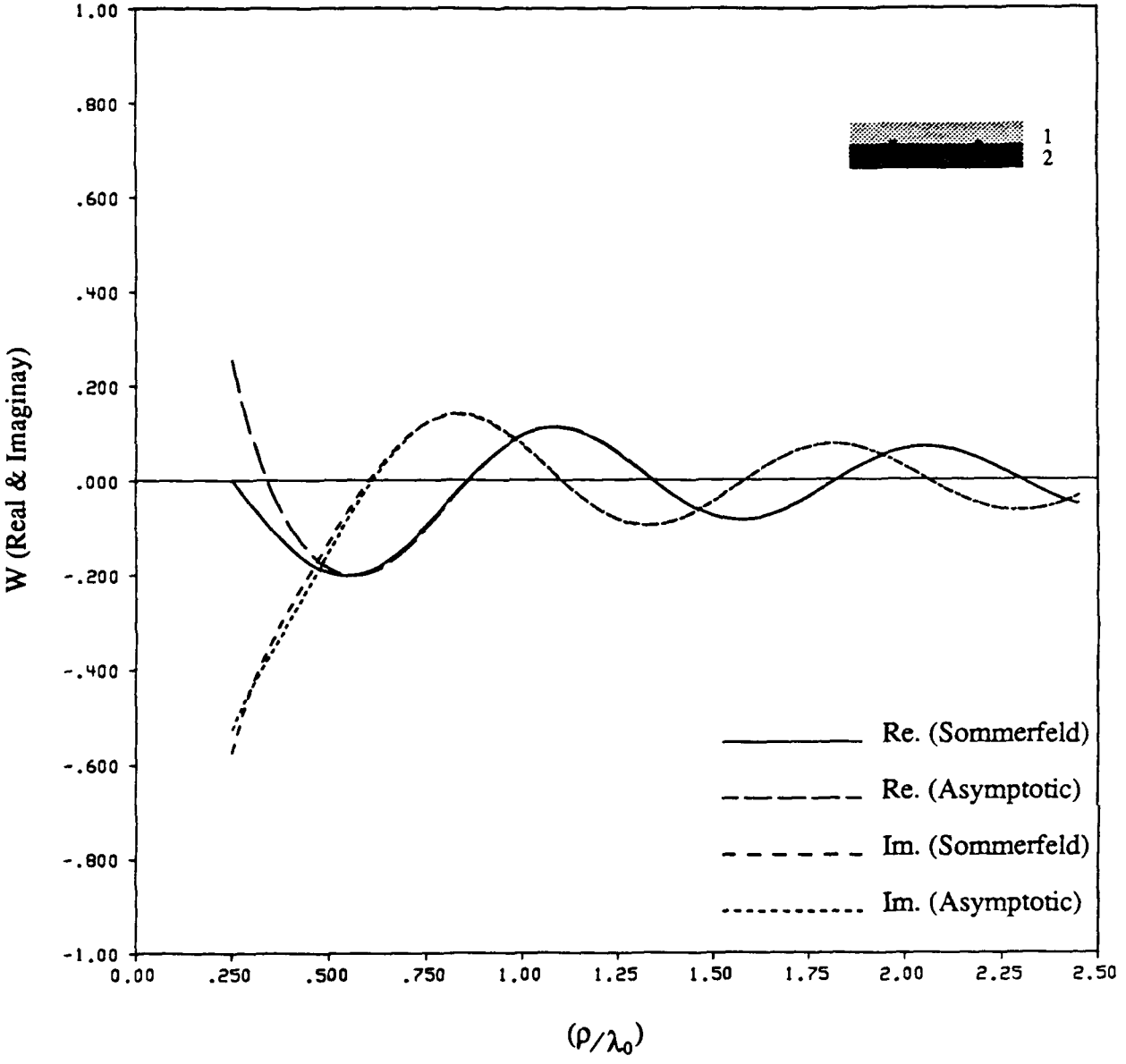

Figure 5.7: Comparison between the numerical integration and asymptotic value of $\mathcal{W}$ versus ρ/λ_0 in (4.17) for $|z - z'| \to 0$.

$$d_1/\lambda_0 = 0.05, \epsilon_{1,t} = 2.25, \epsilon_{1,t}/\epsilon_{1,z} = 0.75, \mu_{1,t} = 1.0, \mu_{1,t}/\mu_{1,z} = 1.0$$
$$d_2/\lambda_0 = 0.05, \epsilon_{2,t} = 3.25, \epsilon_{2,t}/\epsilon_{2,z} = 0.75, \mu_{2,t} = 1.0, \mu_{2,t}/\mu_{2,z} = 1.0$$

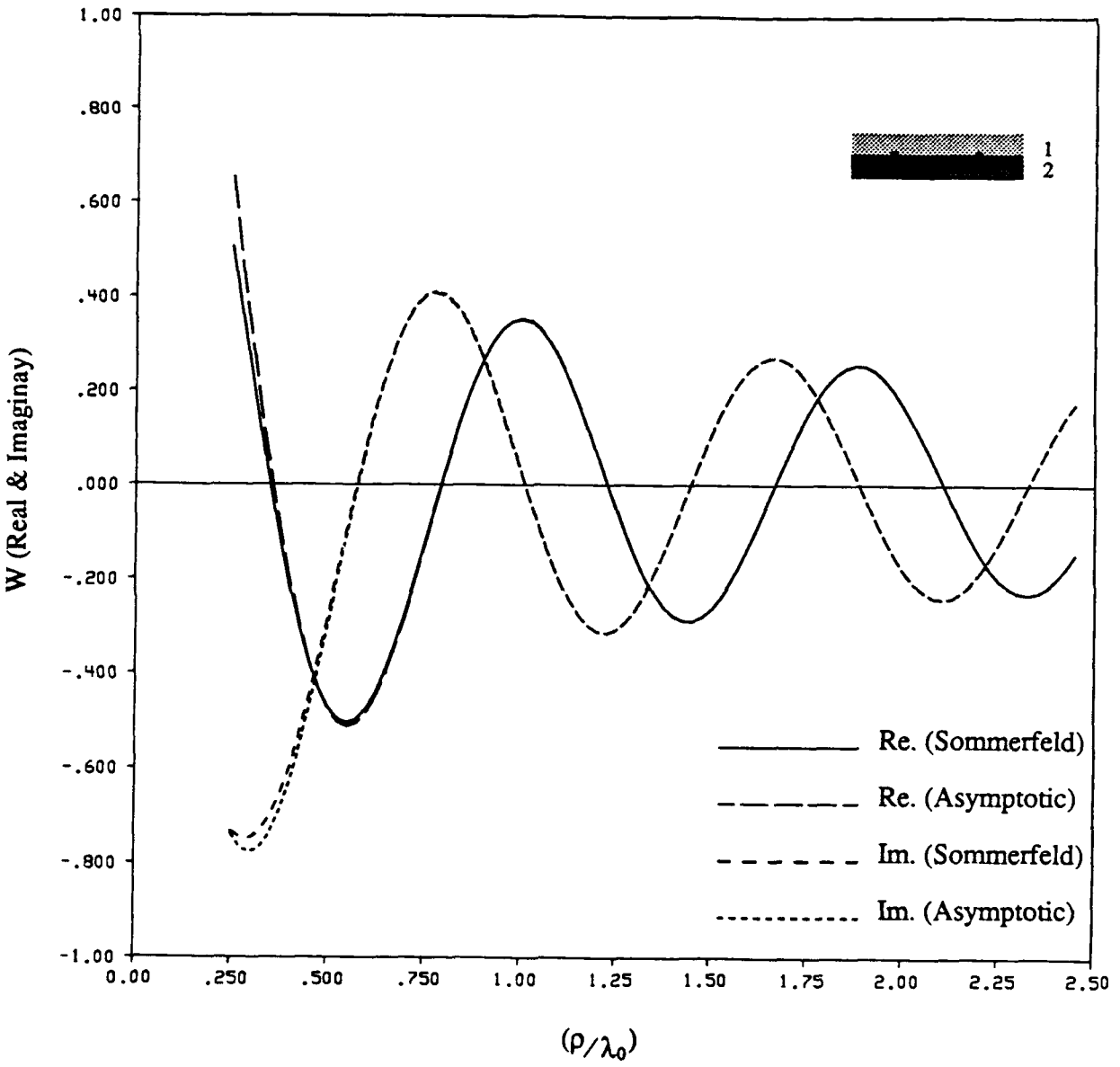

Figure 5.8: Comparison between the numerical integration and asymptotic value of $\mathcal{W}$ versus ρ/λ_0 in (4.17) for $|z - z'| \to 0$.

$d_1/\lambda_0 = 0.05, \epsilon_{1,t} = 3.25, \epsilon_{1,t}/\epsilon_{1,z} = 1.0, \mu_{1,t} = 1.0, \mu_{1,t}/\mu_{1,z} = 1.0$
$d_2/\lambda_0 = 0.03, \epsilon_{2,t} = 9.60, \epsilon_{2,t}/\epsilon_{2,z} = 1.0, \mu_{2,t} = 1.0, \mu_{2,t}/\mu_{2,z} = 1.0$

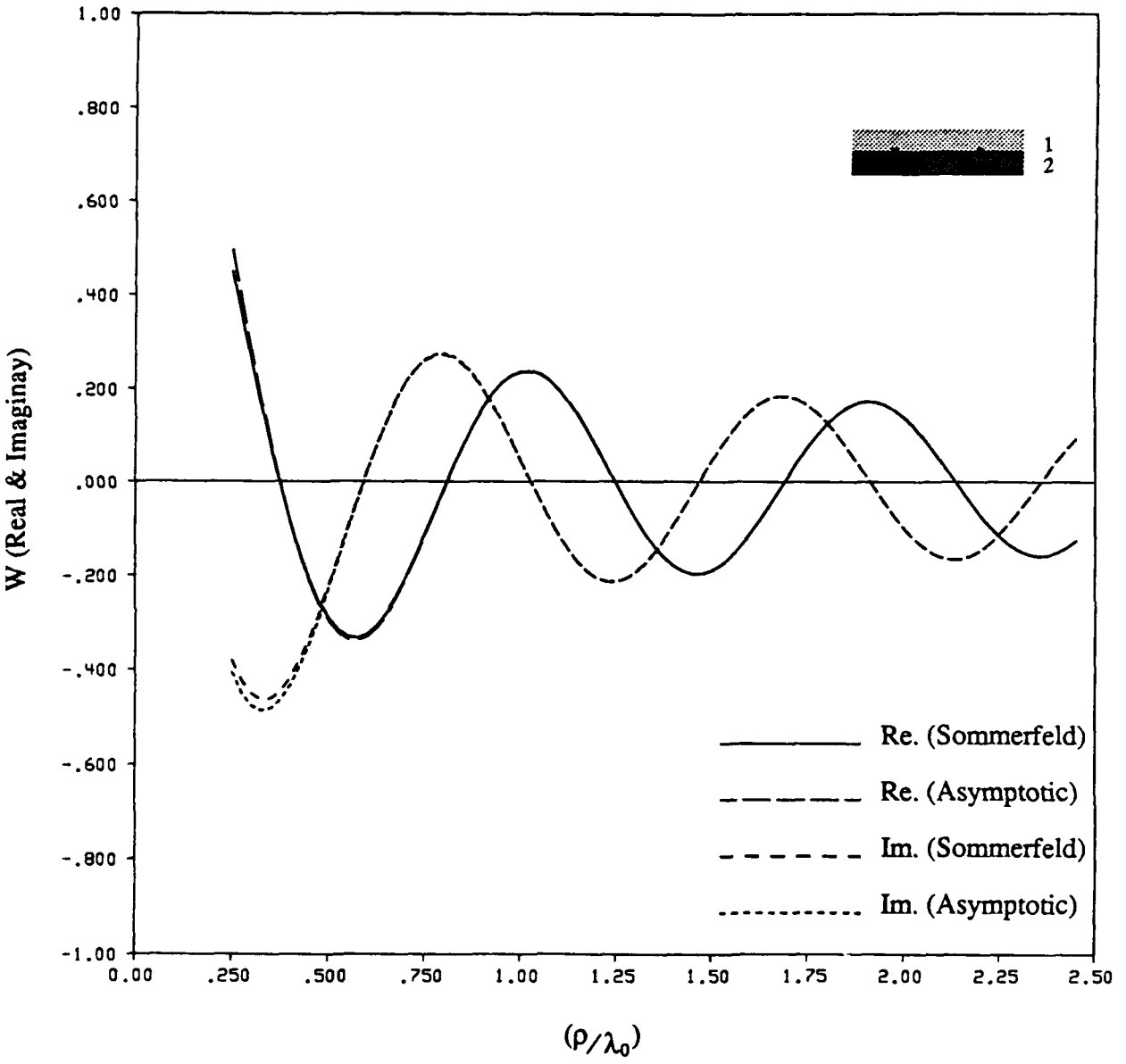

Figure 5.9: Comparison between the numerical integration and asymptotic value of $\mathcal{W}$ versus ρ/λ_0 in (4.17) for $|z - z'| \to 0$.

$$d_1/\lambda_0 = 0.05, \epsilon_{1,t} = 3.25, \epsilon_{1,t}/\epsilon_{1,z} = 1.5, \mu_{1,t} = 1.0, \mu_{1,t}/\mu_{1,z} = 1.0$$
$$d_2/\lambda_0 = 0.03, \epsilon_{2,t} = 9.60, \epsilon_{2,t}/\epsilon_{2,z} = 0.9, \mu_{2,t} = 1.0, \mu_{2,t}/\mu_{2,z} = 1.0$$

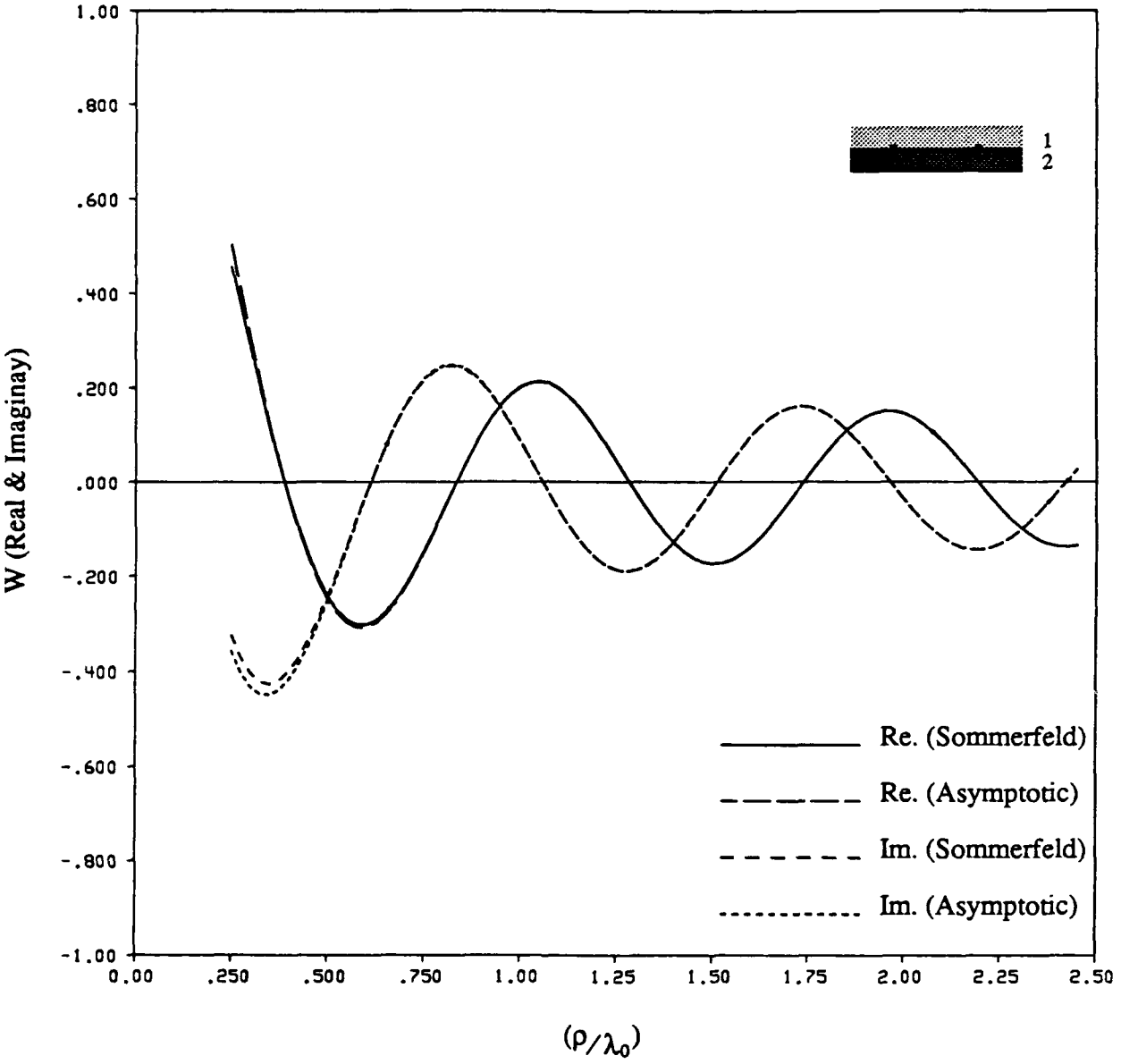

Figure 5.10: Comparison between the numerical integration and asymptotic value of $\mathcal{W}$ versus ρ/λ_0 in (4.17) for $|z - z'| \to 0$.

$$d_1/\lambda_0 = 0.05, \epsilon_{1,t} = 3.25, \epsilon_{1,t}/\epsilon_{1,z} = 0.5, \mu_{1,t} = 1.0, \mu_{1,t}/\mu_{1,z} = 1.0$$
$$d_2/\lambda_0 = 0.03, \epsilon_{2,t} = 9.60, \epsilon_{2,t}/\epsilon_{2,z} = 0.5, \mu_{2,t} = 1.0, \mu_{2,t}/\mu_{2,z} = 1.0$$

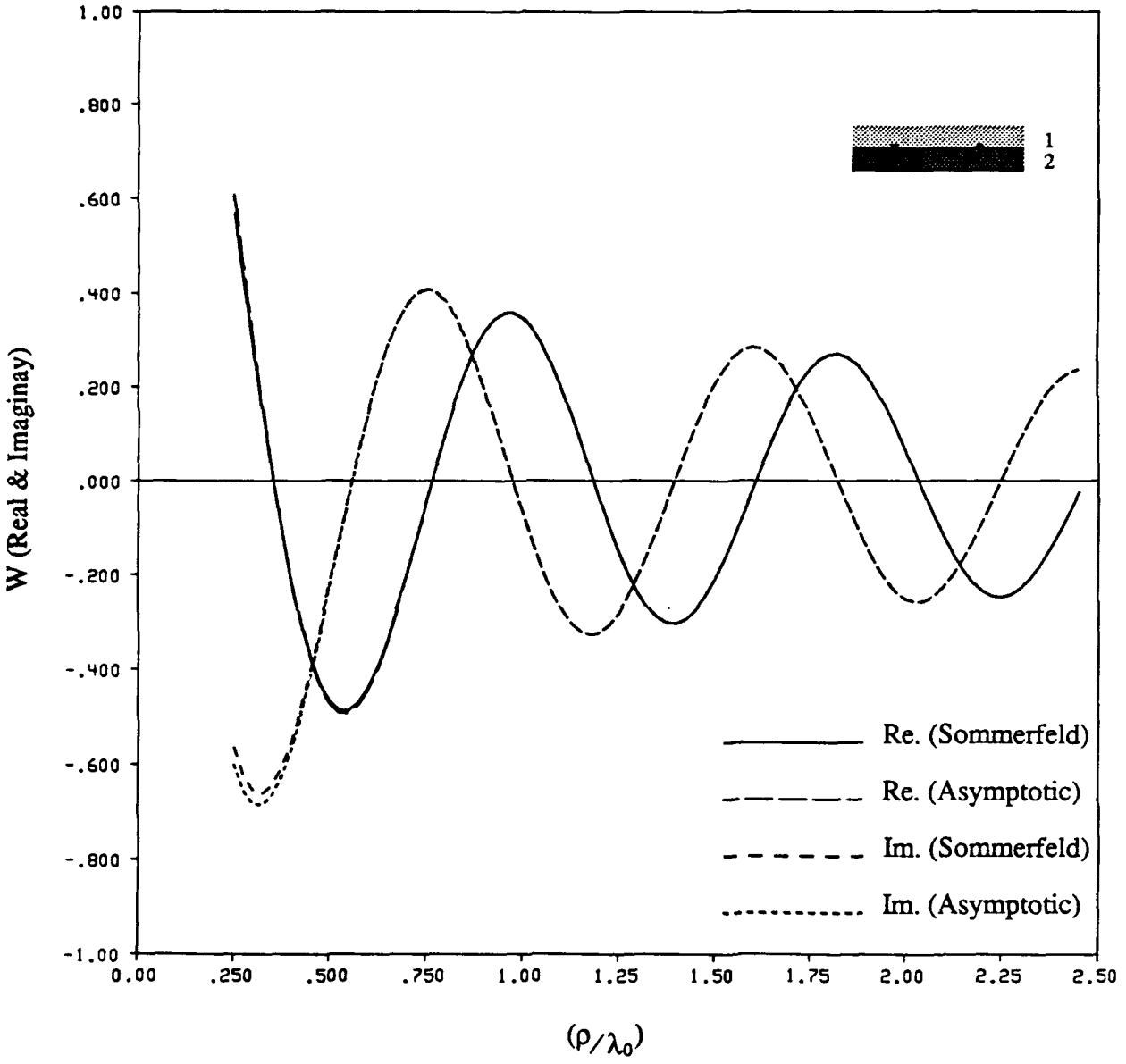

Figure 5.11: Comparison between the numerical integration and asymptotic value of $\mathcal{W}$ versus ρ/λ_0 in (4.17) for $|z - z'| \to 0$.

$$d_1/\lambda_0 = 0.05, \epsilon_{1,t} = 3.25, \epsilon_{1,t}/\epsilon_{1,z} = 1.0, \mu_{1,t} = 1.0, \mu_{1,t}/\mu_{1,z} = 1.0$$
$$d_2/\lambda_0 = 0.03, \epsilon_{2,t} = 2.25, \epsilon_{2,t}/\epsilon_{2,z} = 1.0, \mu_{2,t} = 1.0, \mu_{2,t}/\mu_{2,z} = 1.0$$

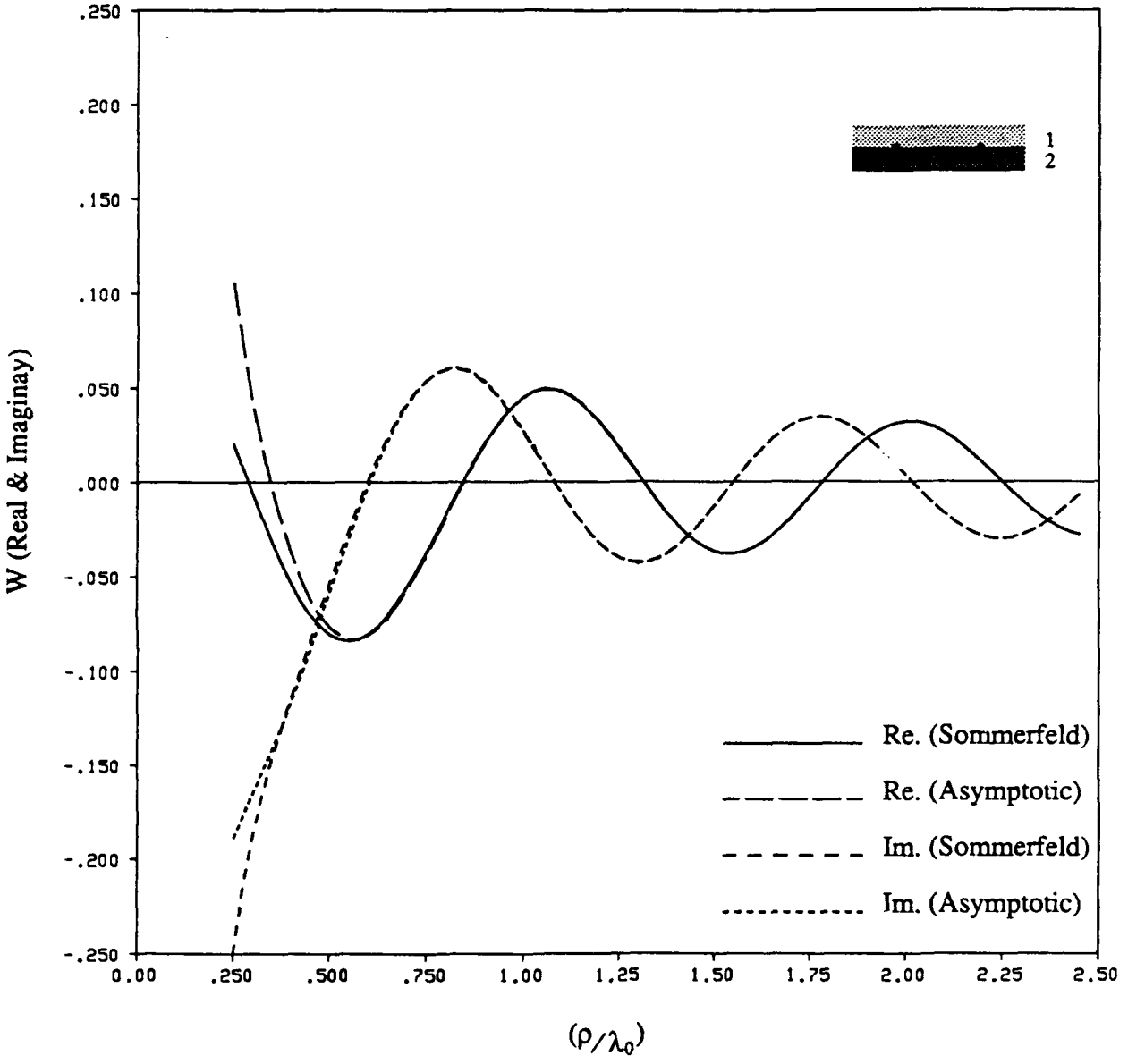

Figure 5.12: Comparison between the numerical integration and asymptotic value of $\mathcal{W}$ versus ρ/λ_0 in (4.17) for $|z - z'| \to 0$.

$$d_1/\lambda_0 = 0.03, \epsilon_{1,t} = 2.25, \epsilon_{1,t}/\epsilon_{1,z} = 1.0, \mu_{1,t} = 1.0, \mu_{1,t}/\mu_{1,z} = 1.0$$
$$d_2/\lambda_0 = 0.06, \epsilon_{2,t} = 9.60, \epsilon_{2,t}/\epsilon_{2,z} = 1.0, \mu_{2,t} = 1.0, \mu_{2,t}/\mu_{2,z} = 1.0$$

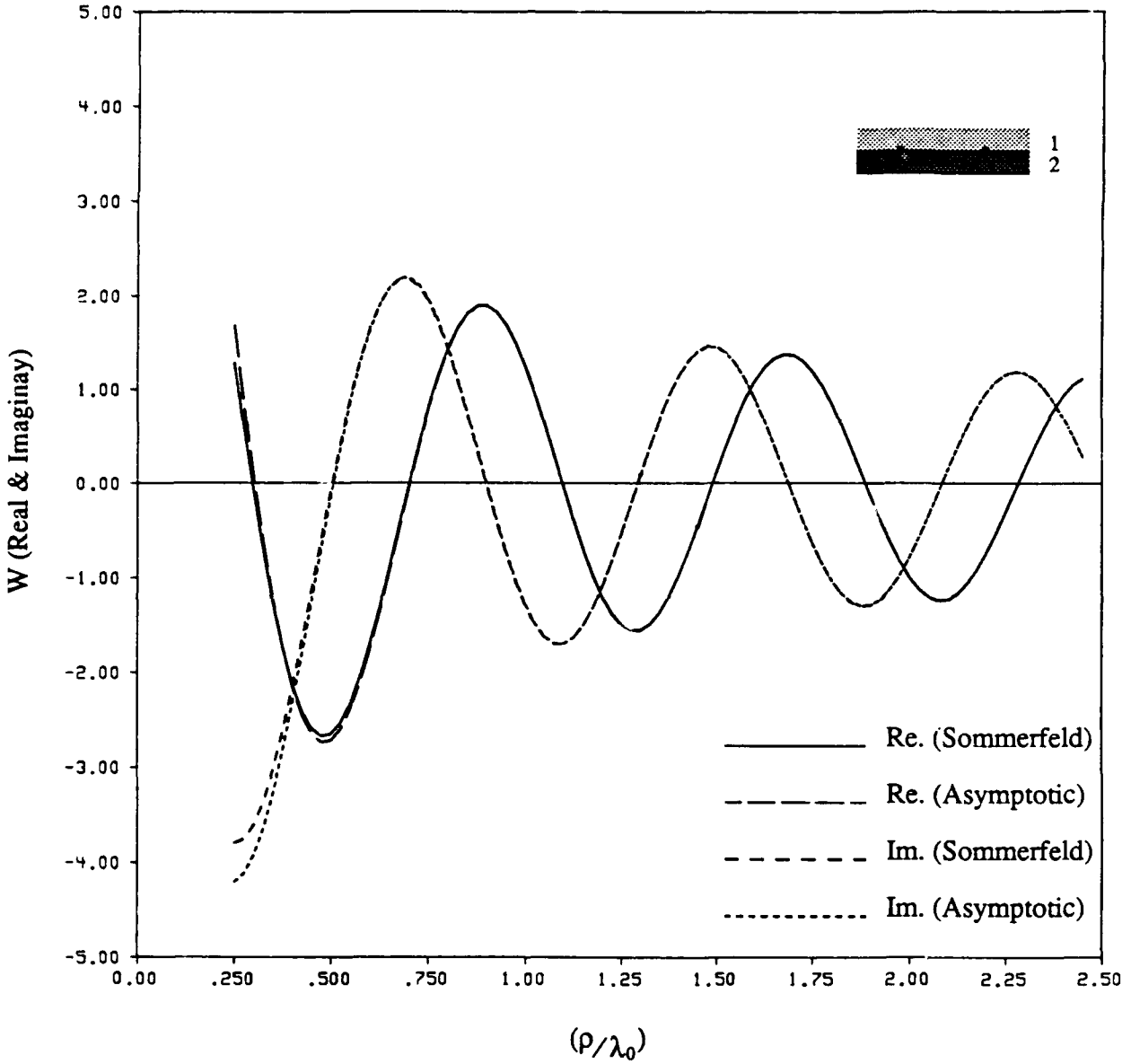

Figure 5.13: Comparison between the numerical integration and asymptotic value of $\mathcal{W}$ versus ρ/λ_0 in (4.17) for $|z - z'| \to 0$.

$d_1/\lambda_0 = 0.05, \epsilon_{1,t} = 2.25, \epsilon_{1,t}/\epsilon_{1,z} = 1.0, \mu_{1,t} = 1.0, \mu_{1,t}/\mu_{1,z} = 1.0$

$d_2/\lambda_0 = 0.05, \epsilon_{2,t} = 3.25, \epsilon_{2,t}/\epsilon_{2,z} = 1.0, \mu_{2,t} = 1.0, \mu_{2,t}/\mu_{2,z} = 1.0$

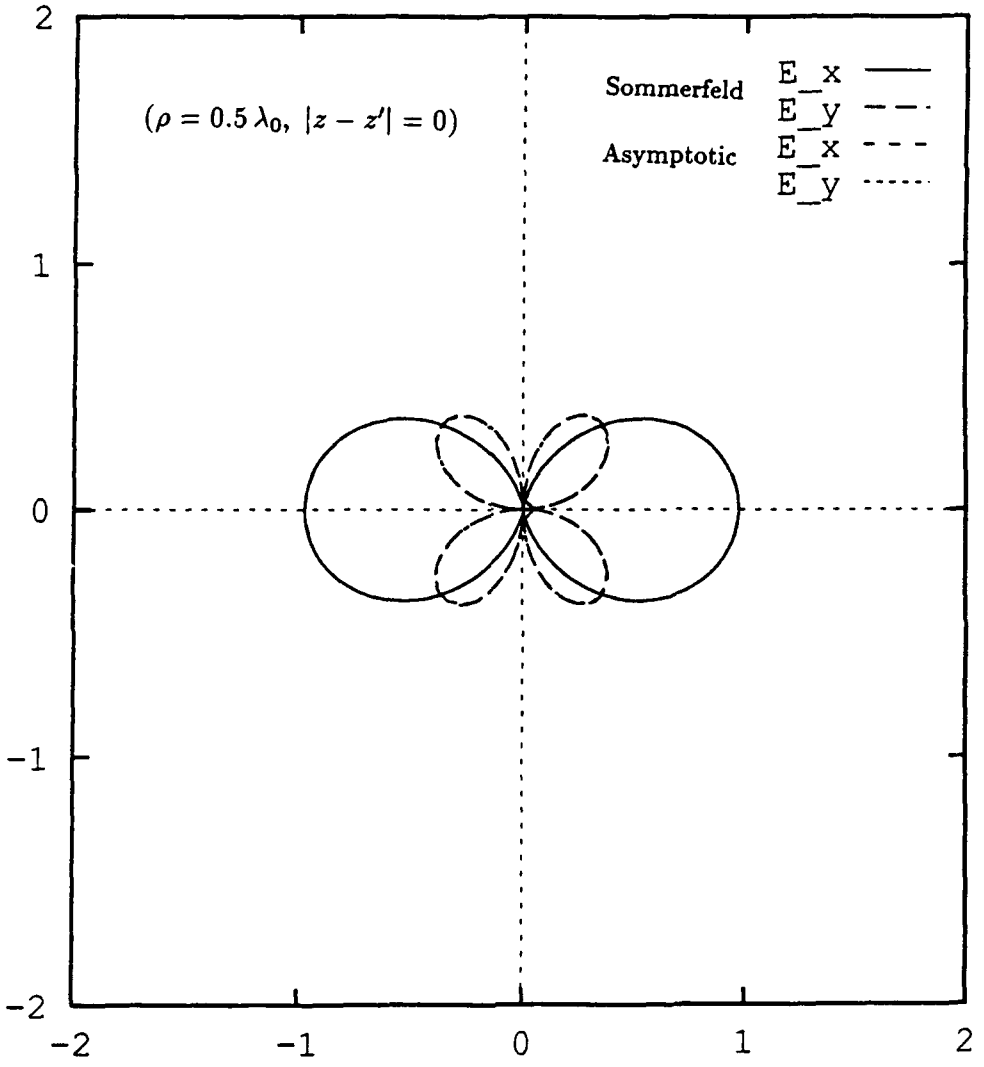

Figure 5.14: Comparison between the numerical integration and asymptotic value of electric fields E_x and E_y of a horizontal electric dipole current point source over the planar interface of the two anisotropic uniaxial slab at observation points (ρ, ϕ) versus ϕ at $(\rho = 0.5\,\lambda_0, |z - z'| = 0)$ after incorporating (4.17) into (3.14)-(3.17).

$d_1/\lambda_0 = 0.05, \epsilon_{1,t} = 2.25, \epsilon_{1,t}/\epsilon_{1,z} = 1.5, \mu_{1,t} = 1.0, \mu_{1,t}/\mu_{1,z} = 1.0$

$d_2/\lambda_0 = 0.05, \epsilon_{2,t} = 3.25, \epsilon_{2,t}/\epsilon_{2,z} = 1.5, \mu_{2,t} = 1.0, \mu_{2,t}/\mu_{2,z} = 1.0$

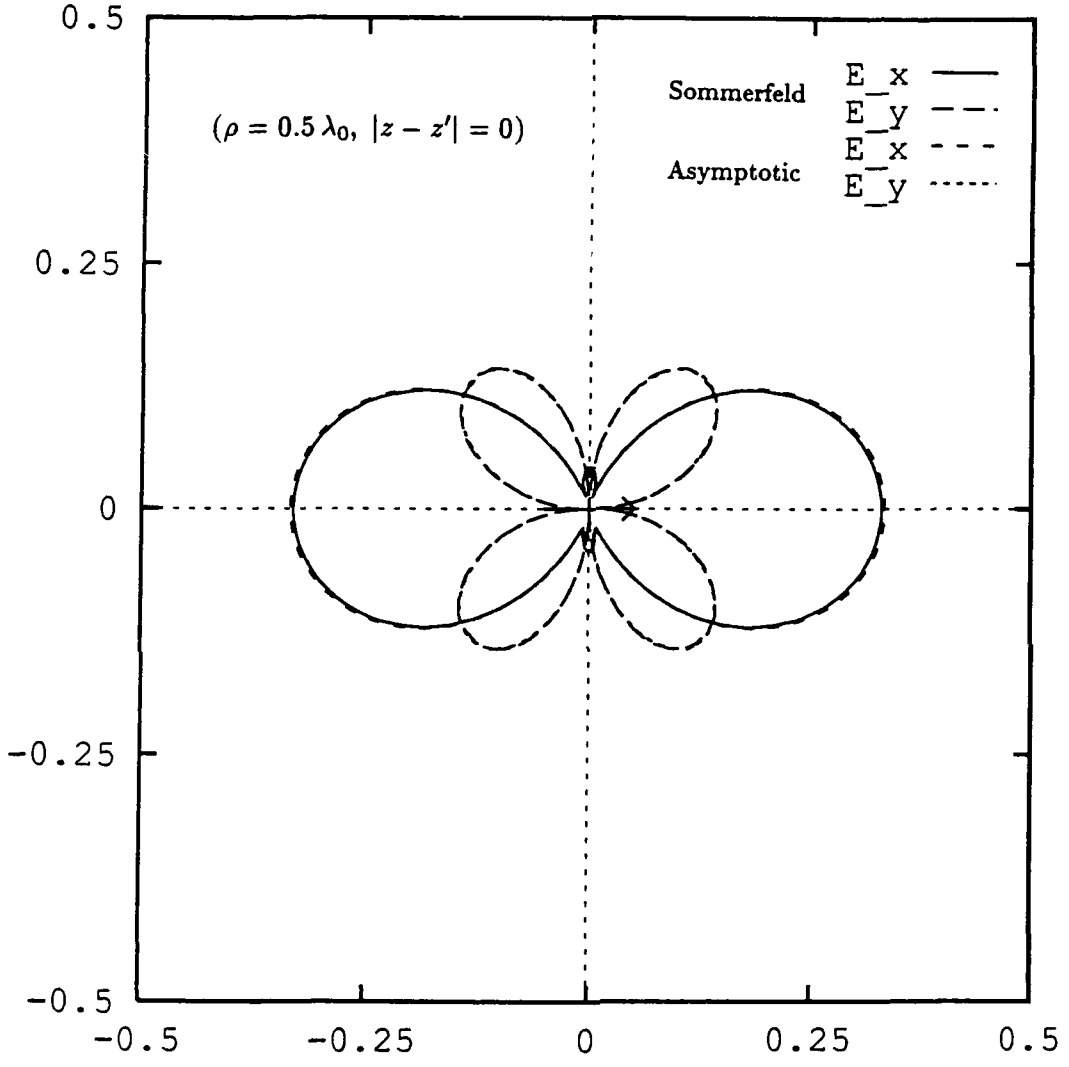

Figure 5.15: Comparison between the numerical integration and asymptotic value of electric fields E_x and E_y of a horizontal electric dipole current point source over the planar interface of the two anisotropic uniaxial slab at observation points (ρ, ϕ) versus ϕ at $(\rho = 0.5\,\lambda_0, |z - z'| = 0)$ after incorporating (4.17) into (3.14)-(3.17).

$d_1/\lambda_0 = 0.05, \epsilon_{1,t} = 2.25, \epsilon_{1,t}/\epsilon_{1,z} = 0.75, \mu_{1,t} = 1.0, \mu_{1,t}/\mu_{1,z} = 1.0$

$d_2/\lambda_0 = 0.05, \epsilon_{2,t} = 3.25, \epsilon_{2,t}/\epsilon_{2,z} = 0.75, \mu_{2,t} = 1.0, \mu_{2,t}/\mu_{2,z} = 1.0$

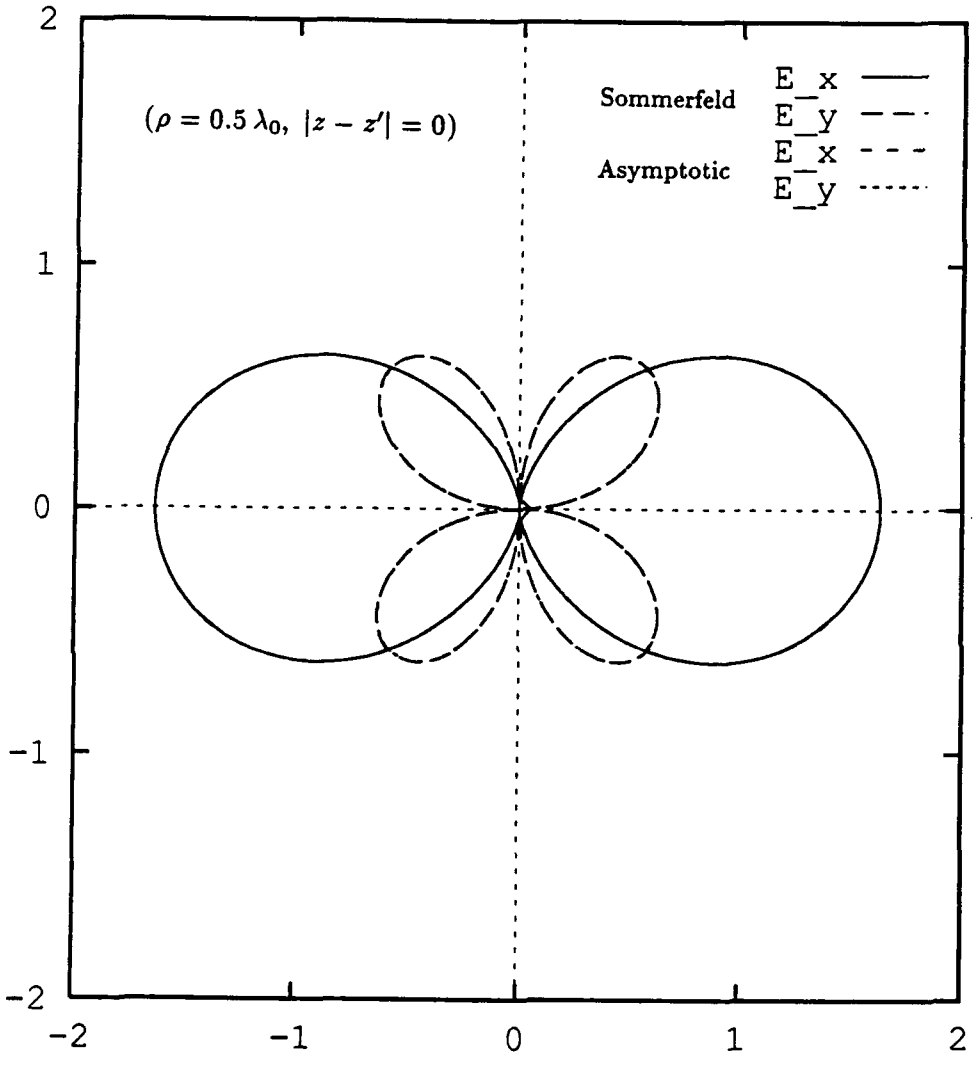

Figure 5.16: Comparison between the numerical integration and asymptotic value of electric fields E_x and E_y of a horizontal electric dipole current point source over the planar interface of the two anisotropic uniaxial slab at observation points (ρ, ϕ) versus ϕ at $(\rho = 0.5\,\lambda_0, |z - z'| = 0)$ after incorporating (4.17) into (3.14)-(3.17).

$d_1/\lambda_0 = 0.05, \epsilon_{1,t} = 3.25, \epsilon_{1,t}/\epsilon_{1,z} = 0.5, \mu_{1,t} = 1.0, \mu_{1,t}/\mu_{1,z} = 1.0$
$d_2/\lambda_0 = 0.03, \epsilon_{2,t} = 9.60, \epsilon_{2,t}/\epsilon_{2,z} = 0.5, \mu_{2,t} = 1.0, \mu_{2,t}/\mu_{2,z} = 1.0$

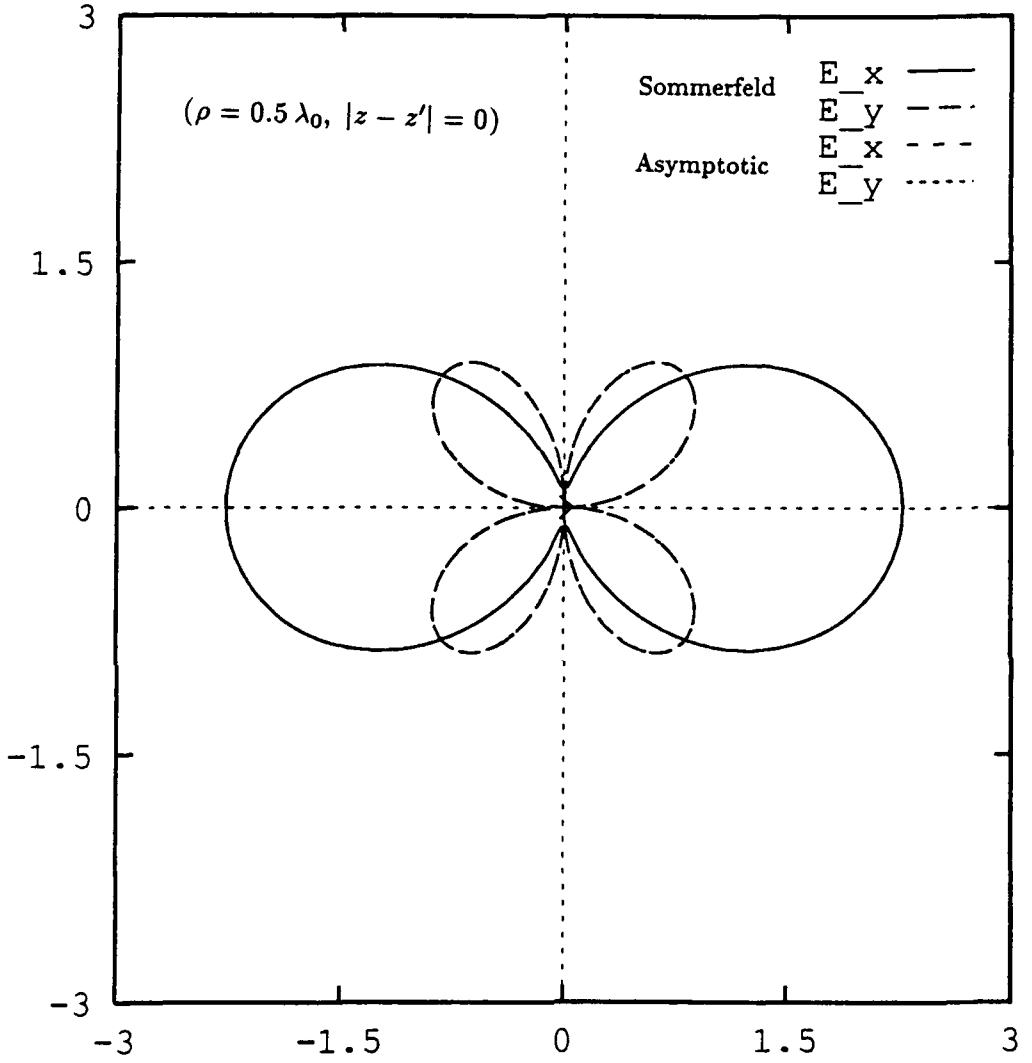

Figure 5.17: Comparison between the numerical integration and asymptotic value of electric fields E_x and E_y of a horizontal electric dipole current point source over the planar interface of the two anisotropic uniaxial slab at observation points (ρ, ϕ) versus ϕ at $(\rho = 0.5\,\lambda_0, |z - z'| = 0)$ after incorporating (4.17) into (3.14)-(3.17).

Chapter 6

Conclusions, Discussions and Directions of Future Research

A relatively simple and accurate closed asymptotic form of the electric dyadic Green's function for a double-layered anisotropic uniaxial grounded slab is developed. The asymptotic representation provides an accurate solution even for a very small separation of the source and observation points (a few tenths of a free space wavelength). The asymptotic closed form dyadic Green's function has been cast in such a form that the physical behavior of the electromagnetic fields due to anisotropy of the medium reveals itself through a simple mathematical parameters. Thus, the physical understanding of the interaction of the spatially confined source with an anisotropic (uniaxial) double-layered grounded slab is greatly enhanced through our asymptotic closed form representation of the dyadic Green's function. In addition two efficient numerical integration schemes based on singularity removal technique and radially propagating integral representation of the Green's dyadic are also presented. In contrast to the representations developed in this study, the Sommerfeld type integral converges slowly for large and even moderately large separation between the source and observation points. The representations developed here do not exhibit this difficulty. Hence a systematic numerical algorithm is developed which can efficiently be used to compute the dyadic Green's function of the anisotropic (uniaxial) double-layered grounded slab for the entire range of the separation of source and observation points. These solutions are expected to be useful in the moment method solution to a wide variety of the anisotropic uniaxial grounded slab problems.

Some related solutions such as the dyadic Green's function for electric as well as magnetic point currents in a general uniaxial multilayered material media have been developed in a form which provide useful physical interpretations; these solutions are important in many applications involving uniaxial stratified media, such as in the design of high performance large phased arrays and frequency selective surfaces (FSS), as well as in the analysis of multilayered guided wave structures.

It is believed that the derivations of the Green's function for multi-layered anisotropic (uniaxial) media, as well as the efficient asymptotic closed form approximation to the dyadic Green's function for anisotropic (uniaxial) double-layered grounded slab are novel; and because it is an efficient solution to a canonical problem, it has applications in a variety of disciplines; such as, monolithic microwave and millimeter waves integrated circuits, inte-

grated optics, non-destructive evaluation (NDE), and geophysical prospecting. As mentioned earlier, the conventional spectral integral of the Green's dyadic is highly oscillatory and contains branch points and pole singularities that are on, or close to, the path of integration. Hence, the numerical evaluation of the spectrum integrals is in general very time consuming and becomes prohibitively expensive as the separation of the source and observation points increases in the lateral direction.

The utility of our efficient asymptotic closed form approximation for the Green's dyadic can hardly be overemphasized.

During the Phase II of our research effort we will perform the following :

a) During Phase I of our work, we have gained a great deal of physical insight into the electromagnetic source interaction with anisotropic media. Owing to the closed form expression for the asymptotic dyadic Green's function for anisotropic double-layered grounded slab, the effect of anisotropy reveals itself through different mathematical parameters. Because of the presence of ten parameters (five for each anisotropic layer including the thickness of the layer) extensive numerical simulation must be performed to completely characterize a source excited anisotropic double-layer geometry. We will perform such an extensive numerical simulation during Phase II.

b) We will extend our dyadic Green's function analysis to include the Green's dyadic due to magnetic point current. This analysis allows us to expand the applicability of our method to aperture coupled and co-planar integrated circuit devices.

c) We intend to develop a computer aided engineering (CAE) code to analyze monolithic microwave and millimeter wave integrated planar elements as shown in Figures 6.1, 6.2, and 6.3. This will include: 1) the analyses of passive microwave and millimeter wave integrated circuits such as design of arbitrary bends, discontinuities, filters, and couplers, 2) finite as well as infinite microstrip antenna phased array (including the feeding network), 3) integrated optical devices such as dielectric waveguide with arbitrary bends, and dielectric waveguide couplers all in anisotropic uniaxial double-layered grounded slab environment.

d) We will develop a computer code to analyze the integrated optical components which needs a calculation of the volumetric current distribution. To be more specific, we will analyze a dielectric waveguide, with arbitrary bends, residing within an anisotropic (uniaxial) double-layered grounded slab. This configuration is a canonical high frequency transmission channel of the electromagnetic energy, and its analysis is of great interest to the optical community. It is noteworthy that because we have an efficient Green's dyadic of the anisotropic double-layered structure, the only unknown we have is the volumetric current within the transmission channel, which we will solve for by our efficient conjugate gradient - fast Fourier transform (GC-FFT) method that we will explain shortly. Nevertheless, because of the presence of the open boundaries the finite element analysis of this class of problems is very time consuming; it takes perhaps (10-100) times more computational effort than our volume-integral formulation which utilizes the newly developed efficient dyadic Green's function as a kernel.

e) In the past, we have used the unit pulse function, defined on a regular three-dimensional grid, to discretize the volume-integral equation. The advantage of this discretization scheme is that it creates a resulting matrix Toeplitz-Hankel, which greatly facilitates the computation and storage demands on the computer. Pulse functions however do not provide continuity of the currents from one cell to another, so it is desirable to consider other functions that do provide this continuity. Recently, we have introduced splines that are derived from higher-order convolutions of the unit pulse, which, of course, are also defined on the same regular grid as are the pulse functions. We have also introduced the reciprocal bases over the same regular grid, which are orthogonal to the spline functions. When we use our higher-order splines as expansion functions and the associated reciprocal bases as a testing function to discretize the volume-integral equation, we will retain the desirable feature of the Toeplitz-Hankel matrix in our system of linear equations as well as the continuity of the currents.

It is also possible to use higher-order shape functions, that are typically used in the finite-element method, to discretize the volume-integral equation. The advantage of higher-order shape functions is that they not only provide the continuity of sources, but also they can easily conform to the shape of the scatterer, and thereby give a more accurate discretized version of the continuum. However, due to the irregular three-dimensional grid producing by this discretization scheme, the resulting matrix may not be in Toeplitz or Hankel form.

We will utilize both discretization techniques (higher-order splines, and higher order shape functions) for our volume-integral equation. We will study the advantages of each method to our problem. We will also look into the use of combination of both discretization methods to take advantage of both discretization methods. This can be done by using the finite element shape functions only in the boundary regions and the higher-order splines in the rest of the body of scatterer. This hybrid method, although it leads to a complex discretization procedure, is expected to produce more accurate results than the original higher-order spline technique that makes an staircase approximation of the outer boundary of the scatterer.

We will also study the degree of the complexity of the discretization procedure and make a decision in the early stages of Phase II as to which method is more suitable for the discretization of our volume-integral equation.

f) Conjugate gradient method and its pre-conditional version is a very powerful tool to solve a system of matrix equations. When it can be combined with the Fast Fourier Transform (FFT) algorithm, it will create an efficient and powerful computational algorithm over an affordable computer memory space. We have considerable experience in the use of the conjugate gradient algorithm and the FFT in both the frequency-and time-domain in our previous SBIR projects. This efficiency, which does not seem to be present in any other computational algorithms, is the basis of the use of our new higher-order splines and reciprocal basis functions which indeed produces a Toeplitz-Hankel matrix.

We will use the conjugate gradient together with the fast Fourier transform during Phase II. We will also address the issue of the pre-conditioning conjugate gradient. From our experience, the pre-conditioning, if used properly, can extensively accelerate the convergence rate of the conjugate gradient algorithm.

g) One of the interesting features of our newly developed efficient asymptotic closed form dyadic Green's function is that it is amenable to transient electromagnetic problems for double-layered anisotropic slab (or half space). This implies that an inverse fast Fourier transform of the weighted average of our closed form approximation of the Green's dyadic over a proper frequency band can create a correct response for a prescribed time dependent electric point current source. It should be pointed out, however, that for the low frequency components, where the lateral separation of the source and observation points are considered to be (electrically) small, an efficient numerical algorithm based on singularity removel technique, should be used to compute the Green's dyadic.

We will set up a transient scattering problem of a perfectly conducting strip within the anisotropic (uniaxial) slab when a time dependent electric source is located over the slab.

It is noteworthy that our transient analysis will directly be applied for the bandwidth analysis of the monolithic microwave and millimeter wave integrated circuits and the three dimensional optical transmission channels.

h) Since the geometry of the proposed model can be very complex, we will explore the employing of a user-friendly graphical pre- and post-processor interface under X-windows. This step is a crucial step toward the commercialization of our microwave and millimeter wave integrated circuit (MIMIC) software product.

i) We have gained a good deal of knowledge about the transputers, and other accelerator boards that can be installed on the 386/486 workstation. These boards offer large-scale computing in a workstation environment. We are also investigating the applicability of the Intel Hypercubes (MIMD), MasPar (SIMD), and WAVETRACER (SIMD) architectures to the solution of our volume-integral equation. The crucial feature of any architecture that is applied to our problem is that it be able to execute the fast Fourier transform (FFT) very rapidly. We will thoroughly investigate the guidelines that should be followed in order that our computer aided engineering (CAE) code will be executable on massively parallel machines, as well as on workstations with the accelerator boards.

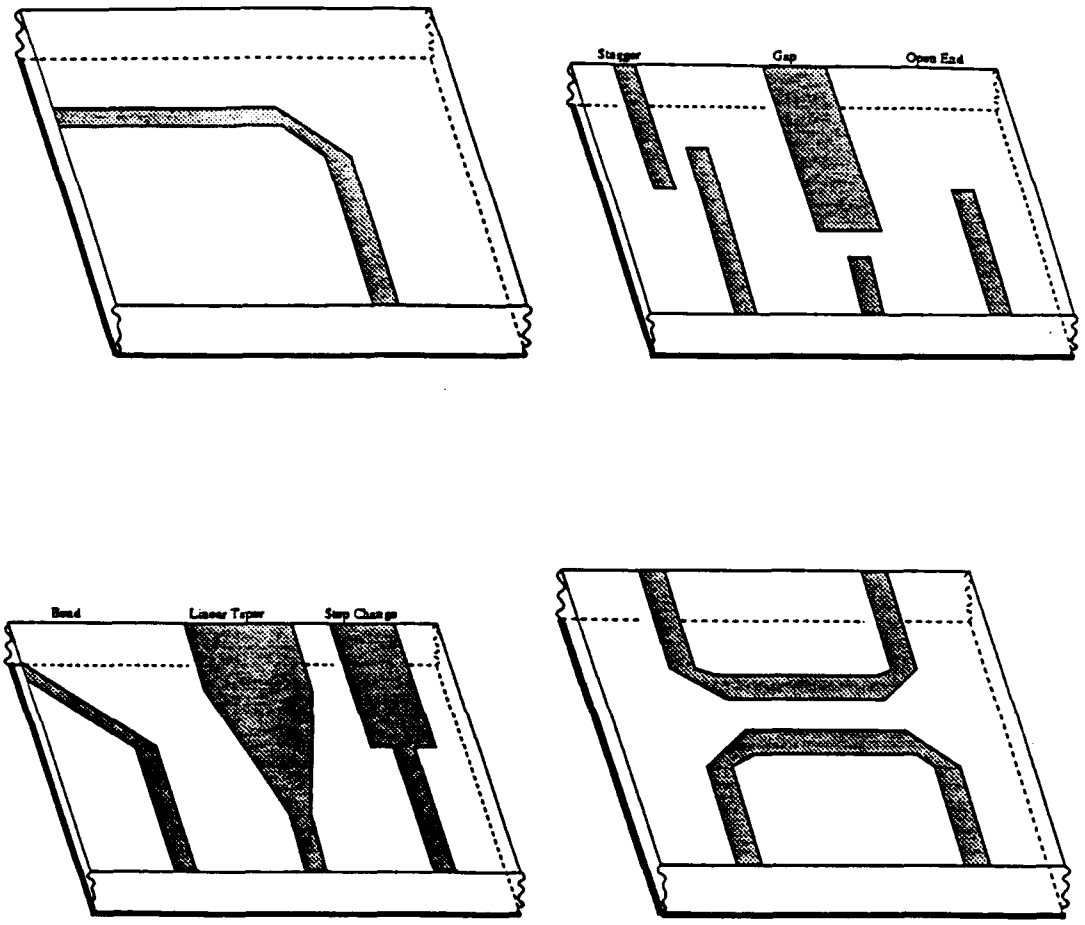

$$\bar{\bar{\epsilon}}_i = \epsilon_{i,t}\mathbf{I}_t + \epsilon_{i,z}\hat{\mathbf{z}}\hat{\mathbf{z}} \;\; ; \;\; \bar{\bar{\mu}}_i = \mu_{i,t}\mathbf{I}_t + \mu_{i,z}\hat{\mathbf{z}}\hat{\mathbf{z}}$$

Figure 6.1: Various bends, junctions, discontinuities, and couplers in single-layered anisotropic uniaxial slab used in monolithic microwave and millimeter wave integrated circuit (MMMIC) designs

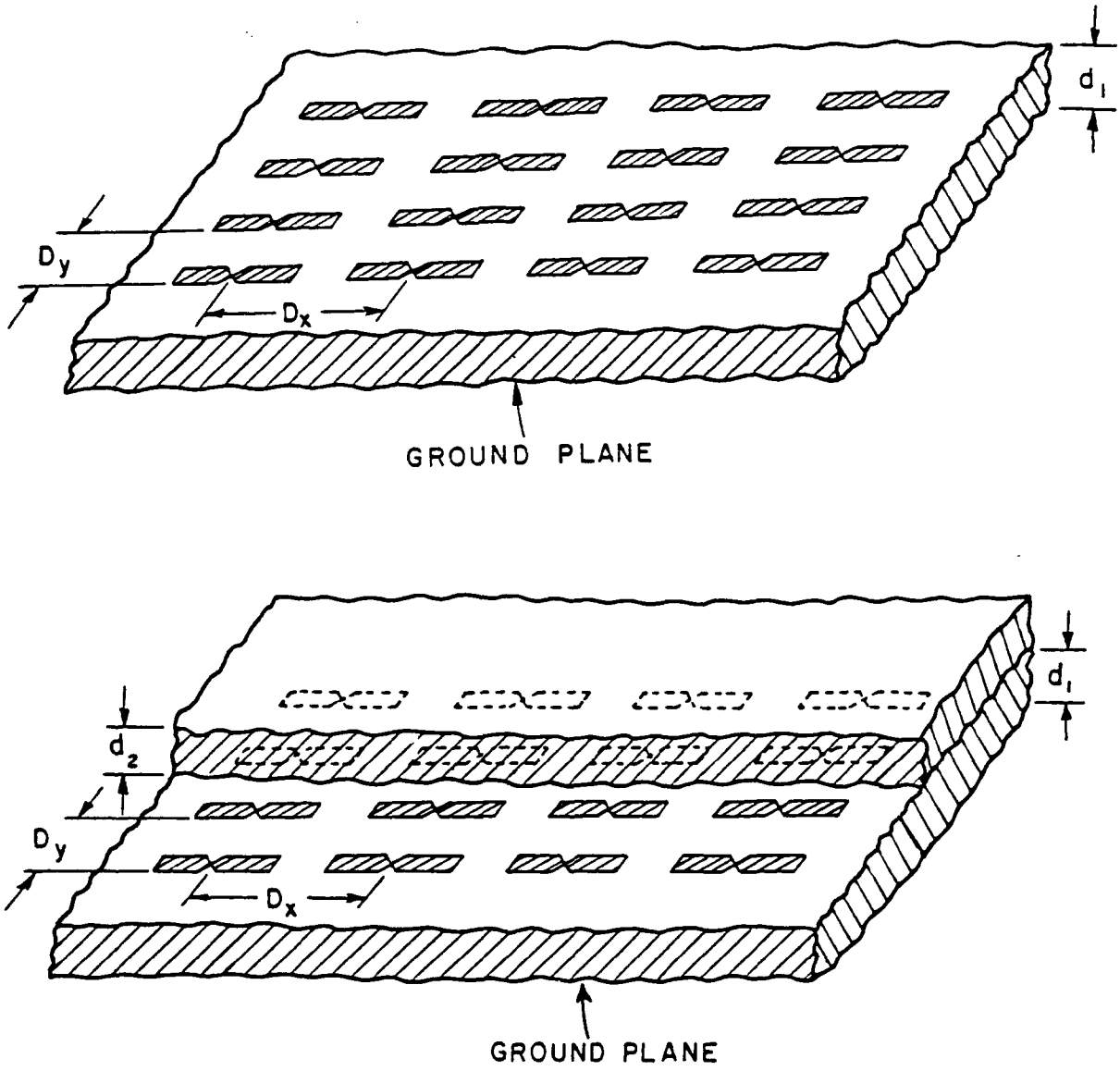

$$\bar{\bar{\epsilon}}_i = \epsilon_{i,t}\mathbf{I}_t + \epsilon_{i,z}\hat{z}\hat{z} \;\; ; \;\; \bar{\bar{\mu}}_i = \mu_{i,t}\mathbf{I}_t + \mu_{i,z}\hat{z}\hat{z}$$

Figure 6.2: Finite micrstrip phased array in single as well as double layered grounded anisotropic uniaxial slab

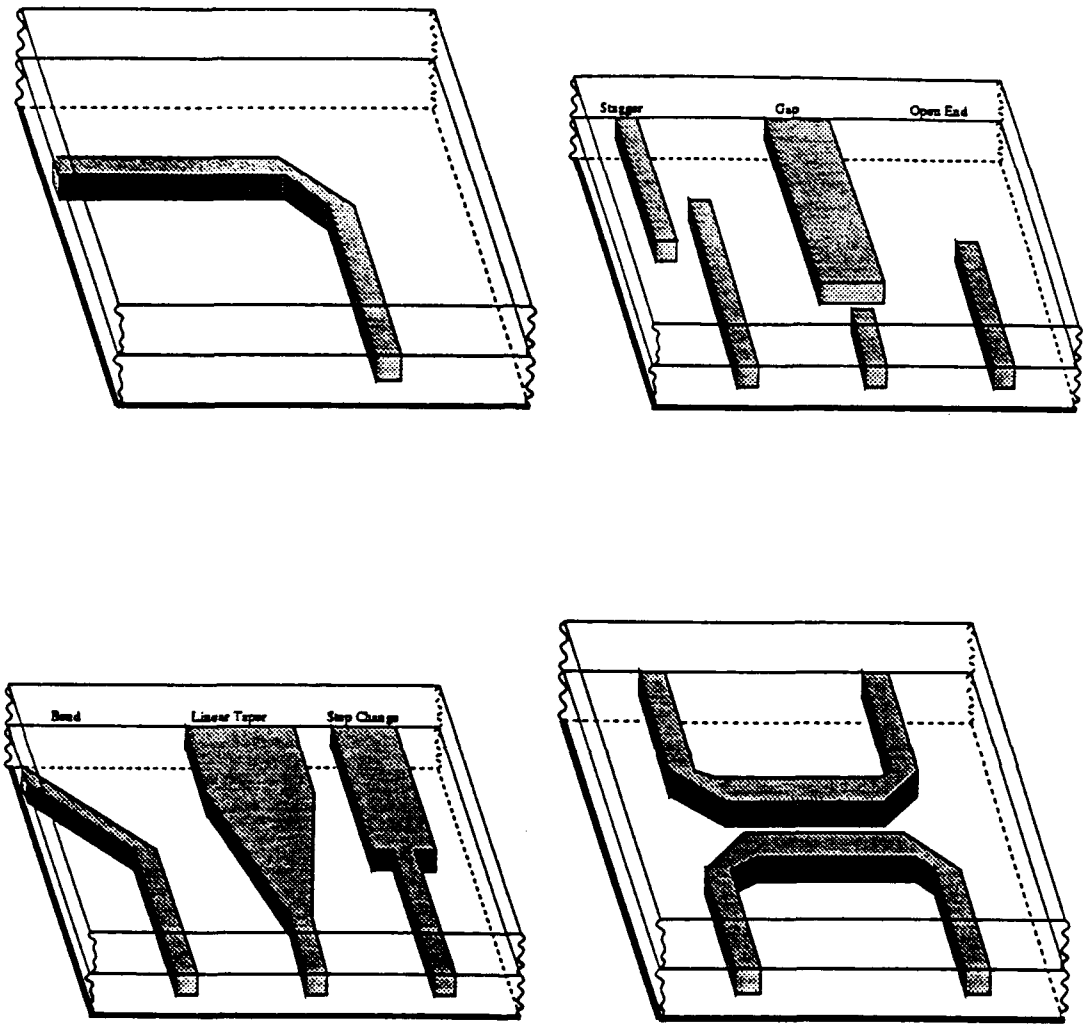

$$\bar{\bar{\epsilon}}_i = \epsilon_{i,t}\mathbf{I}_t + \epsilon_{i,z}\hat{z}\hat{z} \;\; ; \;\; \bar{\bar{\mu}}_i = \mu_{i,t}\mathbf{I}_t + \mu_{i,z}\hat{z}\hat{z}$$

Figure 6.3: Different bends, junctions, and couplers of dielectric waveguides in double-layered anisotropic uniaxial slab used in millimeter wave and optical circuit designs

Chapter 7

Appendices

7.1 Appendix A: Eigenvalues and Eigenmodes for General Uniaxial Media

In this appendix the explicit expression for the eigenmode κ_α and the eigen vector-wave $\mathit{\Pi}_\alpha(\mathbf{r}, \mathbf{k}_t)$ for a general uniaxial anisotropic material where ($\bar{\bar{\epsilon}} = \epsilon_t \mathbf{I}_t + \epsilon_z \hat{\mathbf{z}}\hat{\mathbf{z}}$; $\bar{\bar{\mu}} = \mu_t \mathbf{I}_t + \mu_z \hat{\mathbf{z}}\hat{\mathbf{z}}$) will be derived.

As stated earlier in (2.17), the eigenvectors $\mathit{\Psi}_\alpha^{\gtrless}(\boldsymbol{\rho})$ corresponding to $\pm\kappa_\alpha$ can be expressed as,

$$\mathit{\Psi}_\alpha^{\gtrless}(\boldsymbol{\rho}) = \frac{1}{2\pi}\mathit{\Psi}_\alpha^{\gtrless} e^{-j\mathbf{k}_t\cdot\boldsymbol{\rho}} \;\; ; \;\; \mathit{\Psi}_\alpha^{\gtrless} = \begin{pmatrix} \mathbf{E}_{t,\alpha} \pm \mathbf{E}_{z,\alpha} \\ \pm\mathbf{H}_{t,\alpha} + \mathbf{H}_{z,\alpha} \end{pmatrix} = \begin{pmatrix} Z_\alpha \mathbf{e}_\alpha \pm \mathbf{e}_{z,\alpha} \\ \pm\mathbf{h}_\alpha + \mathbf{h}_{z,\alpha} \end{pmatrix} \quad , \qquad \text{(A.1)}$$

where $\mathbf{e}_\alpha, \mathbf{h}_\alpha$ and $\mathbf{e}_{z,\alpha}, \mathbf{h}_{z,\alpha}$ are normalized mode-vectors transverse and parallel to z respectively, for the eigenvalues of $\pm\kappa_\alpha$, and Z_α is the mode impedance; and their explicit values can be found from the source-free solution of (2.7). Thus, after substituting $\nabla_t \longrightarrow -j\mathbf{k}_t$, $\frac{\partial}{\partial z} \longrightarrow -j\kappa_\alpha$ in (2.14), $\bar{\bar{\epsilon}}_{tt} = \epsilon_t \mathbf{I}_t$, and $\bar{\bar{\mu}}_{tt} = \mu_t \mathbf{I}_t$ one will have,

$$\begin{aligned} \omega\epsilon_0 \left[\epsilon_t \mathbf{I}_t - \frac{1}{\omega^2\epsilon_0\mu_0\mu_z}\mathbf{k}_t\mathbf{k}_t\right]\cdot(\hat{\mathbf{z}}\times\mathbf{e}_\alpha) &= \kappa_\alpha Y_\alpha \mathbf{h}_\alpha \\ \omega\mu_0 \left[\mu_t \mathbf{I}_t - \frac{1}{\omega^2\epsilon_0\mu_0\epsilon_z}\mathbf{k}_t\mathbf{k}_t\right]\cdot(\hat{\mathbf{z}}\times\mathbf{h}_\alpha) &= -\kappa_\alpha Z_\alpha \mathbf{e}_\alpha \;, \end{aligned} \qquad \text{(A.2)}$$

where $Y_\alpha \equiv \frac{1}{Z_\alpha}$.

Because one is ultimately interested in the guided (z-propagating) representation of the vector-wave, one can introduce a right handed coordinate basis of the form $(\hat{\mathbf{z}}, \hat{\mathbf{k}}_t', \hat{\mathbf{k}}_t'')$, where the unit vector $\hat{\mathbf{k}}_t'$ is defined by the decomposition of $\mathbf{k} = \hat{\mathbf{k}}_t' k_t + \hat{\mathbf{z}}\kappa_\alpha$ and $\hat{\mathbf{k}}_t'' = \hat{\mathbf{z}} \times \hat{\mathbf{k}}_t'$. Let us now substitute an *ansatz* $(\mathbf{e}_1, \mathbf{h}_1)$ for $\alpha = 1$:

$$\mathbf{e}_1 \;=\; \hat{\mathbf{k}}_t' \;, \qquad \text{(A.3)}$$

$$\mathbf{h}_1 \;=\; \hat{\mathbf{z}} \times \mathbf{e}_1 = \hat{\mathbf{k}}_t'' \;,$$

into (A.2), then one will have

$$\begin{aligned} \omega\epsilon_0\epsilon_t &= \kappa_1 Y_1 \;, \\ -\omega\mu_0\,(\mu_t - \frac{1}{\omega^2\epsilon_0\mu_0\epsilon_z}k_t^2) &= \kappa_1 Z_1 \;, \end{aligned} \tag{A.4}$$

which yields

$$\kappa_1 = \sqrt{k_0^2\mu_t\epsilon_t - \frac{\epsilon_t}{\epsilon_z}k_t^2} \;\;;\;\; Z_1 = \frac{1}{Y_1} = \frac{\kappa_1}{\omega\epsilon_0\epsilon_t} \;, \tag{A.5}$$

where $k_0^2 = \omega^2\epsilon_0\mu_0$. Using (2.13), the normalized longitudinal modevector e_z, h_z can be expressed as,

$$e_{z,1} = -\frac{k_t}{\omega\epsilon_0\epsilon_z} \;\;;\;\; h_{z,1} = 0 \;. \tag{A.6}$$

As is evident from (A.6) the $\alpha = 1$ mode is transverse magnetic TM (or E-mode) with respect to the z-coordinate.

For $\alpha = 2$, one may substitute

$$\begin{aligned} \mathbf{e}_2 &= \hat{\mathbf{k}}_t'' \;, \\ \mathbf{h}_2 &= \hat{\mathbf{z}} \times \mathbf{e}_2 = -\hat{\mathbf{k}}_t' \;, \end{aligned} \tag{A.7}$$

into (A.2),

$$\begin{aligned} -\omega\epsilon_0\,(\epsilon_t - \frac{1}{\omega^2\epsilon_0\mu_0\mu_z}k_t^2) &= \kappa_2 Y_2 \;, \\ \omega\mu_0\mu_t &= \kappa_2 Z_2 \;, \end{aligned} \tag{A.8}$$

which yields

$$\kappa_2 = \sqrt{k_0^2\mu_t\epsilon_t - \frac{\mu_t}{\mu_z}k_t^2} \;\;;\;\; Y_2 = \frac{1}{Z_2} = \frac{\kappa_2}{\omega\mu_0\mu_t} \;. \tag{A.9}$$

Using (2.13), the normalized longitudinal modevector e_z, h_z can be expressed as,

$$e_{z,2} = 0 \;\;;\;\; h_{z,2} = -\frac{k_t}{\omega\mu_0\mu_z} \;. \tag{A.10}$$

As is evident from (A.10), the $\alpha = 2$ mode is transverse electric TE (or H-mode) with respect to the z-coordinate.

The explicit expressions for vector-wave modes of a general uniaxail anisotropic medium can now be obtained (see (2.17) after incorporating (A.3), (A.5), (A.6), (A.7), (A.9), and (A.10) into (A.1).

7.2 Appendix B: Reciprocity and Orthogonality Relations in Anisotropic Media

In this appendix a set of reciprocity and orthogonality relations for anisotropic media will be discussed. These relations are useful in the derivation of the dyadic Green's function for unbounded as well as multi-layered uniaxial anisotropic media.

The Maxwell curl equations for a gyroelectric source excited medium can be expressed as,

$$\begin{aligned} \nabla \times \mathbf{E} &= -j\omega\mu_0\bar{\bar{\mu}}\mathbf{H} - \mathbf{M} \quad , \\ \nabla \times \mathbf{H} &= j\omega\epsilon_0\bar{\bar{\epsilon}} \cdot \mathbf{E} + \mathbf{J} \quad , \end{aligned} \tag{B.1}$$

where $(\mu_0\bar{\bar{\mu}}, \epsilon_0\bar{\bar{\epsilon}})$ are the constitutive tensors of the medium, and $\mathbf{J}$ and $\mathbf{M}$ are electric and magnetic current sources, respectively. One can introduce an associated adjoint medium with the constitutive parameters of $(\mu_0\bar{\bar{\mu}}^+, \epsilon_0\bar{\bar{\epsilon}}^+)$, where in the adjoint medium the Maxwell curl equations can be expressed as,

$$\begin{aligned} \nabla \times \mathbf{E}^+ &= -j\omega\mu_0\bar{\bar{\mu}}^+\mathbf{H}^+ - \mathbf{M}^+ \\ \nabla \times \mathbf{H}^+ &= j\omega\epsilon_0\bar{\bar{\epsilon}}^+ \cdot \mathbf{E}^+ + \mathbf{J}^+ \quad . \end{aligned} \tag{B.2}$$

The appropriate reciprocity relation can be sought by calculating $\nabla \cdot (\mathbf{E} \times \mathbf{H}^+) = \mathbf{H}^+ \cdot \nabla \times \mathbf{E} - \mathbf{E} \cdot \nabla \times \mathbf{H}^+$ and $\nabla \cdot (\mathbf{E}^+ \times \mathbf{H})$, from (B.1) and (B.2) taking their difference:

$$\begin{aligned} \nabla \cdot (\mathbf{E} \times \mathbf{H}^+ - \mathbf{E}^+ \times \mathbf{H}) = \; &+ \; j\omega\epsilon_0 \left(\mathbf{E}^+ \cdot \bar{\bar{\epsilon}} \cdot \mathbf{E} - \mathbf{E} \cdot \bar{\bar{\epsilon}}^+ \cdot \mathbf{E}^+\right) \\ &- j\omega\mu_0 \left(\mathbf{H}^+ \cdot \bar{\bar{\mu}} \cdot \mathbf{H} - \mathbf{H} \cdot \bar{\bar{\mu}}^+ \cdot \mathbf{H}^+\right) \\ &\mathbf{H}^+ \cdot \mathbf{M} + \mathbf{E}^+ \cdot \mathbf{J} + \mathbf{H} \cdot \mathbf{M}^+ - \mathbf{E} \cdot \mathbf{J}^+ \quad . \end{aligned} \tag{B.3}$$

If the transpose of the permiability and permittivity tensors of the medium are the same as the permiability and permittivity tensors of the adjoint medium, $(\bar{\bar{\mu}} = \bar{\bar{\mu}}^+ \; ; \; \bar{\bar{\epsilon}} = \bar{\bar{\epsilon}}^+$, where $(\sim)$ denotes transpose), then one can identify,

$$\begin{aligned} \mathbf{E}^+ \cdot \widetilde{\bar{\bar{\epsilon}}} \cdot \mathbf{E} &= \mathbf{E} \cdot \bar{\bar{\epsilon}} \cdot \mathbf{E}^+ = \mathbf{E} \cdot \bar{\bar{\epsilon}}^+ \cdot \mathbf{E}^+ \quad , \\ \mathbf{H}^+ \cdot \widetilde{\bar{\bar{\mu}}} \cdot \mathbf{H} &= \mathbf{H} \cdot \bar{\bar{\mu}} \cdot \mathbf{H}^+ = \mathbf{H} \cdot \bar{\bar{\mu}}^+ \cdot \mathbf{H}^+ \quad , \end{aligned}$$

and the first four terms of the right hand side will cancel. Upon introducing a closed volume V bounded by the surface S, one will have

$$\oint_S d\mathbf{s} \cdot (\mathbf{E} \times \mathbf{H}^+ - \mathbf{E}^+ \times \mathbf{H}) = \int_V dv \; (-\mathbf{H}^+ \cdot \mathbf{M} + \mathbf{E}^+ \cdot \mathbf{J} + \mathbf{H} \cdot \mathbf{M}^+ - \mathbf{E} \cdot \mathbf{J}^+) \quad . \tag{B.4}$$

Equation (B.4) is the reciprocity relation in an anisotropic (symmetric gyroelectric) medium wherein $(\bar{\bar{\mu}} = \bar{\bar{\mu}} \; ; \; \bar{\bar{\epsilon}} = \bar{\epsilon})$, and the adjoint medium will be the same as its associated medium. A general uniaxial medium is an special case of symmetric gyroelectric medium.

The orthogonality of the z-guided vector-wave modes

$$\mathit{\Pi}_{\alpha}^{\gtrless}(\mathbf{k}_t, \mathbf{r}) = \frac{1}{2\pi} \begin{pmatrix} Z_\alpha \mathbf{e}_\alpha \pm \mathbf{e}_{z,\alpha} \\ \pm \mathbf{h}_\alpha + \mathbf{h}_{z,\alpha} \end{pmatrix} e^{-j\mathbf{k}_t \cdot \boldsymbol{\rho} \mp j\kappa_\alpha z} \tag{B.5}$$

can be inferred by substituting for the divergence operation, $\nabla \cdot = \left(\nabla_t + \hat{\mathbf{z}} \frac{\partial}{\partial z}\right) \cdot$, in (B.3) and applying the surface divergence theorem to a pair of source free fields of $\mathit{\Pi}_{\alpha}^{>}(\mathbf{k}_t, \mathbf{r})$ and $\mathit{\Pi}_{\beta}^{<}(-\mathbf{k}_t', \mathbf{r})$ [22, pages 174–179]; this yields,

$$\begin{aligned} \int_S ds \;\; & \nabla_t \cdot (\pm Z_\alpha \mathbf{e}_\alpha(\mathbf{k}_t) \times \mathbf{h}_\beta(\mathbf{k}_t') - Z_\beta \mathbf{e}_\beta(\mathbf{k}_t') \times \mathbf{h}_\alpha(\mathbf{k}_t))\, e^{-j\boldsymbol{\rho}\cdot(\mathbf{k}_t - \mathbf{k}_t') - jz(\kappa_\alpha \pm \kappa_\beta)} \\ &= \oint_C dl\, \hat{\mathbf{n}} \cdot (\pm Z_\alpha \mathbf{e}_\alpha(\mathbf{k}_t) \times \mathbf{h}_\beta(\mathbf{k}_t') - Z_\beta \mathbf{e}_\beta(\mathbf{k}_t') \times \mathbf{h}_\alpha(\mathbf{k}_t))\, e^{-j\boldsymbol{\rho}\cdot(\mathbf{k}_t - \mathbf{k}_t') - jz(\kappa_\alpha \pm \kappa_\beta)} \qquad \text{(B.6)} \\ &= \frac{\partial}{\partial z} \int_S ds \hat{\mathbf{z}} \cdot (\pm Z_\alpha \mathbf{e}_\alpha(\mathbf{k}_t) \times \mathbf{h}_\beta(\mathbf{k}_t') - Z_\beta \mathbf{e}_\beta(\mathbf{k}_t') \times \mathbf{h}_\alpha(\mathbf{k}_t))\, e^{-j\boldsymbol{\rho}\cdot(\mathbf{k}_t - \mathbf{k}_t') - jz(\kappa_\alpha \pm \kappa_\beta)} \;\; . \end{aligned}$$

The contour integral vanishes because of the radiation condition as $\rho \to \infty$[1]. Thus one will have

$$(\kappa_\alpha \pm \kappa_\beta) \int_S ds \hat{\mathbf{z}} \cdot (\pm Z_\alpha \mathbf{e}_\alpha(\mathbf{k}_t) \times \mathbf{h}_\beta(\mathbf{k}_t') - Z_\beta \mathbf{e}_\beta(\mathbf{k}_t') \times \mathbf{h}_\alpha(\mathbf{k}_t))\, e^{-j\boldsymbol{\rho}\cdot(\mathbf{k}_t - \mathbf{k}_t')} = 0 \quad , \tag{B.7}$$

which yields,

$$\mathbf{h}_\beta \cdot (\hat{\mathbf{z}} \times \mathbf{e}_\alpha) = \delta_{\alpha\beta} \;\; , \tag{B.8}$$

$$\mathbf{e}_\beta \cdot (\mathbf{h}_\alpha \times \hat{\mathbf{z}}) = \delta_{\alpha\beta} \;\; . \tag{B.9}$$

It is noteworthy that the orthogonality relations stated here do not distinguish between the modes for $+\kappa_\alpha$ and $-\kappa_\alpha$, which is, of course, the direct result of the reflection symmetry property of the medium.

[1]The surface divergence theorem is applied to the open surface S here with the radiation condition implied as $\rho \to \infty$.

7.3 Appendix C: Essential expressions related to $\tilde{g}'^{\gtrless}_{ij}(\xi,z,z')$ and $\tilde{g}''^{\gtrless}_{ij}(\xi,z,z')$

In this appendix explicit expressions for $\tilde{g}'^{\gtrless}_{ij}(\xi,z,z')$ and $\tilde{g}''^{\gtrless}_{ij}(\xi,z,z')$ along with the the residues of the surface wave and leaky wave poles, which are related to the roots of D_E and D_H are given. Also, expressions for $N^{\gtrless}_{\substack{E\\H}}(1)$, $\lim_{\xi\to 1}\left[\sqrt{1-\xi^2}\,\frac{d}{d\xi}N^{\gtrless}_{\substack{E\\H}}(\xi)\right]$, $D_{\substack{E\\H}}(1)$, and $\lim_{\xi\to 1}\left[\sqrt{1-\xi^2}\,\frac{d}{d\xi}D_{\substack{E\\H}}(\xi)\right]$ which are employed in Chapter 4 to construct the uniform asymptotic representation of the dyadic Green's function are presented in this appendix.

We first start with TM or (E-mode) terms, $\tilde{g}'^{\gtrless}_{ij}(\xi,z,z')$, and subsequently the TE or (H-mode) terms, $\tilde{g}''^{\gtrless}_{ij}(\xi,z,z')$, will be presented. The functions $\tilde{g}'^{\gtrless}_{ij}(\xi,z,z')$, and $\tilde{g}''^{\gtrless}_{ij}(\xi,z,z')$, can be expressed as

$$\tilde{g}'^{>}_{ij}(\xi,z,z') = \frac{N^{>}_{ij,E}(\xi,z,z')}{D_E(\xi)} \quad , \tag{C.1}$$

$$\tilde{g}''^{>}_{ij}(\xi,z,z') = \frac{N^{>}_{ij,H}(\xi,z,z')}{D_H(\xi)} \, , \tag{C.2}$$

where functions $N_{ij,E}$, D_E, $N_{tt,H}$, and D_H will be defined shortly. Between $\tilde{g}^{>}_{ij}$, and $\tilde{g}^{<}_{ij}$ the following relations hold:

$$\tilde{g}'^{<}_{tt}(z,z') = \tilde{g}'^{>}_{tt}(z',z) \quad , \tag{C.3}$$

$$\tilde{g}'^{<}_{zz}(z,z') = \tilde{g}'^{>}_{zz}(z',z) \quad , \tag{C.4}$$

$$\tilde{g}'^{>}_{zt}(z,z') = -\tilde{g}'^{<}_{tz}(z',z) \quad , \tag{C.5}$$

$$\tilde{g}'^{<}_{zt}(z,z') = -\tilde{g}'^{>}_{tz}(z',z) \quad , \tag{C.6}$$

and

$$\tilde{g}''^{<}_{tt}(z,z') = \tilde{g}''^{>}_{tt}(z',z) \; . \tag{C.7}$$

The functions $N_{ij,E}$, and D_E (in view of (2.18), (2.36), and (2.49)) are defined as

$$N^{>}_{tt,E}(z,z') = \frac{e^{-j\kappa'_2(\overline{z-z'})}(1-e^{-j2\kappa'_2(\overline{z'-z_2})})}{1+e^{-j2\kappa'_2 d_2}}\left[U_1(1+e^{-j2\kappa'_2(\overline{z_1-z})})+U_2(1-e^{-j2\kappa'_2(\overline{z_1-z})})\right] \tag{C.8}$$

$$N^{>}_{tz,E}(z,z') = \frac{e^{-j\kappa_2'(\overline{z-z'})}(1+e^{-j2\kappa_2'(\overline{z'-z_2})})}{1+e^{-j2\kappa_2'\bar{d}_2}}\left[U_1\,(1+e^{-j2\kappa_2'(\overline{z_1-z})})+U_2\,(1-e^{-j2\kappa_2'(\overline{z_1-z})})\right] \tag{C.9}$$

$$N^{<}_{tz,E}(z,z') = -\frac{e^{-j\kappa_2'(\overline{z'-z})}(1-e^{-j2\kappa_2'(\overline{z-z_2})})}{1+e^{-j2\kappa_2'\bar{d}_2}}\left[U_1\,(1-e^{-j2\kappa_2'(\overline{z_1-z'})})+U_2\,(1+e^{-j2\kappa_2'(\overline{z_1-z'})})\right] \tag{C.10}$$

$$N^{>}_{zz,E}(z,z') = \frac{e^{-j\kappa_2'(\overline{z-z'})}(1+e^{-j2\kappa_2'(\overline{z'-z_2})})}{1+e^{-j2\kappa_2'\bar{d}_2}}\left[U_1\,(1-e^{-j2\kappa_2'(\overline{z_1-z})})+U_2\,(1+e^{-j2\kappa_2'(\overline{z_1-z})})\right] \tag{C.11}$$

and

$$D_E(\xi) = U_1(\xi) + j\,\tan\kappa_2'\bar{d}_2\,U_2(\xi)\ , \tag{C.12}$$

where,

$$\begin{aligned} U_1(\xi) &= Z_1\ (Z_0 + j\,Z_1\,\tan\kappa_1'\bar{d}_1) \\ U_2(\xi) &= Z_2\ (Z_1 + j\,Z_0\,\tan\kappa_1'\bar{d}_1)\ , \end{aligned} \tag{C.13}$$

and parameters $\overline{z_i - z_j}$, $\bar{d}_i$, κ_i', are defined as

$$\overline{z_i - z_j} = k_0\,(z_i - z_j)\ ;\ \bar{d}_i = k_0\,d_i\ ;\ \kappa_i' = \sqrt{n_i - n_i'\xi^2}\ ;\ n_i = \mu_{i,t}\,\epsilon_{i,t}\ ;\ n_i' = \frac{\epsilon_{i,t}}{\epsilon_{i,z}}\ , \tag{C.14}$$

and the normalized mode impedance Z_i is defined as

$$Z_i = \frac{\kappa_i'}{\epsilon_{i,t}}\ . \tag{C.15}$$

Note that the parameters κ_i, and Z_i are respectively normalized to k_0 and $\omega\epsilon_0$, and thus $n_0 = n_0' = 1$.

The residue of $\tilde{g}_{ij}^{'\gtrless}(z,z')$ at $\xi = \xi_{p'}$ which is associated with the TM (or E-mode) surface wave or leaky wave mode is given by

$$Res\left(\tilde{g}_{ij}^{'\gtrless}(z,z')\right)_{|\xi=\xi_{p'}} = \frac{N^{\gtrless}_{ij,E}(\xi_{p'})}{\frac{d}{d\xi}D_E(\xi)_{|\xi=\xi_{p'}}}\ , \tag{C.16}$$

where

$$\frac{d}{d\xi}D_E(\xi) = -\xi\Bigg\{Z_1\left[\frac{1}{\kappa_0}+j\frac{n_1'}{\epsilon_1}\left(\frac{\tan\kappa_1'\bar{d}_1}{\kappa_1'}+\frac{\bar{d}_1}{\cos^2(\kappa_1'\bar{d}_1)}\right)\right] + \frac{n_1'}{\epsilon_1\kappa_1'}\left(Z_0+jZ_1\tan\kappa_1'\bar{d}_1\right) + j\left[Z_2\tan\kappa_2'\bar{d}_2\left[\frac{n_1'}{\epsilon_1\kappa_1'}+j\left(\frac{\tan\kappa_1'\bar{d}_1}{\kappa_0}+\frac{n_1'\kappa_0}{\kappa_1'}\frac{\bar{d}_1}{\cos^2\kappa_1'\bar{d}_1}\right)\right] + \frac{n_2'}{\epsilon_2}\left(\frac{\tan\kappa_2'\bar{d}_2}{\kappa_2'}+\frac{\bar{d}_2}{\cos^2(\kappa_2'\bar{d}_2)}\right)\left(Z_1+jZ_0\tan\kappa_1'\bar{d}_1\right)\right]\Bigg\} \quad . \tag{C.17}$$

Also, explicit expressions for $N^{>}_{ij,E}(1)$, $\lim_{\xi\to 1}\left[\sqrt{1-\xi^2}\,\frac{d}{d\xi}N^{>}_{ij,E}(\xi)\right]$, $D_E(1)$, and $\lim_{\xi\to 1}\left[\sqrt{1-\xi^2}\,\frac{d}{d\xi}D_E(\xi)\right]$ are given by

$$N^{>}_{tt,E}(1,z,z') = \frac{e^{-j\sqrt{n_2-n_2'}\,(\overline{z-z'})}\left(1-e^{-j2\sqrt{n_2-n_2'}\,(\overline{z'-z_2})}\right)}{1+e^{-j2\sqrt{n_2-n_2'}\,d_2}} \cdot\Bigg(\left[j\frac{n_1-n_1'}{(\epsilon_1)^2}\tan\sqrt{n_1-n_1'}\,\bar{d}_1\right]\left(1+e^{-j\sqrt{n_2-n_2'}\,(\overline{z_1-z})}\right)+\left[\frac{\sqrt{n_2-n_2'}}{\epsilon_2}\frac{\sqrt{n_1-n_1'}}{\epsilon_1}\right]\left(1-e^{-j2\sqrt{n_2-n_2'}\,(\overline{z_1-z})}\right)\Bigg) \quad , \tag{C.18}$$

$$N^{>}_{tz,E}(1,z,z') = \frac{e^{-j\sqrt{n_2-n_2'}\,(\overline{z-z'})}\left(1-e^{-j2\sqrt{n_2-n_2'}\,(\overline{z'-z_2})}\right)}{1+e^{-j2\sqrt{n_2-n_2'}\,d_2}} \cdot\Bigg(\left[j\frac{n_1-n_1'}{(\epsilon_1)^2}\tan\sqrt{n_1-n_1'}\,\bar{d}_1\right]\left(1+e^{-j\sqrt{n_2-n_2'}\,(\overline{z_1-z})}\right)+\left[\frac{\sqrt{n_2-n_2'}}{\epsilon_2}\frac{\sqrt{n_1-n_1'}}{\epsilon_1}\right]\left(1-e^{-j2\sqrt{n_2-n_2'}\,(\overline{z_1-z})}\right)\Bigg) \quad , \tag{C.19}$$

$$N^{<}_{tz,E}(1,z,z') = -\frac{e^{-j\sqrt{n_2-n_2'}\,(\overline{z-z'})}\left(1-e^{-j2\sqrt{n_2-n_2'}\,(\overline{z'-z_2})}\right)}{1+e^{-j2\sqrt{n_2-n_2'}\,d_2}} \tag{C.20}$$

$$\cdot \left(\left[j \frac{n_1 - n_1'}{(\epsilon_1)^2} \tan \sqrt{n_1 - n_1'} \bar{d}_1 \right] (1 - e^{-j\sqrt{n_2 - n_2'}\,(\overline{z_1 - z})}) + \right.$$

$$\left. \left[\frac{\sqrt{n_2 - n_2'}}{\epsilon_2} \frac{\sqrt{n_1 - n_1'}}{\epsilon_1} \right] (1 + e^{-j2\sqrt{n_2 - n_2'}\,(\overline{z_1 - z})}) \right) \quad ,$$

$$N^{<}_{zz,E}(1, z, z') = \frac{e^{-j\sqrt{n_2 - n_2'}\,(\overline{z - z'})}(1 + e^{-j2\sqrt{n_2 - n_2'}\,(\overline{z' - z_2})})}{1 + e^{-j2\sqrt{n_2 - n_2'}\,d_2}} \tag{C.21}$$

$$\cdot \left(\left[j \frac{n_1 - n_1'}{(\epsilon_1)^2} \tan \sqrt{n_1 - n_1'} \bar{d}_1 \right] (1 - e^{-j\sqrt{n_2 - n_2'}\,(\overline{z_1 - z})}) + \right.$$

$$\left. \left[\frac{\sqrt{n_2 - n_2'}}{\epsilon_2} \frac{\sqrt{n_1 - n_1'}}{\epsilon_1} \right] (1 + e^{-j2\sqrt{n_2 - n_2'}\,(\overline{z_1 - z})}) \right) \quad ,$$

$$\lim_{\xi \to 1} \left[\sqrt{1 - \xi^2}\, \frac{d}{d\xi} N^{>}_{tt,E}(\xi, z, z') \right] = - \frac{e^{-j\sqrt{n_2 - n_2'}\,(\overline{z - z'})}(1 - e^{-j2\sqrt{n_2 - n_2'}\,(\overline{z' - z_2})})}{1 + e^{-j2\sqrt{n_2 - n_2'}\,d_2}}$$

$$\cdot \left(\left[j \frac{\sqrt{n_1 - n_1'}}{\epsilon_1} (1 + e^{-j\sqrt{n_2 - n_2'}\,(\overline{z_1 - z})}) + \right. \right. \tag{C.22}$$

$$\left. \left. + j[\frac{\sqrt{n_2 - n_2'}}{\epsilon_2} \tan \sqrt{n_1 - n_1'} \bar{d}_1 (1 - e^{-j2\sqrt{n_2 - n_2'}\,(\overline{z_1 - z})}) \right) \right] \quad ,$$

$$\lim_{\xi \to 1} \left[\sqrt{1 - \xi^2}\, \frac{d}{d\xi} N^{>}_{tz,E}(\xi, z, z') \right] = - \frac{e^{-j\sqrt{n_2 - n_2'}\,(\overline{z - z'})}(1 + e^{-j2\sqrt{n_2 - n_2'}\,(\overline{z' - z_2})})}{1 + e^{-j2\sqrt{n_2 - n_2'}\,d_2}}$$

$$\cdot \left(\left[j \frac{\sqrt{n_1 - n_1'}}{\epsilon_1} (1 + e^{-j\sqrt{n_2 - n_2'}\,(\overline{z_1 - z})}) + \right. \right. \tag{C.23}$$

$$\left. \left. + j[\frac{\sqrt{n_2 - n_2'}}{\epsilon_2} \tan \sqrt{n_1 - n_1'} \bar{d}_1 (1 - e^{-j2\sqrt{n_2 - n_2'}\,(\overline{z_1 - z})}) \right) \right] \quad ,$$

$$\lim_{\xi \to 1} \left[\sqrt{1 - \xi^2}\, \frac{d}{d\xi} N^{<}_{tz,E}(\xi, z, z') \right] = \frac{e^{-j\sqrt{n_2 - n_2'}\,(\overline{z - z'})}(1 + e^{-j2\sqrt{n_2 - n_2'}\,(\overline{z' - z_2})})}{1 - e^{-j2\sqrt{n_2 - n_2'}\,d_2}}$$

$$\cdot \left(\left[j \frac{\sqrt{n_1 - n_1'}}{\epsilon_1} (1 - e^{-j\sqrt{n_2 - n_2'}\,\overline{(z_1 - z)}}) + \right. \right. \tag{C.24}$$

$$\left. \left. + j[\frac{\sqrt{n_2 - n_2'}}{\epsilon_2} \tan \sqrt{n_1 - n_1'}\,\bar{d}_1 (1 + e^{-j2\sqrt{n_2 - n_2'}\,\overline{(z_1 - z)}}) \right) \right] ,$$

$$\lim_{\xi \to 1} \left[\sqrt{1 - \xi^2}\, \frac{d}{d\xi} N^{<}_{zz,E}(\xi, z, z') \right] = - \frac{e^{-j\sqrt{n_2 - n_2'}\,\overline{(z - z')}} (1 - e^{-j2\sqrt{n_2 - n_2'}\,\overline{(z' - z_2)}})}{1 - e^{-j2\sqrt{n_2 - n_2'}\,\bar{d}_2}}$$

$$\cdot \left(\left[j \frac{\sqrt{n_1 - n_1'}}{\epsilon_1} (1 - e^{-j\sqrt{n_2 - n_2'}\,\overline{(z_1 - z)}}) + \right. \right. \tag{C.25}$$

$$\left. \left. + j[\frac{\sqrt{n_2 - n_2'}}{\epsilon_2} \tan \sqrt{n_1 - n_1'}\,\bar{d}_1 (1 + e^{-j2\sqrt{n_2 - n_2'}\,\overline{(z_1 - z)}}) \right) \right] ,$$

$$D_E(1) = \frac{n_1 - n_1'}{(\epsilon_1)^2} \tan \sqrt{n_1 - n_1'}\,\bar{d}_1 + j\sqrt{n_2 - n_2'}\,\epsilon_2 \frac{\sqrt{n_1 - n_1'}}{\epsilon_1} \tan \sqrt{n_2 - n_2'}\,\bar{d}_2 , \tag{C.26}$$

and

$$\lim_{\xi \to 1} \left[\sqrt{1 - \xi^2}\, \frac{d}{d\xi} D_E(\xi) \right] = - \left[\frac{\sqrt{n_1 - n_1'}}{\epsilon_1} - \frac{\sqrt{n_2 - n_2'}}{\epsilon_2} \tan \sqrt{n_2 - n_2'}\,\bar{d}_2 \tan \sqrt{n_1 - n_1'}\,\bar{d}_1 \right] . \tag{C.27}$$

Also the following relations exists

$$\begin{aligned} N^{<}_{tt,E}(1, z, z') &= N^{>}_{tt,E}(1, z', z) , \\ \lim_{\xi \to 1} \sqrt{1 - \xi^2}\, \frac{d}{d\xi} N^{<}_{tt,E}(z, z') &= \lim_{\xi \to 1} \sqrt{1 - \xi^2}\, \frac{d}{d\xi} N^{>}_{tt,E}(z', z) , \end{aligned} \tag{C.28}$$

$$\begin{aligned} N^{<}_{zz,E}(1, z, z') &= N^{>}_{zz,E}(1, z', z) , \\ \lim_{\xi \to 1} \sqrt{1 - \xi^2}\, \frac{d}{d\xi} N^{<}_{zz,E}(z, z') &= \lim_{\xi \to 1} \sqrt{1 - \xi^2}\, \frac{d}{d\xi} N^{>}_{zz,E}(z', z) , \end{aligned} \tag{C.29}$$

$$
\begin{aligned}
N^{>}_{zt,E}(1,z,z') &= -N^{<}_{tz,E}(1,z',z) \\
\lim_{\xi\to 1}\sqrt{1-\xi^2}\,\frac{d}{d\xi}N^{>}_{zt,E}(z,z') &= -\lim_{\xi\to 1}\sqrt{1-\xi^2}\,\frac{d}{d\xi}N^{<}_{tz,E}(z',z)\ ,
\end{aligned}
\tag{C.30}
$$

$$
\begin{aligned}
N^{>}_{tz,E}(1,z,z') &= -N^{<}_{zt,E}(1,z',z) \\
\lim_{\xi\to 1}\sqrt{1-\xi^2}\,\frac{d}{d\xi}N^{>}_{tz,E}(z,z') &= -\lim_{\xi\to 1}\sqrt{1-\xi^2}\,\frac{d}{d\xi}N^{<}_{zt,E}(z',z)\ .
\end{aligned}
\tag{C.31}
$$

As mentioned earlier, the TE or (H-mode) terms, $\tilde{g}''^{>}_{ij}(\xi,z,z')$, is given by

$$
\tilde{g}''^{>}_{ij}(\xi,z,z') = \frac{N^{>}_{ij,H}(\xi,z,z')}{D_H(\xi)}\ , \tag{C.32}
$$

where the functions $N_{tt,H}$, and D_H (in view of (2.20), (2.36), and (2.49)) are defined as

$$
N^{>}_{tt,H} = \frac{e^{-j\kappa''_2(\overline{z-z'})}(1-e^{-j2\kappa''_2(\overline{z'-z_2})})}{1+e^{-j2\kappa''_2\bar{d}_2}}\left[V_1(1-e^{-j2\kappa''_2(\overline{z_1-z})})+V_2(1+e^{-j2\kappa''_2(\overline{z_1-z})})\right]\ , \tag{C.33}
$$

and

$$
D_H(\xi) = V_2(\xi) + j\,\tan\kappa''_2\bar{d}_2\,V_1(\xi)\ , \tag{C.34}
$$

where

$$
\begin{aligned}
V_1(\xi) &= Y_1\,(Y_0 + jY_1\,\tan\kappa''_1\bar{d}_1)\ , \\
V_2(\xi) &= Y_2\,(Y_1 + jY_0\,\tan\kappa''_1\bar{d}_1)\ ,
\end{aligned}
\tag{C.35}
$$

and the parameter κ''_i is defined as

$$
\kappa''_i = \sqrt{n_i - n''_i\xi^2}\ ;\ n''_i = \frac{\mu_{i,t}}{\mu_{i,z}}\ , \tag{C.36}
$$

and the normalized mode admittance Y_i is given by

$$
Y_i = \frac{\kappa''_i}{\mu_{i,t}}\ . \tag{C.37}
$$

Note that the parameters κ_i, and Y_i are respectively normalized to k_0, and $\omega\mu_0$, and thus $n_0 = n_0'' = 1$.

The residue of $\tilde{g}_{ij}''^{\gtrless}(z,z')$ at $\xi = \xi_{p''}$ which is associated with the TE (or H-mode) surface wave or leaky wave mode is given by

$$Res\left(\tilde{g}_{ij}''^{\gtrless}(z,z')\right)_{|_{\xi=\xi_{p''}}} = \frac{N_{ij,E}^{\gtrless}(\xi_{p''})}{\frac{d}{d\xi}D_H(\xi)}_{|_{\xi=\xi_{p''}}} , \tag{C.38}$$

where

$$\begin{aligned}\frac{d}{d\xi}D_H(\xi) \;=\; & -\xi\left\{Y_2\left[\frac{n_1''}{\mu_1\kappa_1''} + j\left(\frac{\tan\kappa_1''\bar{d}_1}{\kappa_0} + \frac{Y_0\, n_1''}{\kappa_1''}\frac{\bar{d}_1}{\cos^2(\kappa_1'\bar{d}_1)}\right)\right]\right. \\ & + \frac{n_2''}{\mu_2\kappa_2''}\left(Y_1 + jY_0\tan\kappa_1''\bar{d}_1\right) \\ & + j\left[Y_1\tan\kappa_2''\bar{d}_2\left[\frac{1}{\kappa_0} + j\frac{n_1''}{\mu_1}\left(\frac{\tan\kappa_1''\bar{d}_1}{\kappa_1''} + \frac{\bar{d}_1}{\cos^2\kappa_1'\bar{d}_1}\right)\right]\right. \\ & \left.\left. + \left(\frac{n_1''}{\mu_1\kappa_1''}\tan\kappa_2''\bar{d}_2 + \frac{Y_2\, n_2''}{\kappa_2''}\frac{\bar{d}_2}{\cos^2(\kappa_2''\bar{d}_2)}\right)\left(Y_0 + jY_1\tan\kappa_1''\bar{d}_1\right)\right]\right\} .\end{aligned} \tag{C.39}$$

Also, explicit expressions for $N_{tt,H}^{>}(1)$, $\lim_{\xi\to 1}\left[\sqrt{1-\xi^2}\,\frac{d}{d\xi}N_{tt,h}^{>}(\xi)\right]$, $D_H(1)$, and $\lim_{\xi\to 1}\left[\sqrt{1-\xi^2}\frac{d}{d\xi}D_H(\xi)\right]$ are given by

$$\begin{aligned}N_{tt,H}^{>}(1,z,z') = & \frac{e^{-j\sqrt{n_2-n_2''}\,(\overline{z-z'})}\left(1 - e^{-j2\sqrt{n_2-n_2''}\,(\overline{z'-z_2})}\right)}{1 + e^{-j2\sqrt{n_2-n_2''}\,d_2}} \\ & \left(\left[j\frac{n_1-n_1''}{(\mu_1)^2}\tan\sqrt{n_1-n_1''}\,\bar{d}_1\right]\left(1 - e^{-j\sqrt{n_2-n_2''}\,(\overline{z_1-z})}\right) + \right. \\ & \left.\left[\frac{\sqrt{n_2-n_2''}}{\mu_2}\frac{\sqrt{n_1-n_1''}}{\mu_1}\right]\left(1 + e^{-j2\sqrt{n_2-n_2''}\,(\overline{z_1-z})}\right)\right) ,\end{aligned} \tag{C.40}$$

$$\begin{aligned}\lim_{\xi\to 1}\left[\sqrt{1-\xi^2}\,\frac{d}{d\xi}N_{tt,H}^{>}(\xi,z,z')\right] = & -\frac{e^{-j\sqrt{n_2-n_2''}\,(\overline{z-z'})}\left(1 - e^{-j2\sqrt{n_2-n_2''}\,(\overline{z'-z_2})}\right)}{1 + e^{-j2\sqrt{n_2-n_2''}\,\bar{d}_2}} \\ & \cdot\left(\left[\frac{\sqrt{n_1-n_1''}}{\mu_1}\left(1 - e^{-j\sqrt{n_2-n_2''}\,(\overline{z_1-z})}\right) + \right.\right.\end{aligned}$$

$$+j[\frac{\sqrt{n_2 - n_2''}}{\mu_2} \tan \sqrt{n_1 - n_1''}\bar{d}_1(1 + e^{-j2\sqrt{n_2 - n_2''}(\overline{z_1 - z})})\Big)\Big] \quad ,$$

$$D_H(1) = \frac{\sqrt{n_1 - n_1''}}{\mu_1}\left(\frac{\sqrt{n_2 - n_2''}}{\mu_2} - \frac{\sqrt{n_1 - n_1''}}{\mu_1} \tan \sqrt{n_2 - n_2''}\bar{d}_2 \tan \sqrt{n_1 - n_1''}\bar{d}_1\right) \quad , \qquad \text{(C.41)}$$

and

$$\lim_{\xi \to 1}\left[\sqrt{1 - \xi^2}\frac{d}{d\xi}D_H(\xi)\right] = -j\left[\frac{\sqrt{n_2 - n_2'}}{\mu_2} \tan \sqrt{n_1 - n_1''}\bar{d}_1 + \frac{\sqrt{n_1 - n_1''}}{\mu_1} \tan \sqrt{n_2 - n_2''}\bar{d}_2\right] \quad . \qquad \text{(C.42)}$$

Also the following relations exist

$$\begin{aligned} N^{<}_{tt,H}(1, z, z') &= N^{>}_{tt,H}(1, z', z) \\ \lim_{\xi \to 1}\sqrt{1 - \xi^2}\,\frac{d}{d\xi}N^{<}_{tt,H}(z, z') &= \lim_{\xi \to 1}\sqrt{1 - \xi^2}\,\frac{d}{d\xi}N^{>}_{tt,H}(z', z) \quad . \end{aligned}$$

7.4 Appendix D: Limiting values of $\tilde{g}'^{>}_{ij<}(\xi,z,z')$ and $\tilde{g}''^{>}_{ij<}(\xi,z,z')$ as $\xi \to \infty$

In this appendix the limmiting values related to $\tilde{g}'^{>}_{ij<}(z,z')$ and $\tilde{g}''^{>}_{ij<}(z,z')$ as $\xi \to \infty$ which are being used in (3.33) will be given.

Note that

$$\begin{aligned} \lim_{\xi\to\infty} \kappa_i' &= \lim_{\xi\to\infty} \sqrt{n_i - n_i'\xi^2} = -j\xi\sqrt{n_i'} \\ \lim_{\xi\to\infty} \kappa_i'' &= \lim_{\xi\to\infty} \sqrt{n_i - n_i''\xi^2} = -j\xi\sqrt{n_i''} \quad . \end{aligned} \tag{D.1}$$

Hence (see (C.1) - (C.11) and (C.32) - (C.39))

$$\lim_{\xi\to\infty} \tilde{g}'^{>}_{tt}(z,z') \to e^{-\xi\sqrt{n_2'}(\overline{z-z'})} + \frac{\frac{\sqrt{n_1'}}{\epsilon_1} - \frac{\sqrt{n_2'}}{\epsilon_2}}{\frac{\sqrt{n_1'}}{\epsilon_1} + \frac{\sqrt{n_2'}}{\epsilon_2}} e^{-\xi\sqrt{n_2'}(\overline{2z_1-(z+z')})} \quad , \tag{D.2}$$

$$\lim_{\xi\to\infty} \tilde{g}'^{>}_{zt}(z,z') \to e^{-\xi\sqrt{n_2'}(\overline{z-z'})} - \frac{\frac{\sqrt{n_1'}}{\epsilon_1} - \frac{\sqrt{n_2'}}{\epsilon_2}}{\frac{\sqrt{n_1'}}{\epsilon_1} + \frac{\sqrt{n_2'}}{\epsilon_2}} e^{-\xi\sqrt{n_2'}(\overline{2z_1-(z+z')})} \quad , \tag{D.3}$$

$$\lim_{\xi\to\infty} \tilde{g}''^{>}_{tt}(z,z') \to e^{-\xi\sqrt{n_2''}(\overline{z-z'})} + \frac{-\frac{\sqrt{n_1''}}{\mu_1} + \frac{\sqrt{n_2''}}{\mu_2}}{\frac{\sqrt{n_1''}}{\mu_1} + \frac{\sqrt{n_2''}}{\mu_2}} e^{-\xi\sqrt{n_2''}(\overline{2z_1-(z+z')})} \quad , \tag{D.4}$$

Also, as $\xi \to \infty$ the following relations exit:

$$\tilde{g}'^{<}_{tt}(z,z') = \tilde{g}'^{>}_{tt}(z',z) \quad , \tag{D.5}$$

$$\tilde{g}'^{>}_{tz}(z,z') = \tilde{g}'^{>}_{tt}(z,z') \quad , \tag{D.6}$$

$$\tilde{g}'^{<}_{zt}(z,z') = -\tilde{g}'^{<}_{tt}(z',z) \quad , \tag{D.7}$$

$$\tilde{g}'^{<}_{tz}(z,z') = -\tilde{g}'^{>}_{zt}(z',z) \quad , \tag{D.8}$$

$$\tilde{g}'^{>}_{zz}(z,z') = \tilde{g}'^{>}_{zt}(z,z') \ , \tag{D.9}$$

$$\tilde{g}'^{<}_{zz}(z,z') = \tilde{g}'^{>}_{zz}(z',z) \ , \tag{D.10}$$

and

$$\tilde{g}''^{<}_{tt}(z,z') = \tilde{g}''^{>}_{tt}(z,z') \ . \tag{D.11}$$

Bibliography

[1] S. Barkeshli and P. H. Pathak, "An efficient moment method analysis of finite phased arrays of microstrip dipoles using an asymptotic closed form approximation for the planar microstrip Green's function," presented at International IEEE/APS Symposium and National Radio Science Meeting at Syracuse, New York, June 6-10, 1988.

[2] S. Barkeshli, "An efficient moment method analysis of finite phased arrays of strip dipoles in a substrate/superstrate configuration using an asymptotic closed form approximation for the planar double layered microstrip Green's function," presented at International IEEE/APS Symposium and National Radio Science Meeting at San Jose, California, June 26-30, 1989.

[3] J. R. Wait, "Fields of a horizontal dipole over a stratified anisotropic half-space," *IEEE Trans. Antennas and Propagation*, vol. AP-14, pp. 790-792, Nov. 1966.

[4] J. A. Kong, "Electromagnetic field due to dipole antennas over stratified anisotropic media, *Geophysics,* vol. 37, pp. 985-996, 1972.

[5] J. A. Kong, *Electromagnetic Wave Theory.* New York: Wiley Interscience, 1986.

[6] L. B. Felsen and N. Marcuvitz, *Radiation and Scattering of Waves,* Prentice-Hall Englewood Cliffs, New Jersey, 1973, Chapter 7 and 8.

[7] S. M. Ali and S. F. Mahmoud, "Electromagnetic fields of buried sources in stratified anisotropic media," *IEEE Trans. Antennas Propagat.*, vol. AP-27, 671-678, 1979.

[8] C. M. Tang, "Electromagnetic fields due to dipole antennas embedded in stratified anisotropic media," *IEEE Trans. Antennas Propagat.*, vol. AP-27, pp. 665-670, 1979.

[9] Y. S. Kwon and J. J. H. Wang, "Computation of Hertzian dipole radiation in stratified uni-axial anisotropic media," *Radio Science*, vol 21, no. 21, pp. 891-902, Nov.-Dec., 1986.

[10] C. M. Krowne, " Green's function in spectral domain for bi-axial and uni-axial anisotropic planar dielectric structures," *IEEE Trans. Antennas Propagat.*, vol. AP-32, pp. 1273-1281, 1984.

[11] J. L. Tsalamengas, and N. K. Uzunoglo, "Radiation from a dipole antennas in the proximity of a general anisotropic grounded layer," *IEEE Trans. Antennas Propagat.*, vol. AP-33, 165-172, 1985.

[12] W. C. Chew, *Waves and Fields in Inhomogeneous Media,* Van Nostrand Reinhold, New York, 1990.

[13] S. Barkeshli and P. H. Pathak, "On the Dyadic Green's Function For A Planar Multi-layered Dielectric/Magnetic Media," will appear in *IEEE Trans. Microwave Theory Tech.*, January, 1992.

[14] S. Barkeshli, "Electromagnetic dyadic green's function for multi-layered symmetric gyroelectric media," paper submitted for the publication to the Journal of *Radio Science*

[15] P. H. Pathak, "On the Eigenfunction Expansion of Electromagnetic Dyadic Green's Functions, *IEEE Trans. Antennas Propagat.*, vol. AP-31, pp. 837-846, 1983.

[16] A. Papoulis, *The Fourier Integral and Its Applications*, McGraw Hill, 1962.

[17] S. Barkeshli and P. Pathak, "On the dyadic Green's function of an infinite array of dipole source in multilayered dielectric/ferrite media," presented at the International IEEE/APS Symposium and National Radio Science Meeting at Blacksburg, Virginia, June 15-19 1987.

[18] S. Barkeshli, P. H. Pathak, "Radial propagation and steepest descent path integral representations of the planar microstrip dyadic Green's function," *Radio Sci.*, vol. 25, no 2, pp 161-174, March-April 1990.

[19] Barkeshli, S., "An efficient approach for evaluating the planar microstrip green's function and its applications to the analysis of microstrip antennas and arrays," Ph.D. dissertation, The Ohio State University, Department of Electrical Engineering, Columbus, Ohio, 1988.

[20] S. Barkeshli, P. H. Pathak and M. Marin, "An asymptotic closed form microstrip surface Green's function for the efficient moment method analysis of mutual coupling in microstrip antennas," *IEEE Trans. Antennas Propagat.*, vol. 38, No. 9, pp. 1374-1383, Sept. 1990.

[21] E. Arbel and L. B. Felsen, "Theory of radiation from sources in anisotropic media. Part I-General sources in stratified media. Part II- point source in an infinite homogeneous medium," in *Electromagnetic Theory and Antennas* (E. C. Jordan, Ed.),pp 391-459. New York: Pergamon Prss, 1963.

[22] R. E. Collin, *Field Theory of Guided Waves,* McGraw Hill, New York, 1960.

[23] S. Barkeshli and P. H. Pathak, "On a closed form asymptotic representation of the planar single and double layered grounded material slab Green's functions and their applications to an efficient analysis of arbitrary microstrip geometries," presented in the International Conference on Directions in Electromagnetic Wave Modeling, The Weber Research Institute of Polytechnic University, New York City, New York, October 1990.

[24] M. Marin, S. Barkeshli and P. H. Pathak, "On the location of surface and leaky waves poles for the grounded dielectric slab," *IEEE Trans. Antennas Propagat.*, Vol. AP-38, No. 4, pp. 570-573, April 1990.

[25] N. G. Alexopoulos and D. R. Jackson, "Fundamnetal superstrate (cover) effects on printed circuit antennas," *IEEE Trans. Antennas Propagat.*, Vol. AP-32, pp. 807-816, August 1984.

[26] M. Marin and P. H. Pathak, "An asymptotic closed-form representation for the grounded double layer surface Green's function," paper submitted for publication on *IEEE Trans. Antennas Propagat.*

END